②

AD–A213 143

Stability and Scaling of
High Current Cyclic Accelerators
Final Report
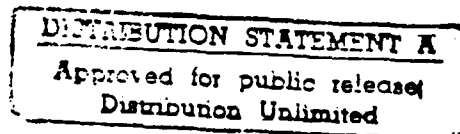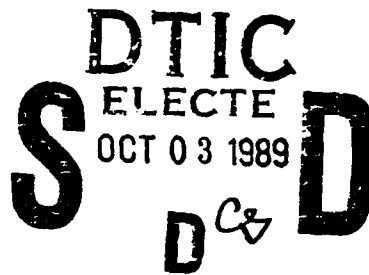SAIC Report SAIC-89/1428
Contract Number N00014-84-C-0518

May 17, 1989

SAIC

Science Applications International Corporation

**DTIC
S ELECTE D
OCT 0 3 1989
D Cv**

89 5 19 146

Stability and Scaling of
High Current Cyclic Accelerators

Final Report

SAIC Report SAIC-89/1428

Contract Number N00014-84-C-0518

May 17, 1989

Submitted to:

Office of Naval Research
800 N. Quincy Street
Arlington, Virginia 22217

Submitted by:

Science Applications International Corporation
1710 Goodridge Drive
McLean, Virginia 22102

TABLE OF CONTENTS

1.0 HISTORICAL INTRODUCTION

Efforts to produce high power, high quality electron beams for use in Navy applications have focused in recent years on techniques to improve the current carrying capacity of the betatron accelerator, first operated by D. Kerst[1,2] in 1940. It was recognized early by Kerst[3] that the current limit in a betatron is due to the defocusing effects of space charge at injection time; space charge effects become rapidly less important as beam energy is increased. One obvious way, therefore, to increase the current is to increase the energy of the injected beam. Of course, there are limits to this strategy; the injector rapidly becomes large and expensive as the energy is increased. Still, this technique has been successfully used to produce high current ($\sim$ 100 A) beams in a betatron.[4,5] By contrast, the largest Kerst betatron[6] achieved currents of about 100 mA using a 100 keV injector.

Besides increasing the energy of injection, other methods have been tried to improve the current limit, including increasing the external focusing strength in various ways and by decreasing the defocusing effect of space charge by the introduction of a background plasma. Devices using this latter approach, called plasma betatrons,[7] never worked very well, even with the addition of an applied toroidal field.[8]

Early attempts to increase the focusing strength of applied magnetic fields had mixed results. Among the earliest were the fixed field, alternating gradient (FFAG) betatron,[9] based upon the (then) newly discovered strong focusing principle[10] and the betatron with added longitudinal field.[11]

Two variations of the FFAG betatron were designed, a radial sector type and a spiral sector type;[3] both use fields that are fixed in time, allowing particle orbits to move radially as energy is increased. The current in these devices is thought to be limited, as in other strong focusing machines, by the tune shift due to space charge. The magnet design in these devices is significantly more complex than for a conventional, weak focusing design.[3]

The addition of a toroidal field to a betatron appears to have been first tried in England shortly after World War II, at the wartime radar establishment at Malvern.[11] It was found that such an additional field *decreased* the current output of the device, the reason being that the electrons tended to intercept the injector after one or a few turns around the machine. This early experiment was soon abandoned but the basic idea, that a longitudinal field could be used to control space charge defocusing, was nonetheless sound; the fundamental problem was to inject and trap a high current beam in the presence of a longitudinal field.

In 1972 Rostoker[12] described theoretically how to form a high density beam of electrons in a torus, using the inductive charging technique pioneered on the HIPAC device.[13]

A few years later he proposed[14] accelerating the resulting high density beam using a flux changing coil, as in a conventional betatron. A similar 'modified betatron' for high current proton beams (not using inductive charging) was proposed by Sprangle and Kapetanakos.[15] On the basis of this theoretical work and some additional studies[16,17] two experimental programs on the modified betatron were begun, one at the University of California at Irvine and another at the Naval Research Laboratory.

The program at Irvine was an outgrowth of some earlier work on electron cloud trapping at Maxwell Laboratories.[18] It was found that a large fraction of the cloud injected by inductive charging could not be accelerated by the betatron field; the suggestion was that electrons were trapped in field bumps produced by the discrete coils used to make the toroidal field. By using a variant of inductive charging the Irvine group was able to produce currents up to 200 A and energies up to 1 MeV (but not both, simultaneously) in a modified betatron.[19]
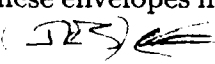
At NRL, extensive analyses were made of injection,[20,21,22] beam equilibria[23] and stability,[24,25,26] and extraction[27] during the design and construction of a larger scale modified betatron, designed to produce a 50 MeV, 10 kA electron beam. The technical obstacles to injection and trapping and to chamber design have proven to be difficult to overcome, however. Recently, the successful injection of a 2-3 kA beam has been achieved using an internal diode injector arrangement.[22]

One of the problems with both the conventional and modified betatrons is their sensitivity of the radial location of the equilibrium orbit to the particle energy, a feature which complicates the injection and trapping of large currents. It was first recognized by Mondelli and Roberson,[28] in the course of their study of the Racetrack Induction Accelerator, that the use of an $\ell=2$ stellarator field will significantly reduce this sensitivity. It was subsequently suggested[29] that the addition of an $\ell=2$ stellarator field to a modified betatron could improve its current carrying capacity. In a test of this prediction, stellarator windings were added to the betatron at Irvine. A 200 A beam was accelerated to 2 MeV in the device;[30] smaller currents were subsequently accelerated to 10 MeV.

The present report presents theoretical results produced with ONR support at SAIC, on the stability and scaling of compact electron accelerators using continuous strong focusing in the form of stellarator windings. The work reported here has been mainly analytical in nature but has also involved the development and use of a variety of computer programs needed to assist various aspects of the study. (See Appendix C.) During the contract we have attempted to address in some considerable detail every major physics issue which would affect the design of accelerators using stellarator fields. Generally speaking, these issues divide into two broad categories: beam equilibria and matching and beam stability;

each of these may be further sub-divided into single particle and collective phenomena.

Beam equilibria are states in which focusing and defocusing forces are in balance. Collections of non-interacting single particles, launched with a distribution of initial conditions, are defocused by the finite beam emittance and focused by external fields. For strong focusing systems there typically exist regions of parameter space in which particle orbits are stable, separated by so-called stopbands, in which the motion is unstable. For non-interacting particles, every collection of initial conditions in a stable system represents an equilibrium. It is possible to construct special equilibria, so-called matched solutions, whose macroscopic properties (e.g. beam shape) repeat periodically with the same period as the focusing system; these have been constructed generally for 1-D systems by Courant and Snyder.[31] In the case of realistic transport systems in which the focusing system changes qualitatively from section to section, numerical analysis is necessary in order to analyze the change in beam properties. A single particle code, SPIRAL, has been constructed for this purpose. This code and its use in performing beam matching calculations from a diode, through a focusing (compression) section and into $\ell = 2$ stellarator transport section are described below.

Once space charge forces are considered, the situation becomes more complex; only in the simple case of a uniform elliptical beam can equilibria be constructed analytically. In the case that the two transverse degrees of freedom are decoupled this was shown by Kapchinskii and Vladimirskii;[32] the resulting K-V equilibria are represented by the usual K-V envelope equations. The stability of these envelopes in a bumpy-torus ($\ell=0$) stellatron, has been studied under this program.[33]

When the transverse degrees of freedom of particle motion are coupled, as in the $\ell=2$ stellatron, the analysis of beam equilibria and stability becomes more complex. Gluckstern[34] appears to have been the first to construct a K-V type of equilibrium for a continuously rotated quadrupole field; Chernin[35] carried out the analysis including a longitudinal field. There remained, however, the question of how small departures from these equilibria behaved. To answer this question, an envelope type of equation governing these systems was required. Such an equation was developed and the stability of the K-V $\ell=2$ stellatron distribution was studied under this program.[36] A code, XYENV, was written to integrate the generalized envelope equation in an arbitrary focusing system, including the effect of space charge for a uniform elliptical beam. It has been used to study the matching problem from longitudinal to stellarator fields in the presence of space charge forces and will continue to be used as a design tool for transport line design.

Beam stability issues, like the issue of envelope stability, naturally divide themselves into single particle and collective effects. The most basic stability question for the stella-

tron, that of the nature of the stopband for single particle motion, was answered in the original paper of Roberson, Mondelli and Chernin.[29] Other single particle instabilities are inevitably present in real machines, however, in the form of orbital resonances due to the presence of field errors. Both linear and non-linear resonances have been investigated in some detail;[37,38] our conclusion is that they are potentially rather serious for the stellatron and may act to limit the achievable current and energy of the device. Some evidence of the ability to cross high order resonances has been reported by the Irvine group.[39] One interesting theoretical finding is the tendency of a strong longitudinal field to reduce the tune shift due to space charge.

Collective beam modes have also been investigated during this effort. In particular, an extensive study was reported[40] on the negative mass instability in the stellatron, and its coupling to transverse modes. An eigenvalue problem for the growth rate was formulated and solved numerically; in addition, the eigenvalue problem was solved approximately, in the smooth approximation, and the resulting dispersion relation reproduced the numerical results to very good accuracy. It was shown that the correct dispersion relation was just that for the modified betatron,[26] under the replacement of a single term, to include the smoothed effect of the stellator field.

Another collective mode of a beam in a stellarator field was identified by Hughes and Godfrey.[41] This is a short wavelength, transverse electromagnetic mode involving a resonance between the betatron oscillations of the beam and a vacuum waveguide mode. Linear growth rates can be significant under some circumstances and computer simulations have shown[41] that this instability can be disruptive. There is some evidence that self beam energy spread due to space charge will help stabilize this mode. Avoidance of this instability requires careful design of the beam transport line.

During the course of this work, it became clear that recirculating induction linacs hold promise for solving some of the problems facing a betatron, even one using strong focusing: for the stellatron, as for the modified betatron, injection and extraction remain key problems. Also, the relatively slow acceleration cycle of a betatron allow time for the growth of beam instabilities. Finally, the weight of a high power betatron and associated power supplies and shielding looked formidable.

Based on the early theoretical work of Mondelli and Roberson[28] on a racetrack recirculator using stellarator fields, on the experimental efforts on recirculation of Wilson,[42] and on the work of Birx[43] on branched magnetics, a spiral line inductor accelerator (SLIA) was proposed[44] in 1985. The SLIA uses a continuous beam line which passes through an accelerator module multiple times. This design vastly reduces the difficulty of injection and extraction and, since the effective accelerating gradient is much larger than in a betatron,

instabilities have much less time to grow; one finds, for example, that the long wavelength negative mass instability in the bends is not nearly as important as in a betatron. Also in the SLIA, the weight of the power supplies is reduced by resetting and re-using the induction module cores between beam passes. Finally, the use of static fields in the transport line allow very low field errors to be achieved.

While solving many problems of the closed orbit, betatron-type accelerators the SLIA introduces at least one important new physics/design issue: the beam break-up instability. This instability is due to the off-axis passage of a beam through an accelerating module which excites an electromagnetic cavity mode which, in turn, further deflects the beam. It has proven to be the single most important current limiting instability in the ATA accelerator.[45] Techniques for its control, including careful cavity design and strong focusing are under investigation. SAIC has developed a numerical code, BBUSH, which tracks a beam through an arbitrary configuration of gaps and transport lines. It was used in our analysis of the effect of sextupole windings on stabilization of the bbu.[46]

The Spiral Line Induction Accelerator was favorably reviewed by the JASON committee in June 1986 and was very highly rated for Navy and other applications in the extensive, DARPA/Services sponsored review, the Net Technical Assessment of the Tactical Applications of Relativistic Charged Particle Beam Weapons, conducted during 1986-87.

The remainder of this report provides technical details on the work performed at SAIC under ONR support. Three main sections, on beam equilibria and matching, on beam stability and on the Spiral Line Induction Accelerator follow. Each section includes a discussion of work performed and summarizes our results. Some details are given in Appendices: Appendix A includes reprints of published papers, Appendix B is a list of conference presentations and Appendix C is a list of brief description of computer codes written in the course of this work. A final section gives our conclusions and recommendations.

2.0 TECHNICAL ACCOMPLISHMENTS

This section describes the technical work done with ONR support on the physics and design issues affecting high current electron accelerators using stellarator focusing. Two broad areas are discussed: beam equilibria and matching (Section 2.1), and beam stability (Section 2.2). A third section (2.3) describes how our studies of these issues led to the proposal of the Spiral Line Induction Accelerator, now presently under assessment for Naval tactical requirements. Each section and subsection contains a summary of our approach to a problem and our main results and conclusions. Some details are provided in Appendices.

2.1 Beam Equilibria and Matching

In a periodic, strong focusing transport system a matched beam is defined as one whose macroscopic properties (beam radii and orientation) repeat with the period of the focusing system; matched beams are typically defined to be monoenergetic. While never precisely realized in practice, the nature of a matched solution for a particular focusing system is important to know so that the dependence of the beam size on its current, energy emittance and on the applied focusing strength can be estimated. One would also like to know the form of the matched solution so that a beam may be prepared, as much as is practical, in a matched state before launching into the transport system.

2.1.1 Self-Consistent Treatment of Space Charge

For a continuously twisted quadrupole, with no added longitudinal field, Gluckstern[34] has described K-V type equilibria; the form of these equilibria when a longitudinal field is present has been worked out by Chernin.[35] The approach is to identify constants of motion for the single particle equations of motion, assuming a uniformly populated, elliptical beam and then to find a function of these constants–a solution of Vlasov's equation–which reproduces the uniform beam. The correct function of constants of motion turns out to be a delta function of a particular argument, in close analogy to the distribution function used by Kapchinsky and Vladimirsky[32] in their now classic work. Once the distribution function is found, it is straightforward to calculate beam radii as functions of system parameters, assuming certain emittances, or phase-space areas, are known. For non-zero current the functions are implicit, due to the dependence of the single particle betatron frequencies on the current; a numerical technique to solve for the equilibrium beam radii as functions of various system parameters was developed. Details of the calculation with numerical examples, are given in the paper of reference (36), included in Appendix A.

In order to study the behavior of beams away from equilibrium, it is necessary to have a formalism which describes a beam in coupled focusing systems, like the stellarator. It is possible to formulate a general envelope equation for a coupled system, including space

6

charge for a uniform beam by using the notion of rms quantities. This was carried out during the present program and is described in the following section. A full accounting is given in reference (36).

2.1.2 General Formulation of the Envelope Equation

When the two transverse degrees of freedom, x and y, of particle motion are linearly coupled, the K-V envelope equations no longer apply to the beam. In some simple cases, like solenoid focusing, it is possible to transform to a rotating frame (e.g. the Larmor frame) in which the single particle equations of motion decouple, but in general the problem is most directly treated, and interpreted, in the laboratory frame.

The derivation of the appropriate envelope equation for coupled systems proceeds in a different manner than the classic derivations of the K-V equations.[32,47] One begins with the paraxial single particle equations of motion, written as

$$v'(s) = M(s)v(s) \qquad (2-1)$$

where $v(s)$ is a 4×1 column vector with elements (x, x', y, y') and $M(s)$ is a 4×4 matrix describing the focusing system; s is the path length variable and a prime mark denotes d/ds. If the beam cross section is a uniformly filled ellipse, then the space charge electrostatic and magnetostatic forces are linear and a space charge term may be included in $M(s)$; the form of this term is given in reference (36).

In the paraxial approximation, all particles in a monoenergetic beam have the same value of longitudinal velocity, $\dot{s}$, therefore all particles in a particular "slice" of the beam remain in that slice. To proceed to an envelope equation which describes the evolution of the rms size of a slice as it propagates through a transport system, one defines the quantities

$$\Sigma_{ij}(s) \equiv\, <v_i(s)v_j(s)> -\, <v_i(s)><v_j(s)> \qquad (2-2)$$

for $i, j = 1, 2, 3, 4$ where the angle brackets denote an average over particles in a slice. The beam covariance matrix Σ satisfies

$$\Sigma'(s) = M(s)\Sigma(s) + (M(s)\Sigma(s))^T \qquad (2-3)$$

by virtue of Eq. (2-1); in Eq. (2-3), ^{T} denotes transpose. Equation (2-3) is the generalization of the K-V envelope equations, the purely spatial components Σ_{11}, Σ_{33}, and $\Sigma_{13} = \Sigma_{31}$ defining the axes and orientation of the rms beam ellipse. Given an initial value for the beam matrix, Eq. (2-3) allows it to be calculated at any point downstream from the

7

launching point. In practice such an initial value may be easily calculated by an electron gun code, at the entrance to the transport system, for example.

To recover the K-V envelope equations for decoupled 2×2 systems, we begin by noting that M and Σ are of 2×2 block diagonal form for decoupled systems, assuming $\Sigma(0)$ is. Defining $\sigma_{xx} \equiv \Sigma_{11}$, $\sigma_{x'x'} \equiv \Sigma_{22}$, and $\sigma_{xx'} \equiv \Sigma_{12} = \Sigma_{21}$ the equations for the x-coordinate may be written out using Eq. (2-3) as:

$$\sigma'_{xx} = 2\sigma_{xx'} \tag{2-4}$$

$$\sigma'_{xx'} = \sigma_{x'x'} + (-k_x^2 + \tilde{I}q_{xx})\sigma_{xx} \tag{2-5}$$

$$\sigma'_{x'x'} = 2(-k_x^2 + \tilde{I}q_{xx})\sigma_{xx'} \tag{2-6}$$

where $k_x^2 \equiv -M_{21}$ contains the external focusing strength, $\tilde{I} \equiv \nu/(\beta^2\gamma^3)$, $\nu = $ Budker's parameter, and

$$q_{xx} \equiv \frac{1}{\sigma_{xx}^{1/2}(\sigma_{xx}^{1/2} + \sigma_{yy}^{1/2})} \quad . \tag{2-7}$$

(The space charge term, derived in reference (36), has been included in Eqs. (2-4, 5, 6).) Equations (2-4)-(2-6) are coupled non-linear equations but they do admit a simple constant of motion, the un-normalized emittance ϵ_x defined by

$$\epsilon_x^2 = 16[\sigma_{xx}\sigma_{x'x'} - \sigma_{xx'}^2] \quad . \tag{2-8}$$

Using Eq. (2-4) to eliminate $\sigma_{xx'}$ and Eq. (2-8) to eliminate $\sigma_{x'x'}$ one may find a single equation for σ_{xx}. If we define

$$r_x \equiv 2\sigma_{xx}^{1/2} \quad , \tag{2-9}$$

the factor 2 arising from the relation between a radius and an rms radius of an ellipse, the resulting equation for r_x is

$$r_x'' + k_x^2 r_x - \frac{4\tilde{I}}{r_x + r_y} - \frac{\epsilon_x^2}{r_x^3} = 0 \tag{2-10}$$

which, along with the analogous equation for r_y, are the K-V envelope equations.

When coupling between x and y motion is present, it is necessary in general to integrate Eq. (2-3) numerically. A computer program, XYENV, has been written for this purpose. The program allows a completely general specification of the paraxial fields as functions

8

of axial distance. It has been used to study the envelope oscillations in the stellatron and beam matching problems in the SLIA. As an example of the latter, we consider the behavior of a beam, initially matched in a uniform solenoid, as it propagates into a stellarator field.

Figure 2-1 shows plots of the major and minor beam radii versus distance (z) along the system for different values of beam current. The beam starts out at $z = -20$ cm matched in a 2.98 kG longitudinal field; this value is chosen so that the 1 MeV beam has a 20 cm Larmor wavelength. The beam emittance is taken to be $\epsilon_n = 0.3I_{kA}^{1/2}$, except for the zero current case for which we have taken $\epsilon = 0.1$ rad-cm. A stellarator field with on-axis gradient of 500 G/cm and period 9 cm is slowly turned on using a "tanh" function, in such a way that Maxwell's equations are always satisfied in linear order; at $z = 0$ the stellarator field has reached half strength. One sees in the figure the development of oscillations in the major and minor beam radii; the amplitude of the oscillations is seen to be fairly insensitive to beam current in this example. In other cases one finds that certain modes of envelope oscillation are linearly unstable, leading to large oscillation amplitudes. This situation is analyzed in reference (36). (See Appendix A.)

2.1.3 Beam Matching: The SPIRAL Code

As mentioned earlier, special equilibria exist called matched solutions in which macroscopic properties repeat periodically with the period of the focusing system. For an actual – as opposed to ideal – magnetic field system, there exist coil windings which include feeds and coil terminations as well as winding errors and physical winding constraints. To design a magnetic focusing system with these limitations that is matched to the desired beam properties of a device requires certain numerical capabilities. Many of these capabilities exist in the code SPIRAL.

The SPIRAL code has been developed and is used as a magnetic field coil design tool. It computes the magnetic focusing fields from actual coil geometries, including feeds and terminations. SPIRAL is a fully three-dimensional code which calculates the magnetic fields using a Boit-Savart solver and has the capability to track single-particle trajectories through magnetostatic fields. The code has many diagnostics, one being the ability to map out the magnetic field structure in several ways, and another being the ability to track the evolution of beam emittance and particle phase-space through a device. SPIRAL can also initiate several distribution functions, including the K-V distribution as well as a simple uniform beam distribution with specified emittance and divergence.

As an example, consider the focusing system in the SLIA experiment in which a beam is to be matched from a diode source, through a compression region and into a combination solenoid/stellarator transport section (see Fig. 2-2). The stellarator in this system is an $\ell = 2$ (quadrupole) winding. Since the stellarator fields are to be turned either on or off

Beam Matching from Solenoid to Stellarator Field
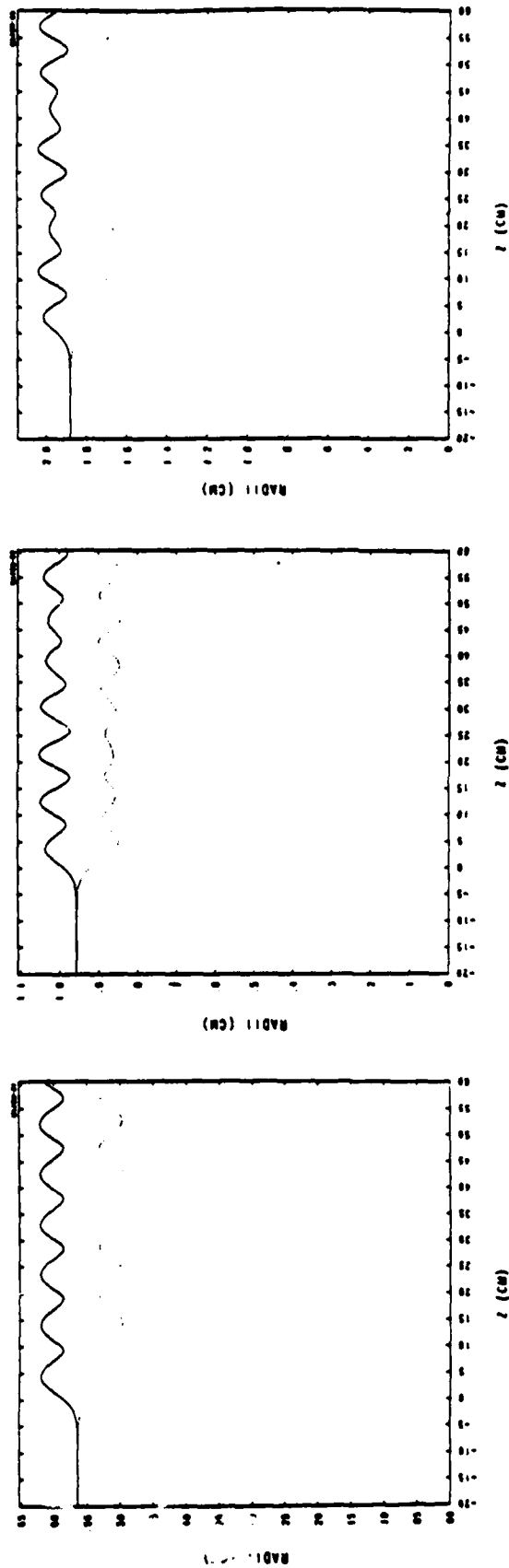
$I = 40 \text{ kA}$

$\epsilon = 0.68$ rad-cm

$I = 5 \text{ kA}$

$\epsilon = 0.24$ rad-cm

$I = 0$

$\epsilon = 0.1$ rad-cm

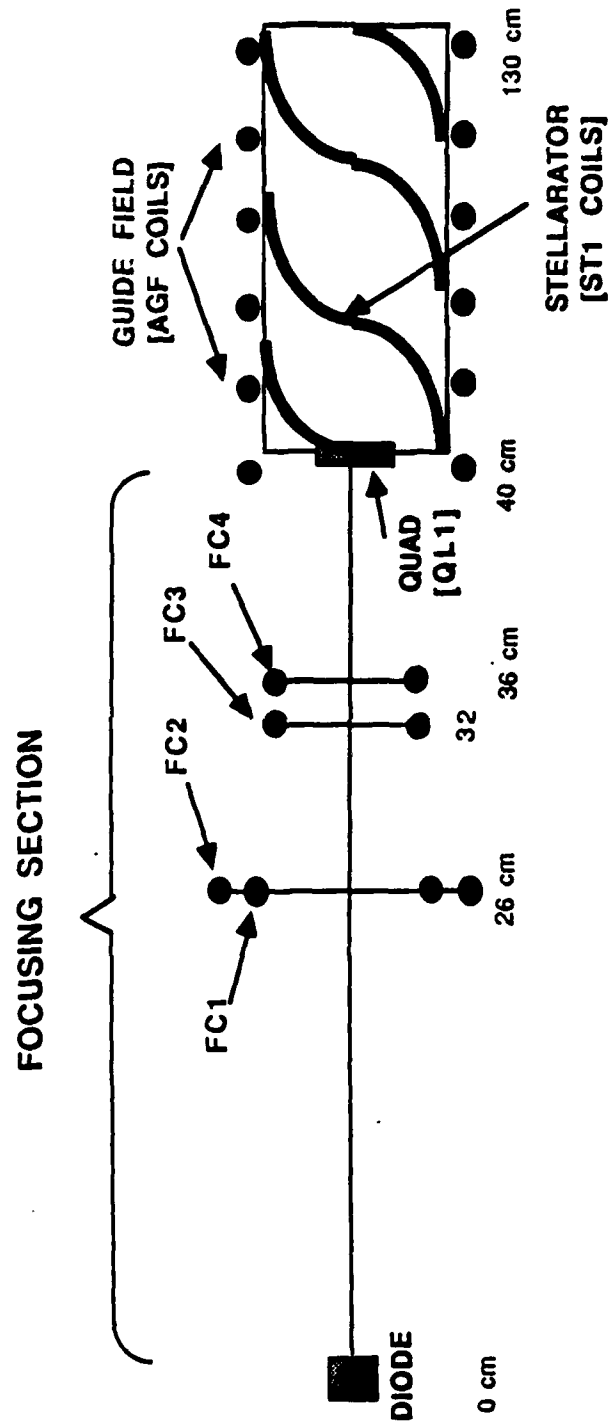Figure 2-1 Beam radii versus distance for different beam currents.

Figure 2-2 Magnetic field system configuration.

in the SLIA, the system was designed such that the compression region was to match the beam (energy 0.6 MeV and current 800 A) into the solenoidal field only. The stellarator fields and any compensation magnets must work independently and provide minimal beam disruption. In addition, it is desired that the stellarator coils begin at roughly the same axial position as the solenoidal windings.

Using SPIRAL, it was found that shifting the stellarator windings to begin about 8.2 cm further down axially and putting a discrete quadrupole magnet centered at the opening of the stellarator coils at a relative angle of 45° (see Table 2-1) provided a reasonable match with minimal beam disturbance. Plots of the longitudinal single-particle trajectories are shown in Fig. 2-3 for the compression/solenoidal configuration with and without the stellarator fields. Also, Fig. 2-4 shows the transverse beam emittance for the same two cases. It can be seen from the plots that the quadruople compensation coil and stellarator coil placement provide minimum disruption of the beam as compared with the compression/solenoidal system alone.

2.2 Beam Stability

Three fundamental types of stability have been investigated for the stellatron configuration: single particle stability, envelope stability and collective stability. The basic stability criterion for single particle motion in a linear, error-free stellarator field was given in reference 29; two pass-bands and two stop-bands were found to exist in the parameter space describing the focusing system. The derivation in reference 29 includes the dc space charge effect of a uniform, round beam. In the sections which follow we will assume that the fundamental stability criteria are satisfied and go on to discuss the types of instability which can still occur under these conditions.

2.2.1 Orbital Resonances

Simple considerations balancing external focusing forces against the defocusing effects of space charge lead to very large estimates for the limiting current in cyclic accelerators. Much more stringent limits become apparent, however, when constraints on beam stability are investigated. One interesting potential source of instability is the resonant excitation of betatron oscillations due to field and focusing errors. When extra focusing fields are added to the basic weak focusing betatron field, the possibilities for exciting disruptive orbital resonances may become quite numerous. Avoidance of certain dangerous resonances is essential for beam confinement. Since the betatron frequencies are in general dependent both on beam energy and current, avoidance of resonances places definite limits on these accelerator parameters.[48]

When field errors are present, a particle in a stellatron is subject to a periodic perturbation of its orbit as it travels around the device. If the period of the perturbation is

10

Longitudinal Trajectories
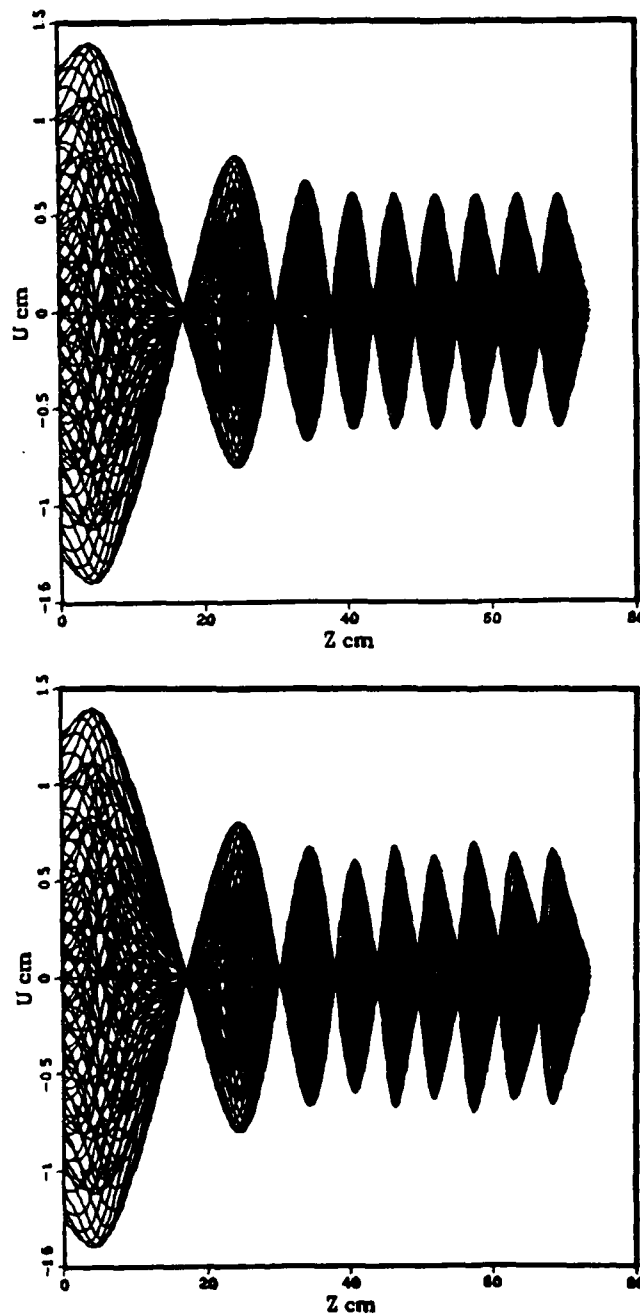
Figure 2-3 Longitudinal phase-space plots of u vs. z for the compression/solenoidal coil system of Table 2-1. a) Without, and b) with the quadrupole/stellarator coils.

Table 2-1
Magnetic Field Coil Data

MAGNETIC FIELD COIL DATA

Focusing Coil: Single-ring coils at axial position z, radius r, and current I

> **FC1:** $z = 22$ cm, $r = 22$ cm, and $I = 86,000$ amp-turns.
> **FC2:** $z = 22$ cm, $r = 26$ cm, and $I = $ -80,000 amp-turns.
> **FC3:** $z = 5$ cm, $r = 5$ cm, and I -6,200 amp-turns.
> **FC4:** $z = 26$ cm, $r = 5$ cm, and $I = $ -7,200 amp-turns.

AGF - Axial Guide Field Coils: Two stacks of 62 single-ring coils beginning at axial position $z = 33.64$ cm and ending at $z = 138.37$ cm. Inner coil set at $r = 4.585$ cm and outer set at $r = 5.518$ cm, both sets carrying current of $I = 1934.4$ amps.

Stellarator Coils: The stellarator coil set consists of two sets of $l = 2$ helical quadrupole coils, each consisting of two wires spread at an angle α, carrying current I. The quadrupole set begins at axial position z and continues with a pitch length of 18 cm with a total length L, and beginning at a relative angle α_r with respect to a transverse axis. All coils have radius $r = 4.154$ cm and current $I = 3457$ amps.

> **ST1:** $z = 41.416$ cm, $L = 85.462$ cm, $\alpha_r = 45.38°$, $\alpha_s = 4.660°$.
> $z = 41.812$ cm, $L = 84.670$ cm, $\alpha_r = 53.30°$, $\alpha_s = 15°$.

Quadrupole Lenses: The quadrupole lens is defined by an axial beginning position z, an axial length L, a transverse magnetic field gradient strength B', and a relative angle to the stellarator coil sets which is $\theta = 45°$.

> **QL1:** $z = 40.614$ cm, $L = 2$ cm, $B' = 340$ G/m.
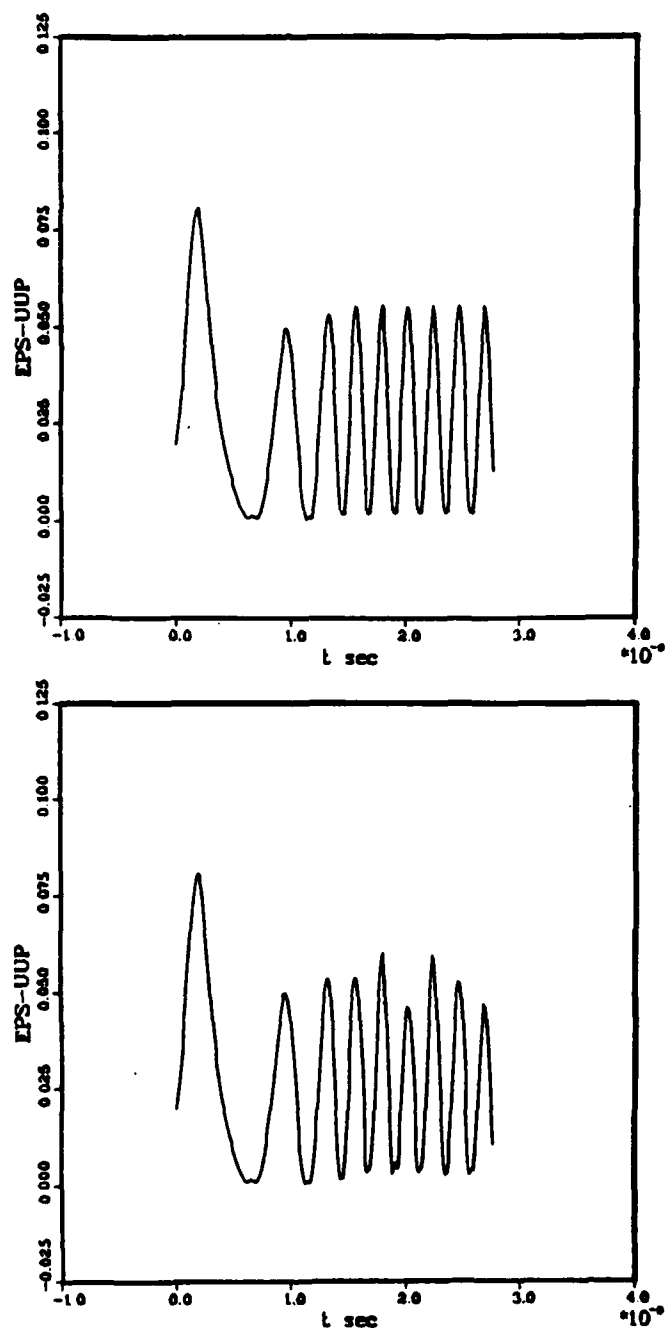
Figure 2-4 RMS emittance plots of $\epsilon_{uu'}$ vs. t for the compression/solenoidal coil system of Table 2-1. a) Without, and b) with the quadrupole/stellarator coils.

not equal or nearly equal to a period of one of the four modes of betatron oscillation, then the resulting driven oscillation remains of finite, usually tolerable amplitude; on the other hand, if there is equality or near equality between the periods of the driving force and a natural betatron mode, transverse oscillation amplitudes can be driven to large values and particles can be lost to the walls or beam emittances can grow intolerably.

It is a fairly simple matter to design a modified betatron or stellatron so that the tunes are away from dangerous integer and half-integer values for low current beams. The dependence of the tunes on current leads to limits on the current, in the usual way, but the functional dependence of the tunes on current is not simple. For example, in the case where only vertical and toroidal fields are present, the fast cyclotron mode tune decreases with increasing current, whereas, the slow drift mode tune *may* increase with current, depending on parameters. For typical designs, the fast mode tune is actually only weakly dependent on current while the slow mode tune, while more sensitive to current, is so slow ($\ll 1$) for all anticipated currents that it is never near a dangerous resonant value, at least when the toroidal field is large.

The most basic resonance is the dipole resonance which occurs when a particle executes an integer number of betatron oscillations around the machine. If this integer is large, the resonance is usually not dangerous and is easily passed through during acceleration. (Experimental evidence of this fact has been reported by the Irvine group.) At low energies the ratio of toroidal to vertical field is usually large and the resonances encountered tend to be of high order. As acceleration proceeds, however, the field ratio can drop to $O(1)$ or less and the more dangerous low number resonances are crossed.

If we include the most general field and focusing errors allowed by Maxwell's equations the equations for the betatron oscillations in the stellatron become

$$(1 + \Delta_1)x'' + \left[\frac{1}{2} + \mu\cos m\theta - \delta + \epsilon_{zo} + \epsilon_{zx}\right]x =$$
$$- \left[\mu\sin m\theta + \epsilon_{zy}\right]y + (b + \epsilon_{\theta o})y' + \Delta_1 - \epsilon_{zo} \qquad (2-11)$$

$$(1 + \Delta_1)y'' + \left[\frac{1}{2} - \mu\cos m\theta + \delta - \epsilon_{zx}\right]y =$$
$$- \left[\mu\sin m\theta + \epsilon_{zy} + \epsilon'_{\theta o}\right]x - (b + \epsilon_{\theta o})x' + \epsilon_{ro} \qquad (2-12)$$

where Δ_1 is the momentum error, μ is a dimensionless quadrupole strength, m is the number of field periods around the device and b is the ratio $B_{\theta o}/B_{zo}$. ϵ_{zo}, ϵ_{zx}, ϵ_{zy}, $\epsilon_{\theta o}$, and ϵ_{ro} are five arbitrary, but presumed small, periodic functions of θ (period 2π)

11

representing errors in B_z, $\partial B_z/\partial r$, $\partial B_z/\partial z$, B_θ, and B_r respectively, and where we have written $n = \frac{1}{2} + \delta$. If we assume that an error term (i.e., the ϵ's) behaves as $\sim \cos k\theta$ for some integer k and if we treat the ϵ's as infinitesimally small, then a perturbative treatment gives a resonance when any of the following conditions hold:

$$\frac{m}{2} \pm \nu_\pm = \pm k \qquad (2-13)$$

$$\left[\frac{m}{2} \pm \nu_\pm\right] \pm \left[\frac{m}{2} \pm \nu_\pm\right] = \pm k \qquad (2-14)$$

where the linear tunes $\nu_\pm$ are given by

$$\nu_\pm^2 = \hat{n} + \frac{1}{4}\hat{m}^2 \pm (\hat{n}\hat{m}^2 + \hat{\mu}^2)^{1/2} \qquad (2-15)$$

$$\hat{m} = m + b/(1 + \Delta_1) \qquad (2-16)$$

$$\hat{n} = \frac{1}{2}/(1 + \Delta_1) + \frac{b^2}{4}/(1 + \Delta_1)^2 \qquad (2-17)$$

$$\hat{\mu} = \mu/(1 + \Delta_1) \qquad (2-18)$$

and where all ($\pm$) signs in (2-13, 14) may be chosen independently. The tunes are real when the stability condition

$$\left|\hat{n} - \frac{1}{4}\hat{m}^2\right| > |\hat{\mu}| \qquad (2-19)$$

is satisfied. Clearly (2-13) represents integer resonances and (2-14) (a slight generalization of) half-integer resonances; (2-14) gives the location of the first stop-band for infinitesimal ϵ's while approximate locations of higher stop-bands involve additional terms of $\pm(m/2 \pm \nu_\pm)$.

When the error terms are of finite size (still small, but no longer infinitesimal) one employs Floquet's theorem to locate the stop- and pass-bands in a standard way.

We present results using Floquet's theorem below for three special cases; in all of these we will set $m = 12$ and $b = 10$.

Case 1: All ϵ's vanish, but $\delta \neq 0$. This case corresponds simply to introducing an asymmetry in the weak focusing field between radial and vertical directions ($n \neq \frac{1}{2}$). In Fig. 2-5 we show the stable and unstable regions of the $\mu - \delta$ plane. The resonance conditions $\nu_+ - \nu_- = m$, of type (2-14) with $k = 0$, occurs when $\mu = 59.75$. Unstable regions of the

12

plane are crossed with solid lines, contours of equal growth rates. (The finite resolution of the grid may miss some growth rate contours.) The five disjoint regions of instability have the following origin: The two regions adjacent to the δ-axis are the extensions into regions of finite μ of the usual ($\mu = 0$) betatron stability condition $0 < n < 1$. The regions adjacent to the line $\mu = 59.75$ is the resonance region where $\nu_+ - \nu_- \approx m$, and the band for $\mu > 95.5$ is the basic instability region where (2-19) is violated for our parameters.

On Fig. 2-5 two points have been labelled A and B in the stable and unstable regions, respectively. In Fig. 2-5A we show results of a particle orbit integration for a stellatron operated at point A; the orbit shown is the projection in the r-z plane. The orbit is clearly well behaved. In Fig. 2-5B we show results of a similar orbit integration for operation at B. The orbit is plotted versus time in Fig. 2-5C where we can see clearly the growth saturation, and turn-over of the oscillation amplitude due to nonlinearities. While the saturation amplitude is not small, this resonance does not seem to be destructive and only appears to couple energy back and forth between two oscillation modes, as in the modified betatron.[49]

Case 2: $\epsilon_{zo} = \epsilon \cos 3\theta$; all other errors vanish. This case considers a periodic error in the vertical field. We illustrate, in Fig. 2-6, the $\mu - \epsilon$ plane where two regions of instability are seen; there is the fundamental instability band where (2-19) is violated for $\mu > 95.5$ and a second band at $\mu \approx 89$ at which one finds the condition $\nu_+ - \nu_- = m + k$ is approximately satisfied; here $\nu_+ \approx 17$, $\nu_- \approx 2$, $m = 12$, $k = 3$. Results of particle orbit integrations at points A and B are given in Figs. 2-6A and 2-6B. In this case we must choose a rather small value of ϵ for our orbit integrations; otherwise the resulting energy error, represented by the inhomogeneous term of (2-11), causes an unacceptably large driven (but non-resonant) oscillation. (Recall that all the error terms in (2-11, 12) are normalized to the vertical field.) The only reason Fig. 2-6 includes such large ϵ values is so that the stop-band could be resolved by the mesh we used when applying the numerical stability test. Near the μ-axis, the stop-band is extremely narrow.

It is interesting to note that for $\mu \approx 81$ there is an integer resonance of the form (2-13), $m/2 - \nu_- = k$, ($\nu_- = k = 3$); since such a resonance is due to the *inhomogeneous* part of (2-11), it does not appear as an unstable band in Fig. 2-6 which, as with Fig. 2-5, is obtained by analysis of only the homogeneous part of (2-11, 12). An orbit integration (not illustrated) shows very strong disruption on this resonance, as expected of a low order integer resonance.

Case 3: $\epsilon_{\theta o} = \epsilon \cos 6\theta$; all other errors vanish. For our final case we consider a small periodic bumpiness in the toroidal field, as would be produced by discrete toroidal field coils. For this case, the stable and unstable regions of the $\mu - \epsilon$ plane are shown in Fig. 2-7. Here we see two unstable regions, the by-now-familiar band for $\mu > 95.5$, and a second
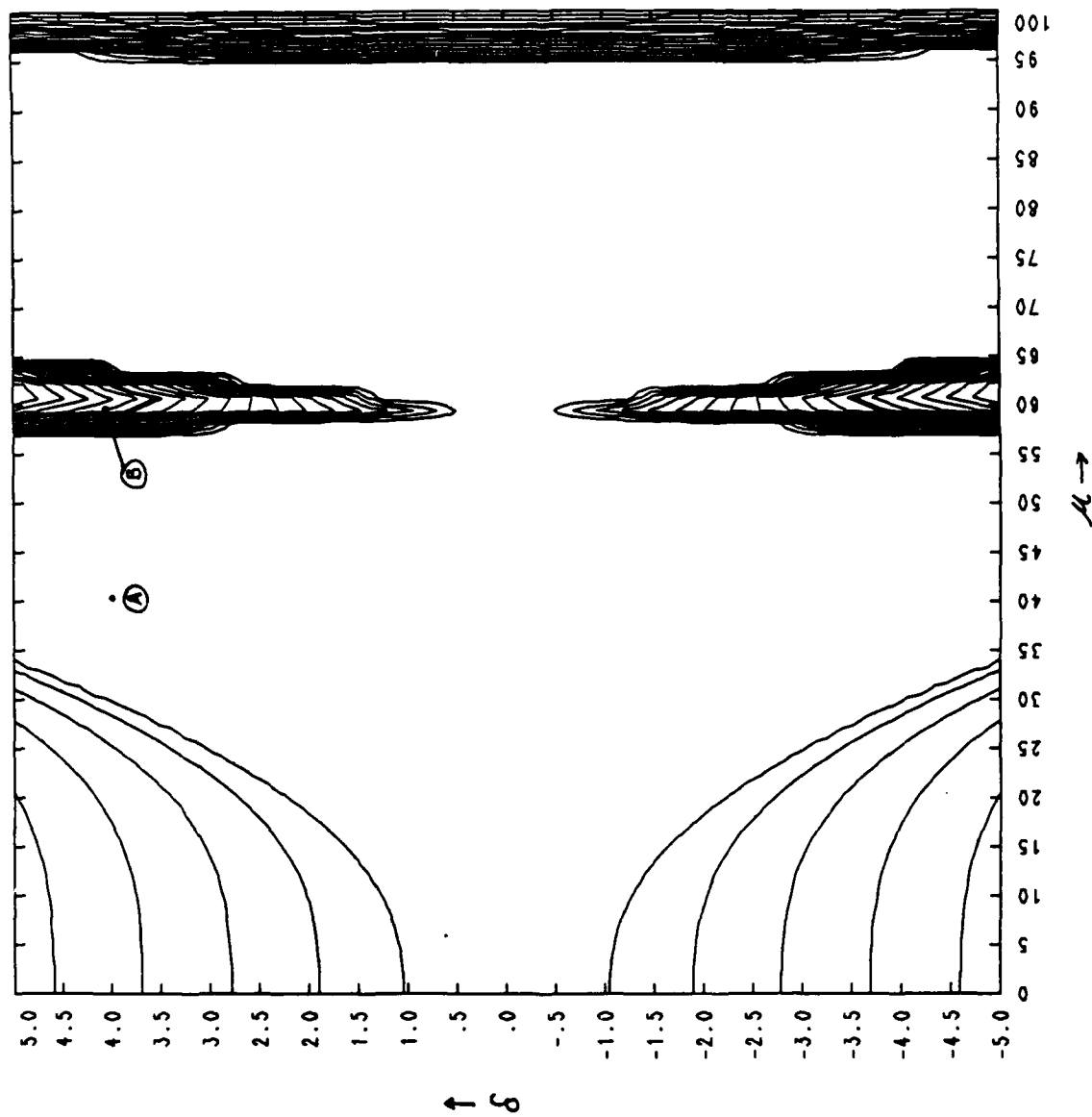
Figure 2-5 The $\mu - \delta$ plane for case 1. The contours are lines of constant growth rate. Points A and B refer to cases for which orbits are shown in Figures 1A and 1B respectively.

Figure 2-5A A particle orbit projection in the transverse plane, for parameters of Figure 1, point A. ($\mu = 40.$, $\delta = 4.$)

Figure 2-5B A particle orbit projection in the transverse plane, for parameters of Figure 2, point B. ($\mu = 59.75$, $\delta = 4$.)

Figure 2-5C Radial position versus time for the particle of Figure 1B. (A "turn" is the time for the particle to go once around the device.)

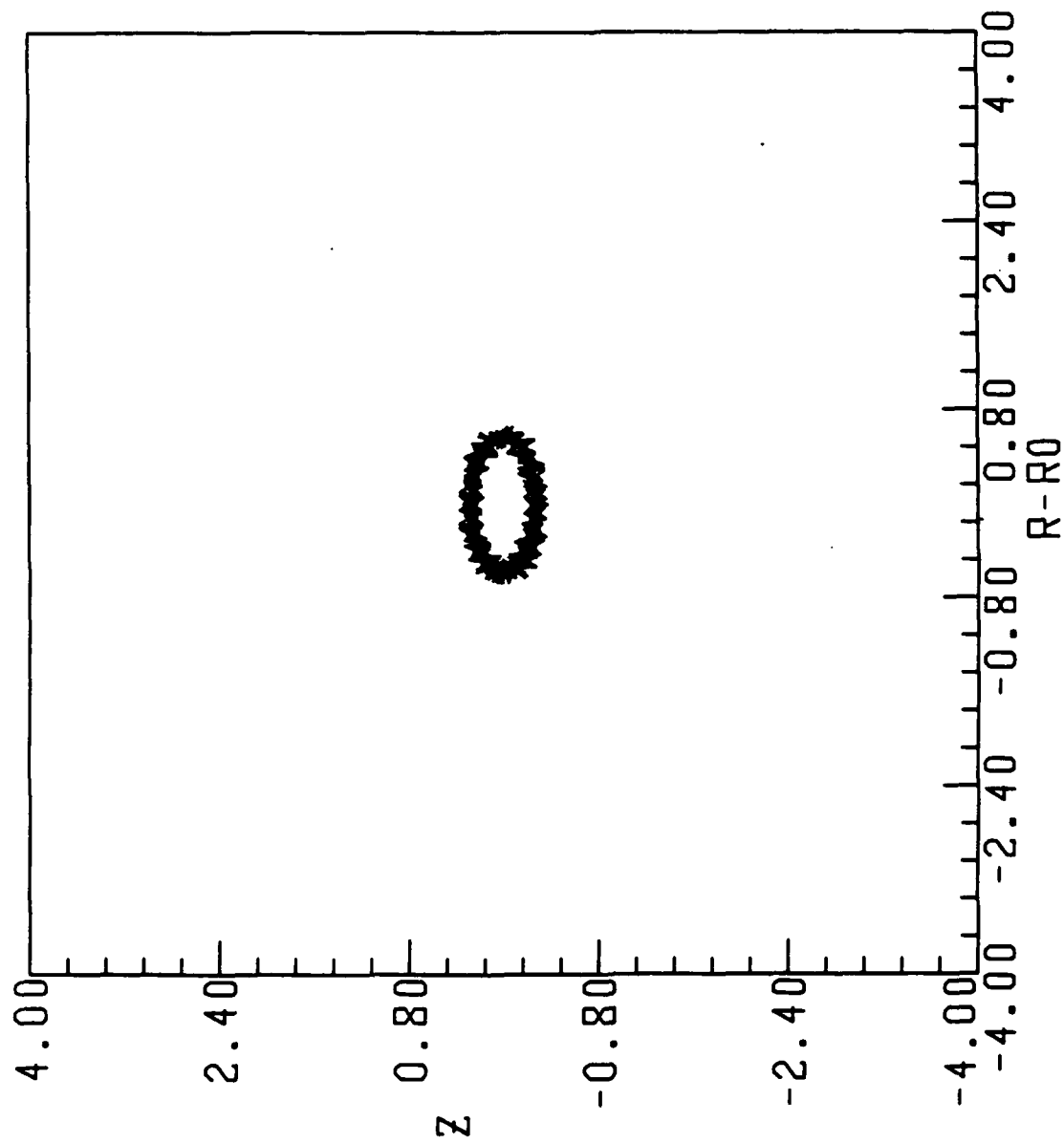Figure 2-6 The $\mu - \epsilon$ plane for case 2.

Figure 2-6A A particle orbit projection in the transverse plane, for parameters of Figure 2, point A. ($\mu = 75.$, $\epsilon = 0.04$)
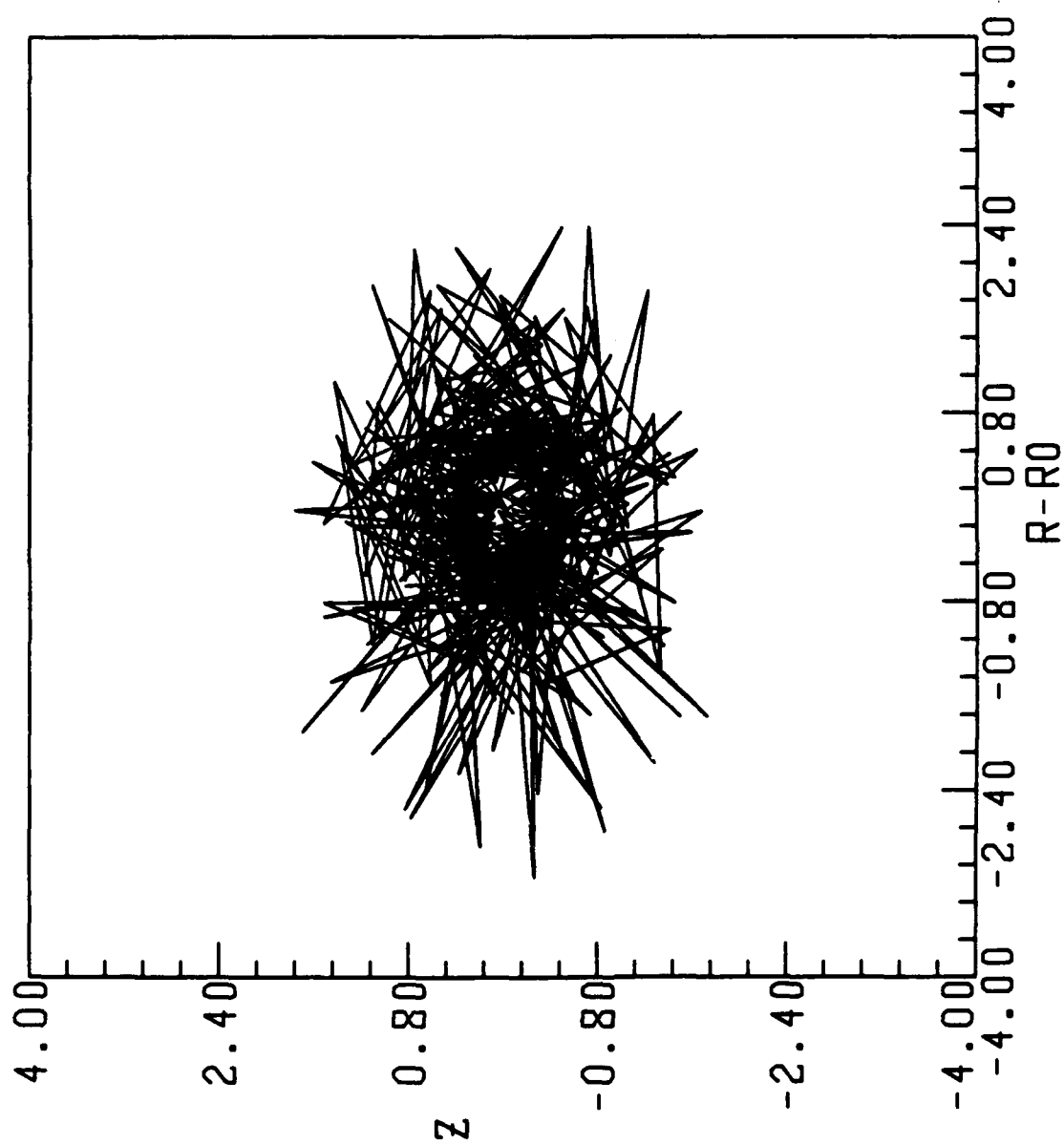
Figure 2-6B A particle orbit projection in the transverse plane, for parameters of Figure 2, point B. ($\mu = 89.$, $\epsilon = 0.04$)
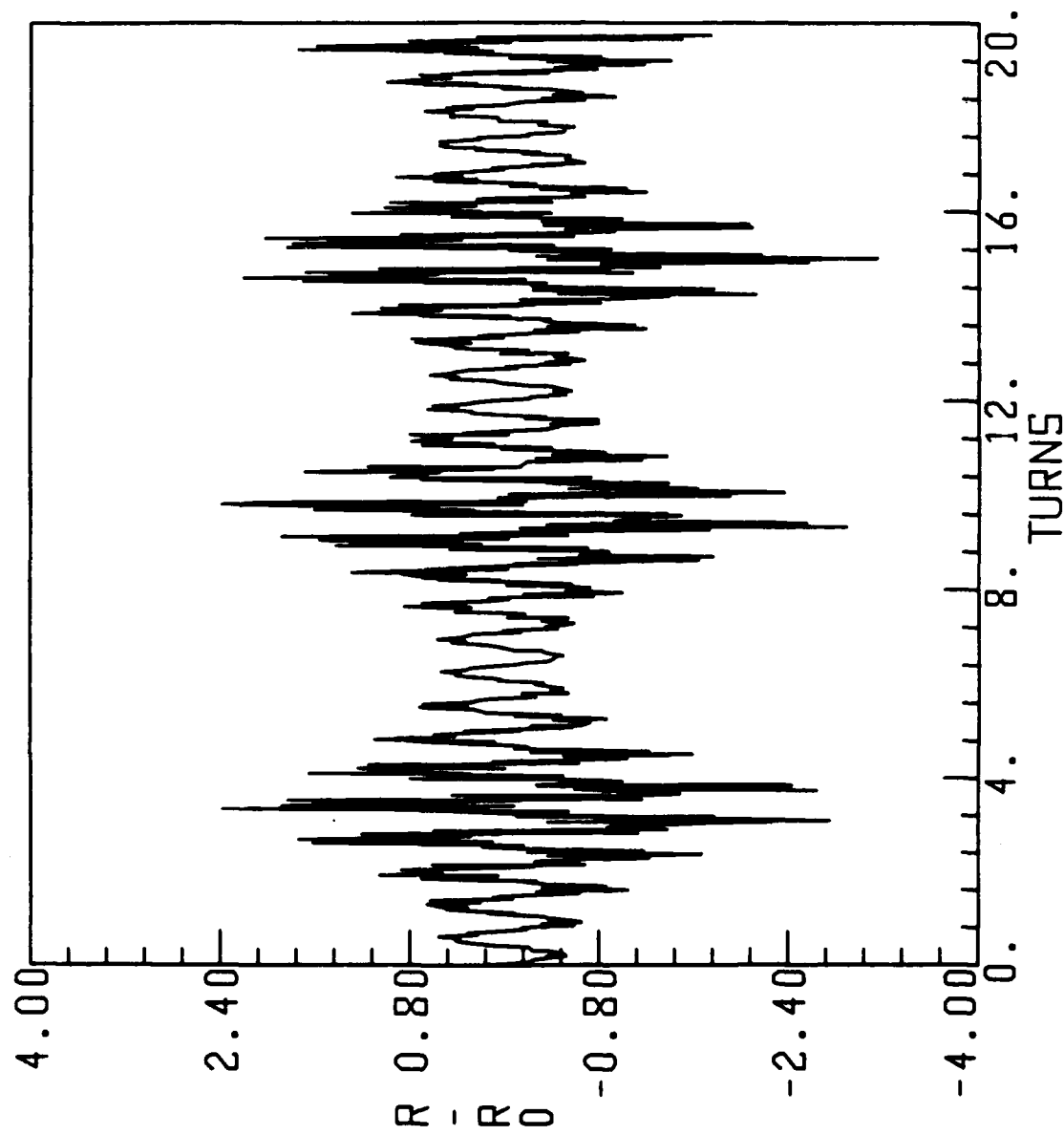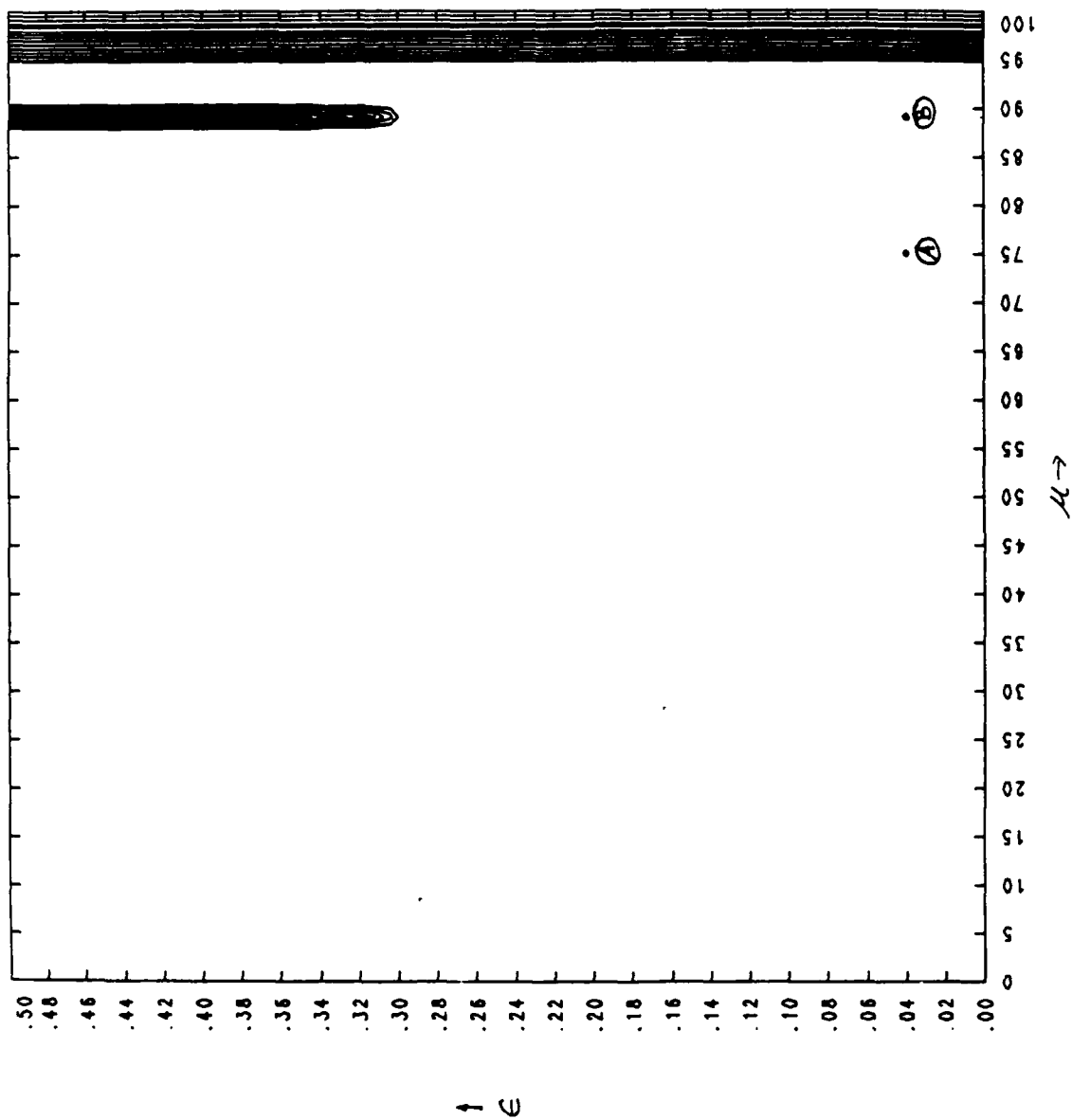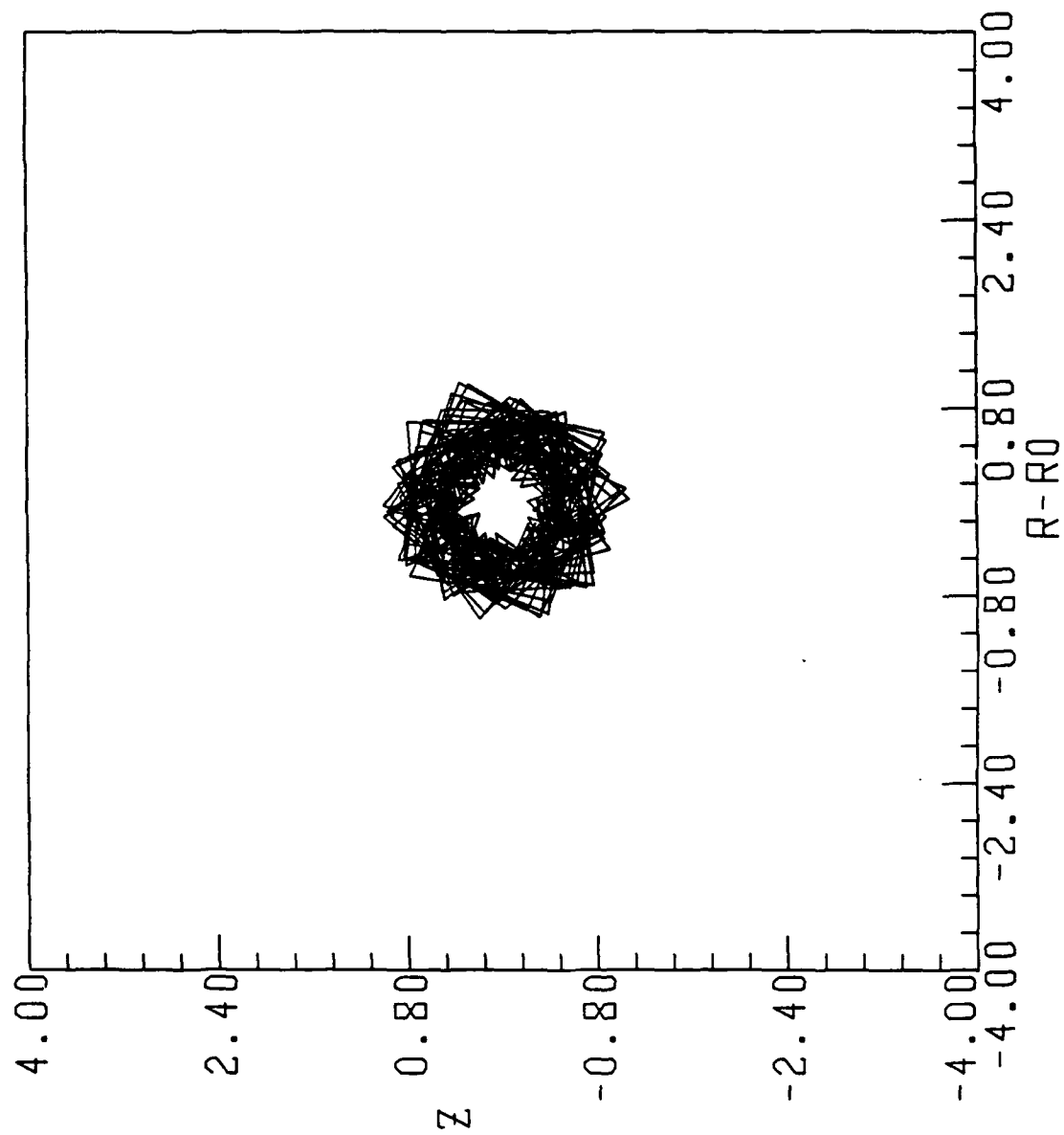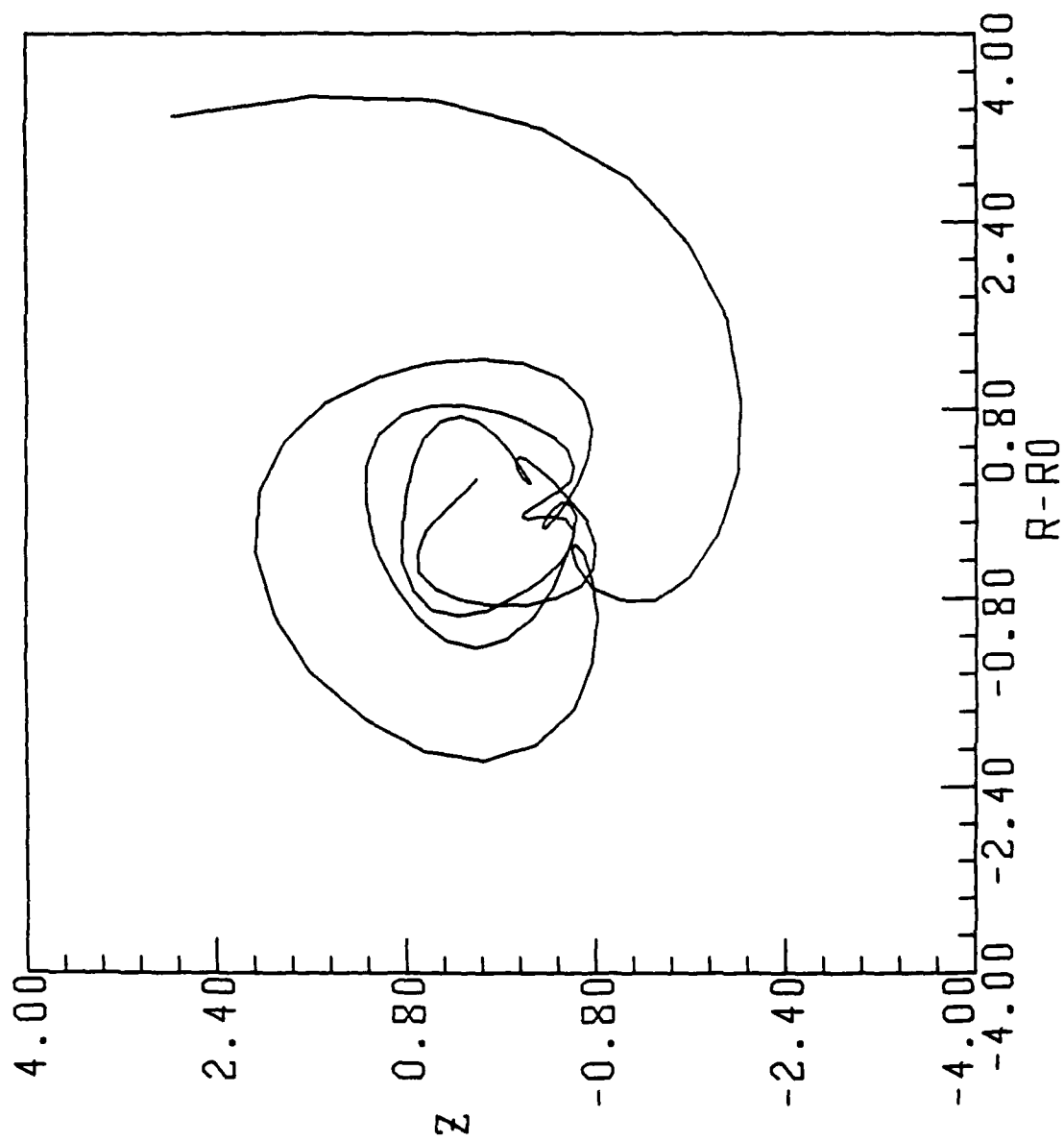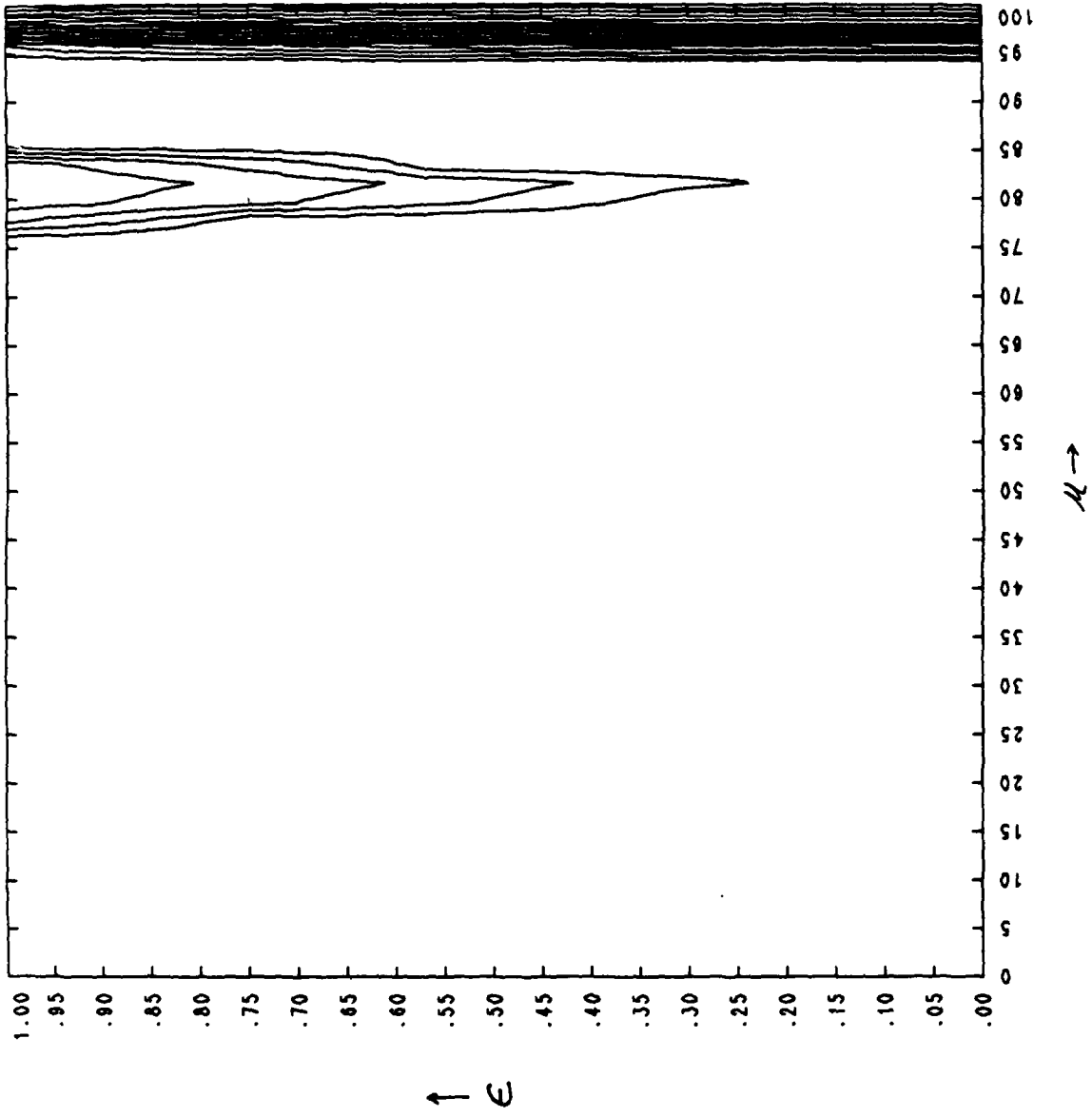
Figure 2-7 The $\mu - \epsilon$ plane for case 3.

near the point $\mu \approx 81$, where one finds that $\nu_- \approx 3$ and a condition of the form (2-14) is satisfied for $k = 6$. Again we have labelled points A and B in the stable and unstable regions; Figs. 2-7A and 2-7B, respectively, illustrate results of particle orbit integrations. In this case, the effects of non-linearities are insufficient to prevent the particle orbit from intersecting the pipe wall, located in this example 4 cm from the axis.

Many other examples could be given, of course; the above three cases were chosen only to illustrate some possibilities.

To give some feeling for the global resonance situation we show, in Fig. 2-8, the contours in the $\mu - b$ plane, for fixed m, on which certain of the conditions (2-13, 14) are satisfied. Clearly it is difficult if not impossible to avoid all resonances. The stellatron experiment at UC Irvine[8] has demonstrated, however, that many high order ($k > 20$) resonances may be passed through with virtually no beam disruption. Plots of the four single particle tunes versus time for a particular shot of the Irvine device are given in Fig. 2-9, clearly showing the crossing of integer values. A plot of beam current versus time for the shot is given in Fig. 2-10 from which one sees that the current is lost gradually, over the course of 50 μs during the second half of the shot, not in the abrupt manner typical of an integer resonance crossing. (An electron makes ≈ 115 revolutions around the device, per microsecond.) It may be, however, that while no single high order resonance is responsible for the current loss, the net effect of crossing many of them in rapid succession may be to induce a type of slow, diffusive particle loss. The above three cases, and other we have considered, support one's intuition that low order (small k) resonances will be more of a problem than large k resonances and may well limit the current and/or the energy attainable in modified-betatron type devices. .

When space charge is included in the calculation of the tunes, one finds that two tunes are decreased and two are increased by the effect of space charge. The tunes all depend on current through the combination current/b, from which we may draw the important conclusion that *the tunes are less sensitive to current the stronger is the toroidal field.* This is an important feature of the toroidal field and immediately suggests the use of a large toroidal field for control of the tune shifts for large currents. While this is correct in principle, a practical consideration may limit its application. Specifically, the toroidal field needs to be large at injection time when space charge effects are large; during subsequent acceleration, then b ($\equiv B_\theta / B_z$) must be kept fixed in order to keep the tunes fixed, that is, B_θ must be raised in direct proportion to the electron momentum. If B_θ starts out large, (initial fields of the order of 1 kG are typical in present experiments), practical limits to the final beam energy become clear. Also, a very large toroidal field will probably complicate the beam ejection problem at the end of the acceleration.
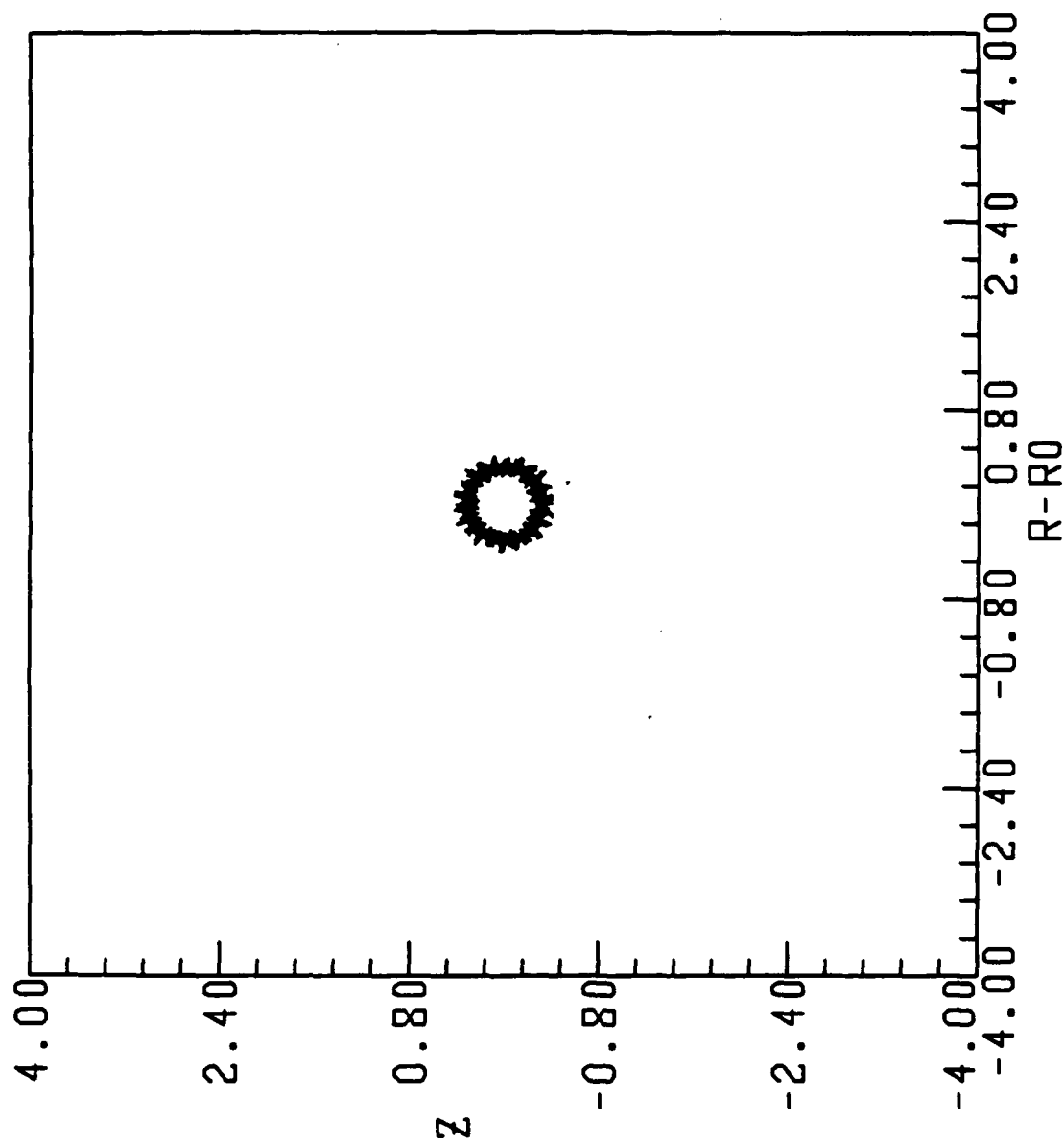
Figure 2-7A A particle orbit projection in the transverse plane, for parameters of Figure 3, point A. ($\mu = 40.$, $\epsilon = 0.75$)
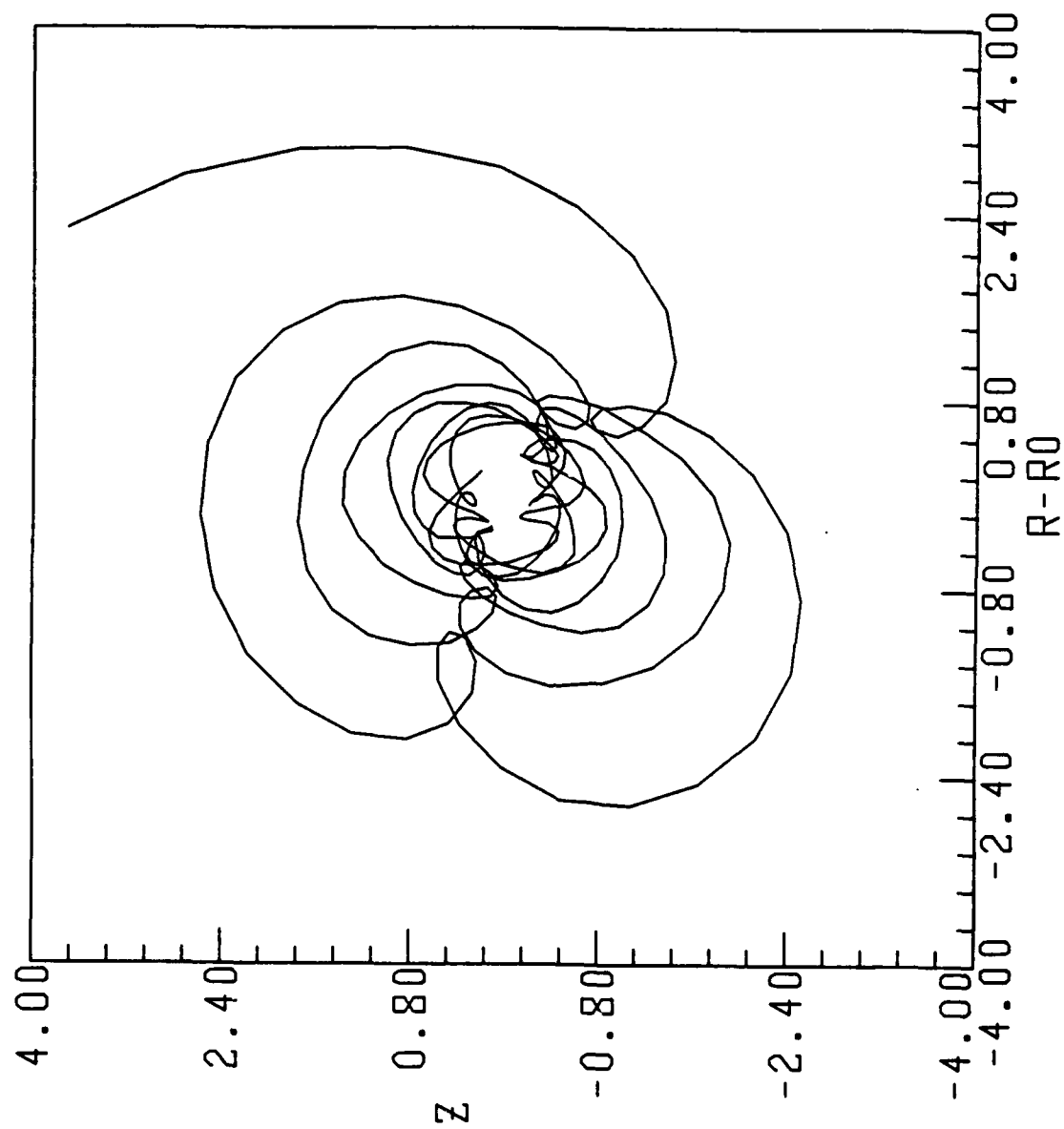
Figure 2-7B A particle orbit projection in the transverse plane, for parameters of Figure 3, point B. ($\mu = 59.75$, $\epsilon = 0.75$)
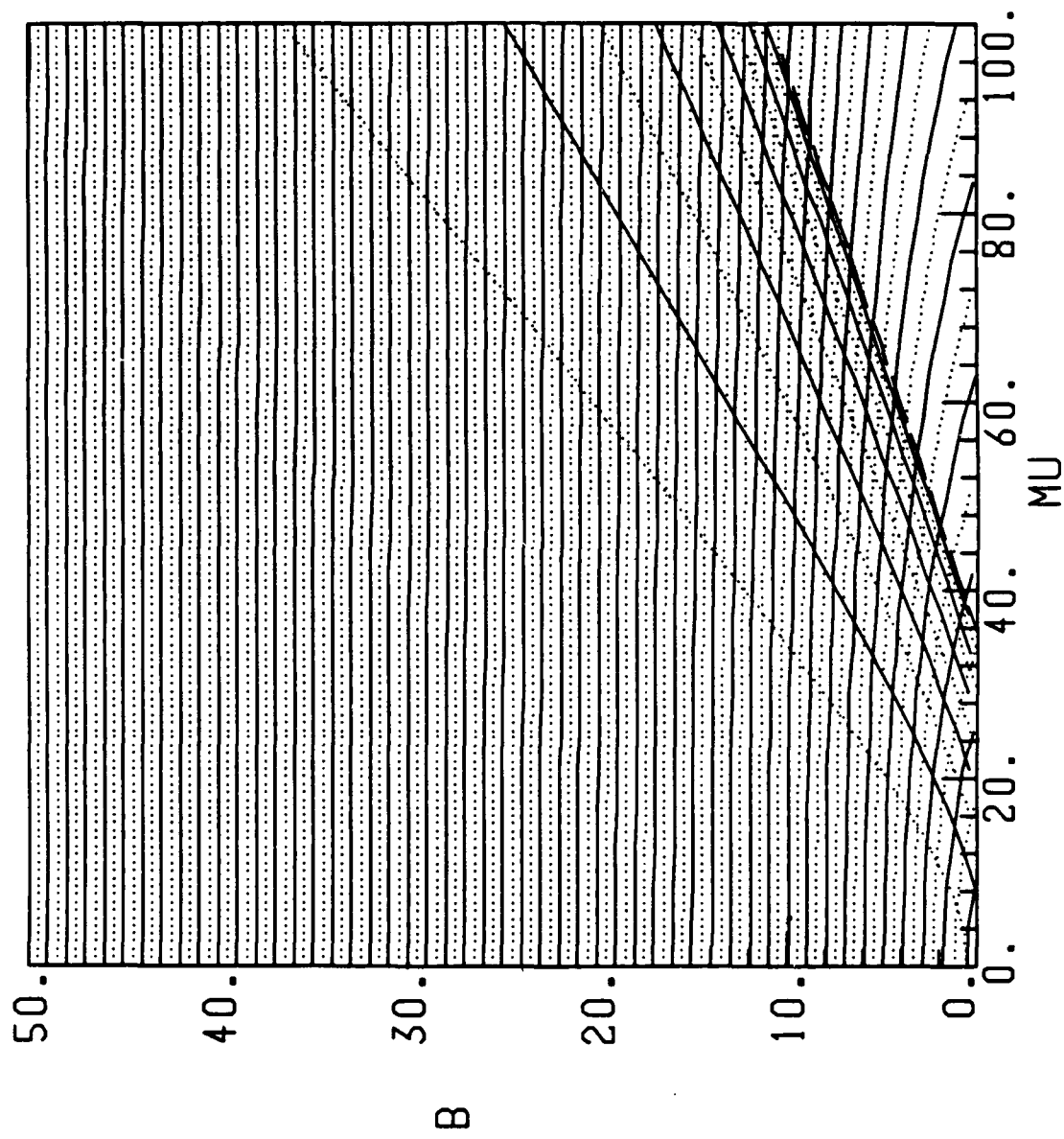
Figure 2-8 The $\mu - b$ plane for $m = 12$, showing contours on which resonance conditions (8a and 8b) are satisfied.
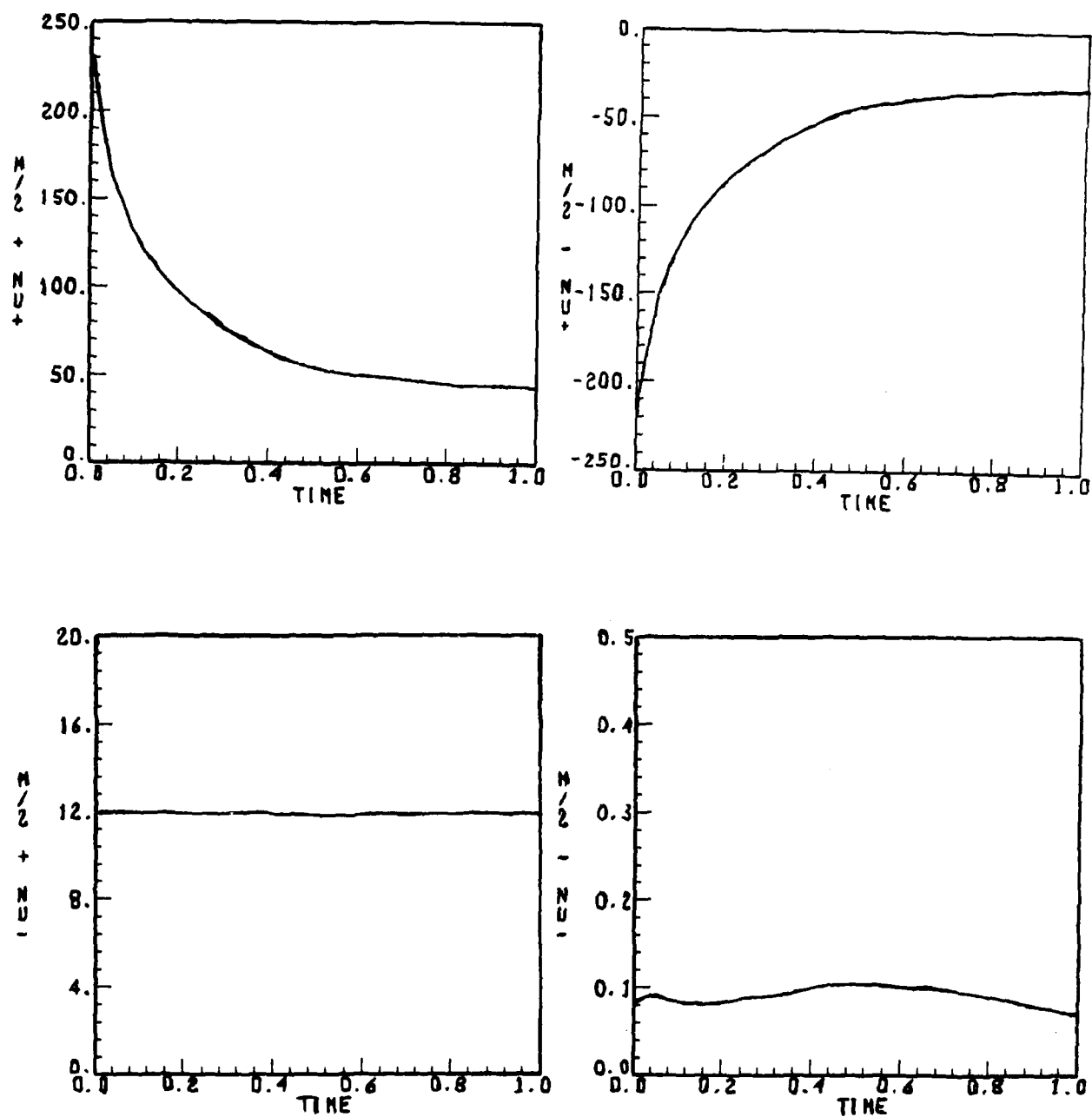
Figure 2-9 Tunes versus a dimensionless time for shot #36772 of the UC Irvine stella-
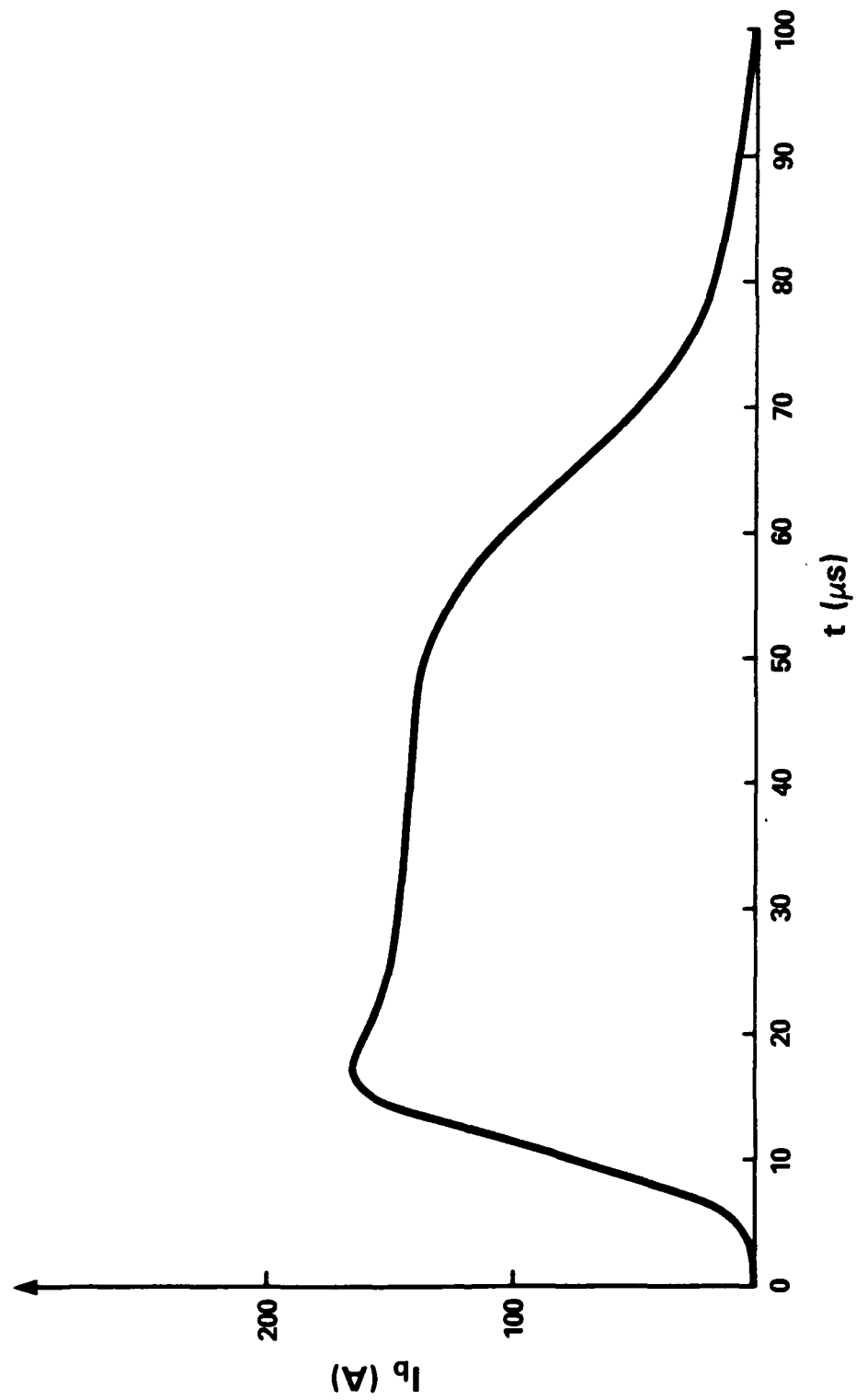tron; the time interval shown is $\approx 90 \ \mu s$.

Figure 2-10 Current versus time for shot #36772.

The resonances described so far are all consequences of *linear* field errors, that is, the single particle equations of motion are still linear in the transverse displacements x and y in the presence of the field errors. A much expanded class of resonances is possible if one considers the effect of non-linearities in the applied fields. A fully general treatment of non-linear resonances would be very complicated but a single interesting example was studied[50] and can be reported on here.

We consider the magnetic field due to four wires carrying current $(I, -I, I, -I)$ wound on a cylinder of radius r_o in a helix of period $2\pi/k$. To leading non-linear order the fields in cylindrical coordinates are

$$B_r(r, \ \theta - kz) \simeq B_o kr \sin 2(\theta - kz)\left[1 + \frac{2}{3}(kr)^2\right] \qquad (2-20)$$

$$B_\theta(r, \ \theta - kz) \simeq B_o kr \cos 2(\theta - kz)\left[1 + \frac{1}{3}(kr)^2\right] \qquad (2-21)$$

$$B_z(r, \ \theta - kz) \simeq -B_o(kr)^2 \cos 2(\theta - kz) \qquad (2-22)$$

where $B_o = 16(Ik/c) \ kr_o K_2'(2kr_o)$. In normalized cartesian coordinates, $2kx \to x$, $2ky \to y$, $2kz \to z$, and $2kct \to t$, the equations of motion are

$$\ddot{x} = \alpha\left\{\frac{1}{2}\dot{y}\left[(x^2 - y^2)\cos z + 2xy \sin z\right]\right.$$
$$\left. + \dot{z}\left[x\left(1 + \frac{1}{12}x^2 + \frac{1}{4}y^2\right)\cos z + y\left(1 + \frac{1}{6}y^2\right)\sin z\right]\right\} \qquad (2-23)$$

$$\ddot{y} = -\alpha\left\{\frac{1}{2}\dot{x}\left[(x^2 - y^2)\cos z + 2xy \sin z\right]\right.$$
$$\left. + \dot{z}\left[y\left(1 + \frac{1}{4}x^2 + \frac{1}{12}y^2\right)\cos z - x\left(1 + \frac{1}{6}x^2\right)\sin z\right]\right\} \qquad (2-24)$$

$$\ddot{z} = -\alpha\left\{\dot{x}\left[x\left(1 + \frac{1}{12}x^2 + \frac{1}{4}y^2\right)\cos z + y\left(1 + \frac{1}{6}y^2\right)\sin z\right]\right.$$
$$\left. - \dot{y}\left[y\left(1 + \frac{1}{4}x^2 + \frac{1}{12}y^2\right)\cos z - x\left(1 + \frac{1}{6}x^2\right)\sin z\right]\right\} \qquad (2-25)$$

where $\alpha = eB_o/4m\gamma kc^2$. These equations have a constant of motion, $P_z + kP_\theta$ where $P_{z,\theta}$ are canonical momenta:

$$\dot{y}x - y\dot{x} + 2\dot{z} + \alpha\left[(x^2 - y^2)\cos z + 2xy \sin z\right]\left[1 + \frac{1}{6}(x^2 + y^2)\right] = \text{constant} \ . \qquad (2-26)$$

15

The linear equations obtained from Eqs. (2-23, 24, 25) by neglecting all non-linear terms have solutions which oscillate in z with frequencies $\frac{1}{2} \pm k_\pm$ where

$$k_\pm = \left[\frac{1}{4} \pm (\alpha/\beta_z)\right]^{1/2} \qquad (2-27)$$

and where $\beta_z = \dot{z}/c$. The basic stability condition for these betatron oscillations is

$$\left|\frac{\alpha}{\beta_z}\right| < \frac{1}{4} \quad . \qquad (2-28)$$

If we return to the non-linear equations and treat the non-linearities perturbatively we see that a non-linear term like $x^3 \cos z$ will oscillate at frequencies $\frac{1}{2} + q$ and $\frac{5}{2} + q$ where q consists of a sum of three of $\pm k_\pm$. In particular, the $\frac{1}{2} + q$ term will be resonant if $q = k_+ - 2k_- = k_-$ or

$$k_+ = 3k_- \qquad (2-29)$$

which occurs when

$$\alpha/\beta_z = 0.2 \quad . \qquad (2-30)$$

Integration of the non-linear equations shows a dramatic instability, even for α/β_z close to 0.2. As an example, if we take $\gamma = 3$ this gives a resonant value for α of 0.1886. Figure 2-11 shows the results of a numerical integration of Eqs. (2-23, 24, 25) for $\alpha = 0.175$. The solution to the linear equations for this α is of course completely well behaved.

The presence of a longitudinal magnetic field, in addition to the twisted quadrupole, changes the values of $k_\pm$ and the stability condition but *not* the resonance condition (2-29). $k_\pm$ becomes

$$k_\pm^2 = \frac{1}{8}\left\{\alpha_z^2 + 2\alpha_z + 2 \pm [\alpha_z^2(\alpha_z + 2)^2 + 4\alpha_o^2]^{1/2}\right\} \qquad (2-31)$$

where

$$\alpha_z = -eB_z/(m\beta\gamma c^2 k) \qquad (2-32)$$

$$\alpha_o \equiv 4\alpha/\beta_z \qquad (2-33)$$

and the linear stability condition becomes

16
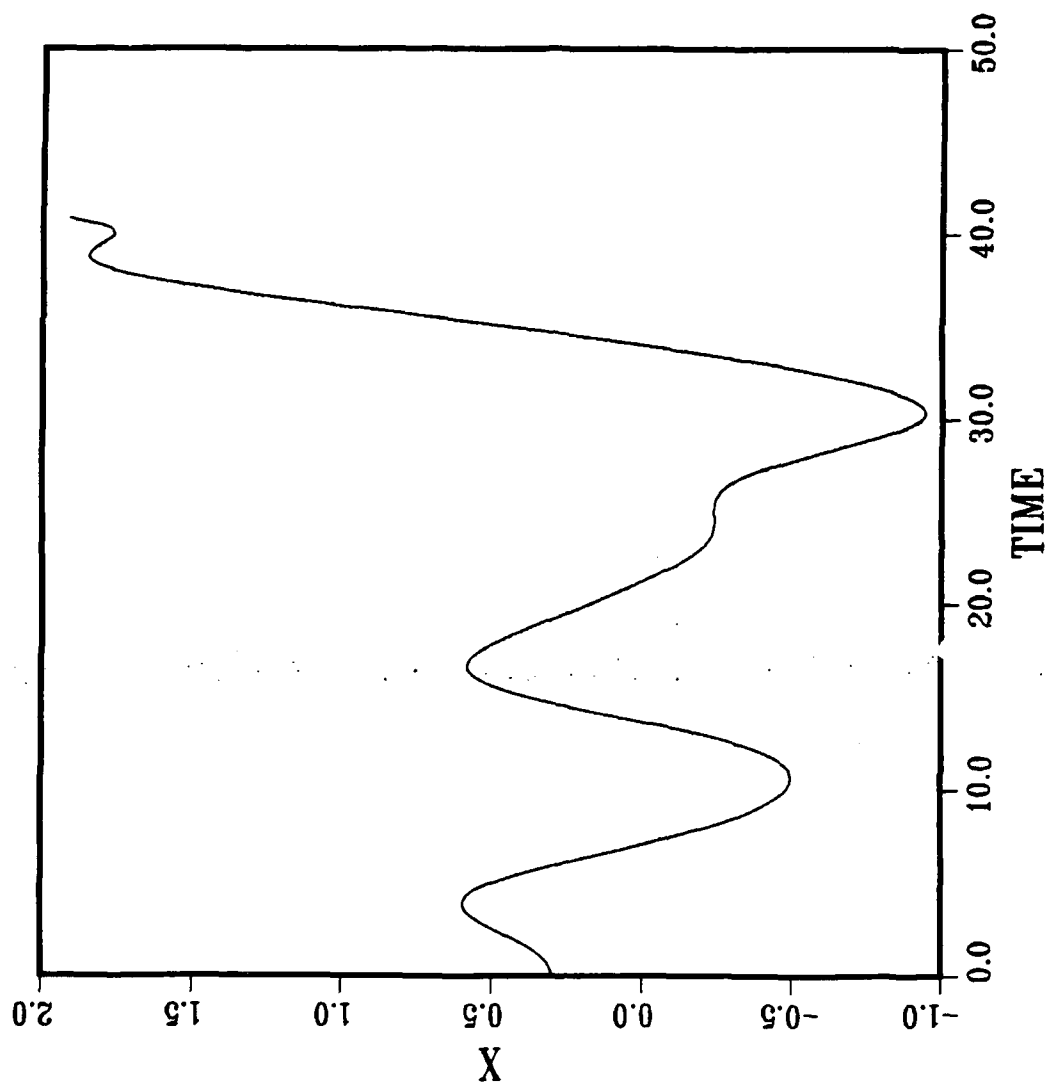
Figure 2-11 x displacement versus time for $\alpha = 0.175$.

$$|\alpha_z + 1| > |\alpha_o| \qquad (2-34)$$

the resonance condition becomes

$$[|\alpha_z + 1|^2 - 9][9|\alpha_z + 1|^2 - 1] + 100\alpha_o^2 = 0 \ . \qquad (2-35)$$

It follows that no resonance is possible if

$$|\alpha_z + 1| < 1/3 \quad \text{or} \quad |\alpha_z + 1| > 3 \ . \qquad (2-36)$$

Figure 2-12 shows the $|\alpha_z + 1| - |\alpha_o|$ plane and the region of linear stability. The dotted curve is a plot of the non-linear resonance condition, Eq. (2-35), which must be avoided in practical designs.

2.2.2 Envelope Stability of $\ell = 0$ Systems

As alternatives to a twisted quadrupole or $\ell = 2$ stellarator field, poloidally symmetric $\ell = 0$ fields have been investigated for use in high current beam transport. Two basic types have been considered, the bumpy-torus betatron[51] which uses toroidal field lines which bulge in and out periodically and the reversing solenoid lens accelerator[52] which uses the focusing action of periodically reversing solenoids which produce field cusps at their ends. We have considered[33] the stability of K-V beam envelopes in the presence of space charge in these two focusing systems, following the approach of Struckmeier and Reiser[54] who treated the stability problem for $\ell = 0$ and $\ell = 2$ discrete element systems.

The K-V envelope equations are

$$X'' + k_x^2(s)X - \frac{2K}{X+Y} - \frac{\epsilon_x^2}{X^3} = 0 \qquad (2-37)$$

$$Y'' + k_y^2(s)Y - \frac{2K}{X+Y} - \frac{\epsilon_y^2}{Y^3} = 0 \qquad (2-38)$$

where $k_{x,y}(s)$ represent external linear focusing, K is the beam perveance, and $\epsilon_{x,y}$ are unnormalized beam emittances. In a torus with $\ell = 0$ focusing these K-V equations hold in the Larmor frame with $\epsilon_x = \epsilon_y \equiv \epsilon$ and

$$k_x^2 = k_y^2 \equiv k^2 = \frac{1}{2r_o^2}\left(1 + \frac{1}{2}b^2(s)\right) \qquad (2-39)$$

17
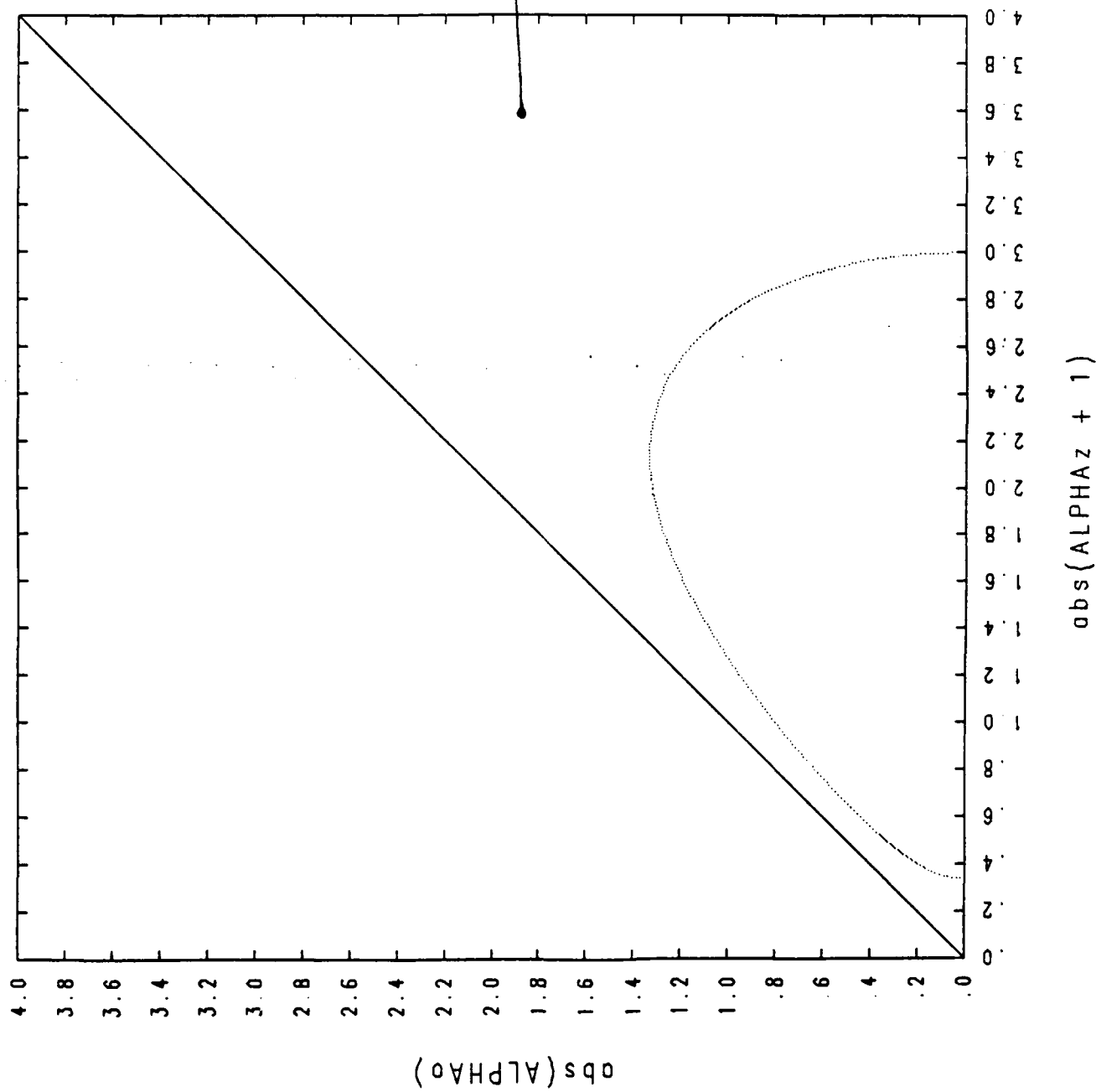
Figure 2-12 Stability plane showing the linearly stable region and the non-linear resonance condition, Eq. (2-35).

where $b(s) \equiv B_{\theta o}(s)/B_{zo}$ and we have taken the betatron field index $n = 1/2$. We will take $b(s)$ to be periodic with period S. In normalized variables the envelope equations become

$$\ddot{x} + \left(\frac{kS}{\pi}\right)^2 x - \frac{2g}{x+y} - \frac{1}{x^3} = 0 \qquad (2-40)$$

$$\ddot{y} + \left(\frac{kS}{\pi}\right) y - \frac{2g}{x+y} - \frac{1}{y^3} = 0 \qquad (2-41)$$

where the dimensionless variable $t \equiv \pi s/S$ has been defined so that the focusing period is π. In Eqs. (2-40, 41), a dot means d/dt and

$$g = KS/\pi\epsilon$$

$$(x,y) = (X,Y)/(\epsilon S/\pi)^{1/2} \quad .$$

The two cases for $b(t)$ corresponding to the bumpy torus (BT) and reversing solenoid lens (RSL) are shown in Figure 2-13. In each case one wishes to know, (1) under what circumstances do matched beam solutions, i.e. periodic solutions with period π exists to Eqs. (2-40, 41), and (2) when are these solutions stable to small perturbations? The second of these questions is of particular practical importance because one would like to know whether a beam launched with nearly the correct, matched initial conditions will remain nearly matched as it propagates through the focusing system.

To find matched beam solutions we set $x = y = R$ in Eqs. (2-40, 41) since a circular matched beam is expected in a symmetric focusing system for a beam with equal emittances in the two transverse planes. One then may find initial conditions $R(0)$ and $\dot{R}(0)$ numerically such that the resulting solution is periodic with period π; such a solution *exists* when the phase shift per period of single particle motion

$$\mu \equiv \int_o^\pi \frac{dt}{R^2} < \pi \quad , \qquad (2-42)$$

which is the condition for stability of betatron oscillations. In the absence of space charge $(g = 0)$, $\mu \equiv \mu_o$; in general $\mu < \mu_o$.

To investigate stability of the matched solutions one carries out a straightforward linearization of Eqs. (2-40, 41), writing

$$x = R + \delta_x \qquad (2-43)$$

$$y = R + \delta_y \quad . \qquad (2-44)$$

18

● **External Focusing Function**

$$\left[\frac{kS}{\pi}\right]^2 = \frac{2}{m^2}\left[1 + \frac{1}{2}\,b^2\right]$$

$$S = \frac{2\pi r_o}{m}$$

$$b^2(t+\pi) = b^2(t)$$

$$b^2(t) = b^2\,(1+\epsilon\,\cos\,2t)^2 \qquad \text{(BT)}$$

$$b^2(t) = \begin{cases} b^2 & 0 \leq t < t_o/2 \quad \text{and} \quad \pi - t_o/2 < t \leq \pi \\ 0 & t_o/2 \leq t \leq \pi - t_o/2 \qquad \text{(RSL)} \end{cases}$$
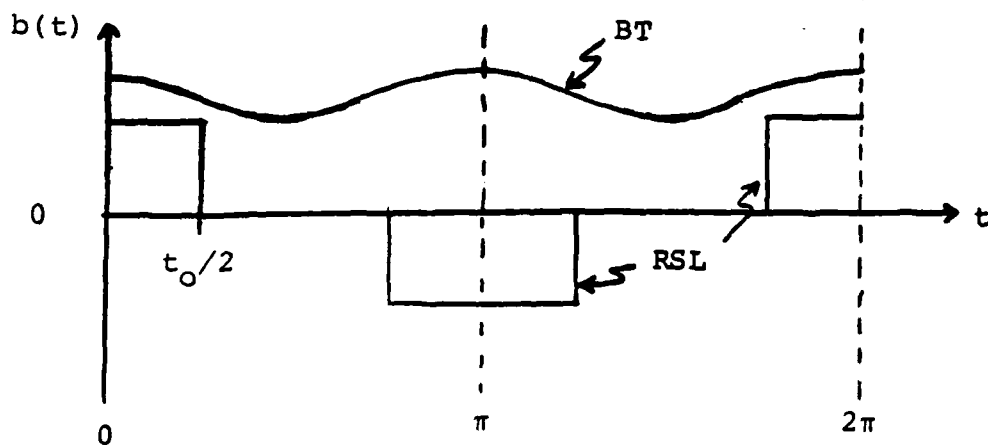
Figure 2-13 External focusing functions for bumpy torus (BT) and reversing solenoid lens (RSL) systems.

Defining $\delta_\pm \equiv \delta_x \pm \delta_y$ one finds that the equations for δ_+ and δ_- are decoupled, representing independent modes of oscillation:

$$\ddot{\delta}_+ + \left[\left(\frac{kS}{\pi}\right)^2 + \frac{g}{R^2} + \frac{3}{R^4}\right]\delta_+ = 0 \qquad (2-45)$$

$$\ddot{\delta}_- + \left[\left(\frac{kS}{\pi}\right)^2 + \frac{3}{R^4}\right]\delta_- = 0 \qquad (2-46)$$

The "+" mode is a monopole or "breather" mode and the "-" mode is a quadrupole or elliptical mode.

Equations (2-45, 46) are linear equations with periodic coefficients to which Floquet's theorem applies. The stability condition is

$$\mu_e < \pi \qquad (2-47)$$

where μ_e is the phase shift per period of either the δ_+ or δ_- equations. This is a more stringent condition than Eq. (2-42), the condition for single particle stability. In fact we have found that Eq. (2-47) implies that

$$\mu_o < \pi/2 \qquad (2-48)$$

for the bumpy torus and RSL systems; this is also the envelope stability condition found by Struckmeier and Reiser.[54] When (2-48) is satisfied the beam current limit is set only by the aperture size or by some other collective effect.

2.2.3 Negative Mass Instability

The negative mass instability in the modified betatron was studied by Sprangle and Vomvoridis.[26] They found that the longitudinal field coupled transverse and longitudinal modes and that the field helped to reduce the growth rate of the instability. Godfrey and Hughes[54] subsequently improved the dispersion relation, and resolved a puzzle about the existence of a growth rate cutoff above a certain critical current, by including toroidal corrections to the first order fields.

When strong focusing fields are added an important feature of the dispersion relation is changed.[40] Since the momentum compaction factor α is greatly reduced, to a value less than one, by the presence of the strong focusing fields, a transition energy is introduced

$$\gamma_t = \alpha^{-1/2} \qquad (2-49)$$

19

below which there is no negative mass effect; the beam consequently is stable for energies below $mc^2\gamma_t$. This transition energy is derived in terms of system parameters (field strengths, periods, etc.) in reference 40, attached here as an appendix.

Reference 40 derives the full linear eigenvalue problem for long wavelength, low frequency collective modes in the stellatron. The eigenvalue problem is then solved in the 'smooth approximation,' which assumes that the wavelength of the perturbation is many stellarator field periods long. This results in a dispersion relation identical in form to that for the modified betatron, under the replacement of a single term; the dispersion relation has been tested against a numerical solution of the eigenvalue problem and excellent agreement has been found. The net effect of the stellarator windings, we have found, is to add a smooth, transverse focusing term which can be large compared to the weak-focusing or space charge defocusing terms; stellarator fields enhance stability in this sense; as a result, increasing the stellarator field strength reduces the negative mass growth rate. Numerical examples given in reference 40 quantify this effect.

2.2.4 Beam-Breakup Instability (BBU)

The BBU is the most serious instability facing the SLIA. The magnitude of the problem can be understood by examining the asymptotic formula for the maximum beam displacement during the beam pulse in the n-th gap, as given by V.K. Neil et al.,[55]

$$\hat{\xi}_n \approx \frac{\exp(\hat{\Gamma}_n)}{\sqrt{16\pi\hat{\Gamma}_n}} \quad , \qquad (2-50)$$

where

$$\hat{\Gamma}_n = 5.49 \times 10^{-4} n Z_\perp[\Omega] \frac{\omega I[kA]}{\omega_0 B_0[kG]} \quad , \qquad (2-51)$$

and where ω = deflecting mode frequency, $\omega_0 = 2\pi$ (785 MHz), I = beam current, and B_0 = solenoidal magnetic field.

This maximum amplitude occurs at a time $\hat{t}_n$, given by

$$\omega\hat{t}_n = 2\hat{\Gamma}_n Q \quad , \qquad (2-52)$$

where Q is the quality factor for the accelerating gap. The beam pulse is assumed to be longer than $\hat{t}_n$.

The coupling impedance, $Z_\perp$, is given in the limit $b \gg w$ by[56]

$$Z_\perp[\Omega] = -730\frac{\omega_0 w}{\omega b^2} Im P_1(\omega) \quad , \qquad (2-53)$$

20

where w is the gap width, b is the pipe radius, and $P_1(w)$ is the cavity response function. Substituting this formula into the expression for $\hat{\Gamma}_n$ yields

$$\hat{\Gamma}_n = -401 \frac{V_f[GeV]I[kA]ImP_1(\omega)}{E_g[MV/cm]B_0[kG]b^2} \quad , \tag{2-54}$$

where E_g is the electric field in the gap, $E_g w$ is the energy gain per gap, and V_f is the final beam energy. In the limit $b \approx w$, Godfrey[57] has shown that the impedance falls as b^{-1} instead of b^{-2}. The ATA gaps satisfy the expression given above, but the SLIA gaps will be better represented by Godfrey's formula.

Figure 2-14 shows contours of constant $\hat{\Gamma}_n = 10$, corresponding to $\hat{\xi}_n \approx 1000$, plotted in the $E_g - b$ plane for various combinations of I and V_f, assuming $ImP_1(\omega) = -0.7$. There is a clear advantage to designing gaps having as large as an E_g as possible. At present LLNL operates at ≈ 200 kV/cm, while Sandia has operated their gaps up to ≈ 400 kV/cm. The limit, set by emission levels over areas of interest, must be experimentally studied with the use of new electrode materials, coatings and conditioning techniques.

The cavity response function has been computed for the deflecting mode in ATA as $ImP_1(\omega) = -1.3$. For a perfectly-coupled gap (ie. with no reflections) the response would be roughly half the ATA value, $ImP_1(\omega) \approx -0.7$. LLNL has designed gaps with nearly optimal coupling, although they have not yet measured their BBU characteristics.

The BBU can be detuned through the use of nonlinear focusing fields. Solenoidal and quadrupole focusing forces are both linear in the transverse displacement from the matched reference orbit. The use of quadrupole focusing in the SLIA, therefore, does not substantially affect the BBU. It acts only as an additional solenoidal focusing field. In the smooth approximation this additional focusing can be calculated to be[58]

$$B_{eff} = B_0 \left[1 + \frac{\epsilon_q^2}{2} \right] \quad , \tag{2-55}$$

where ϵ_q is proportional to the quadrupole field strength. For $\epsilon_q < 1$, the quadrupole focusing yields only a modest reduction in the BBU growth rate compared with the result with B_0 alone. By adding a sextupole field to the transport system, however, the focusing fields will be quadratic in the displacement from the reference orbit, and the growth of the BBU will be strongly affected.[46] The nonlinear transverse focusing causes the betatron wavelengths of the electrons to depend on the amplitude of their displacement from the reference orbit. As the BBU instability drives the beam electrons off axis, therefore, their response to the BBU driving mode becomes detuned, thereby preventing them from exciting that mode in accelerating gaps downstream. Ion focusing also defeats the BBU by
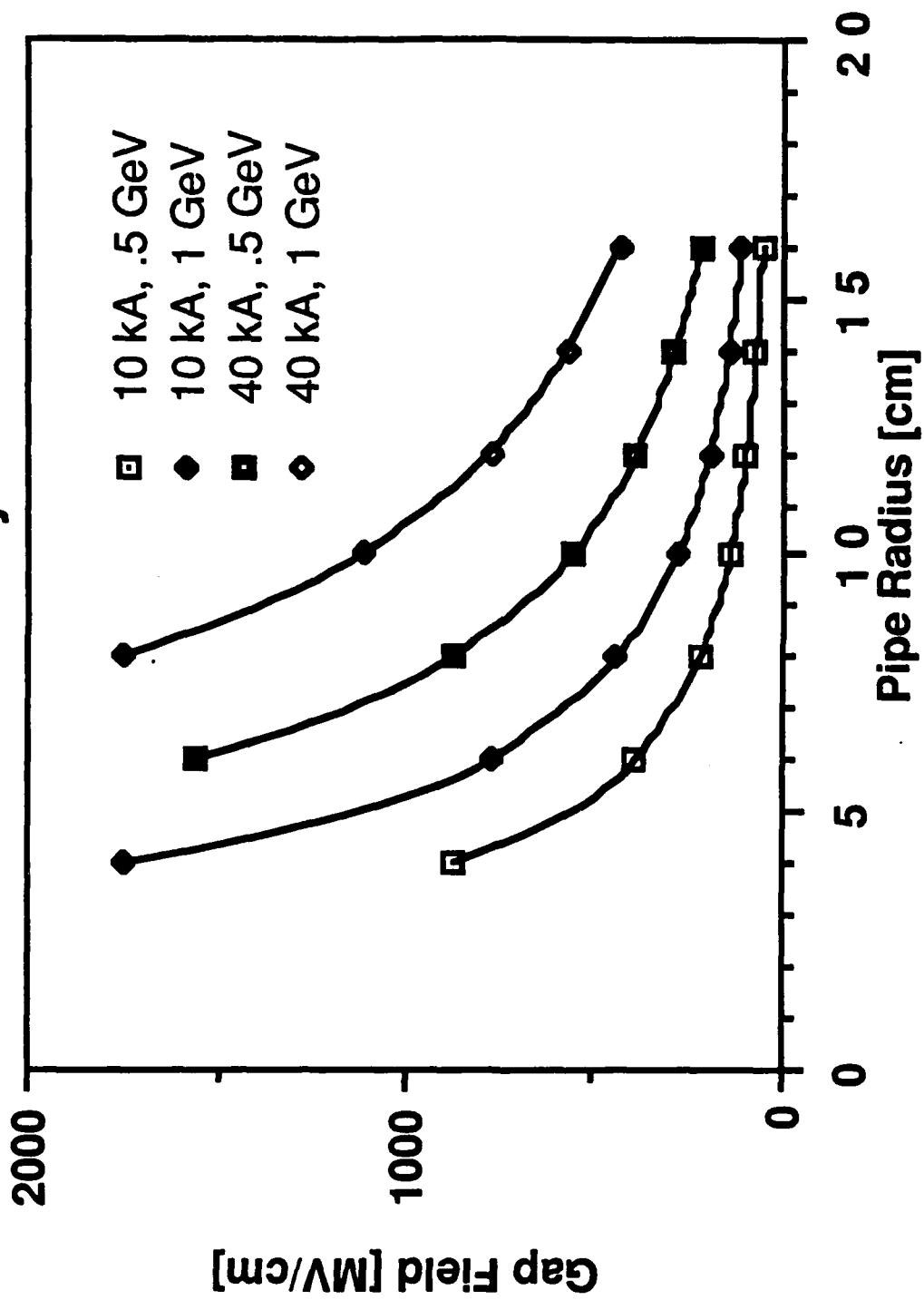
21

Figure 2-14 Contours for $\hat{T}_n = 10$.

introducing a spread in betatron wavelength.[45] Since the SLIA is planned to operate without IFR guiding, magnetic focusing systems that can spoil the BBU have been explored. A twisted sextupole winding appears to offer great promise in this regard.

The twisted sextupole field is the equivalent of an $l = 3$ stellarator field, whose components may be expressed (to quadratic order in x and y) as

$$B_x \approx \frac{27}{16}\epsilon_s B_0 \alpha^2 [2xy \cos(3\alpha s) - (x^2 - y^2)\sin(3\alpha s)] \qquad (2-56)$$

$$B_y \approx \frac{27}{16}\epsilon_s B_0 \alpha^2 [(x^2 - y^2)\cos(3\alpha s) + 2xy \sin(3\alpha s)] \ . \qquad (2-57)$$

These fields add to the other fields (longitudinal field, quadrupole field, and vertical field on the bends) in the SLIA configuration.

The current that must be used to excite a continuous sextupole winding to produce a desired shear in the field on axis depends strongly on the radius of the sextupole coil, as shown in Figure 2-15. The parameter ϵ_s on that figure measures the sextupole field strength. When $\epsilon_s = 1$, the amplitude of the sextupole field equals the solenoidal field, B_0. Figure 2-15 is plotted for $B_0 = 5$ kG. For the SLIA, where the vacuum vessel has a radius of 3 cm, the current required in the sextupole coils will be ≈ 240 kA for $\epsilon_s = 6$. While this current is large, the inductance of the sextupole winding is small, as is the energy associated with this field.

The effect of this field is illustrated in Figure 2-16. This figure shows the beam profile after passing through 800 gaps. The beam pulse is 30 ns long, and $t = 0$ on the figure corresponds to the time that the beam head passes the 800th gap. The gaps in this example are modeled by an impulse model developed by V.K. Neil et al.[55] The gap characteristics are assumed similar to those in ATA ($Z_\perp/Q = 10$ Ω, $Q = 4$, a deflecting mode frequency of 785 MHz, and energy gain per cavity of 0.3 MeV). The final energy of this accelerator would be 241 MeV (1 MeV injected + 800 gaps × 0.3 MeV/gap). The transport system between gaps is similar to that planned for the SLIA ($B_0 = 5$ kG, quadrupole field amplitude of $\epsilon_q = 0.3$, quadrupole pitch length of $L_q = 18$ cm), with the addition of a continuously-twisted sextupole field ($\epsilon_s = 6$ and $L_s = 18$ cm). The incident electron beam at the first gap has a current of 10 kA, an energy of 1 MeV, and is off-axis by 10^{-4} cm. The beam is injected without energy spread, and the model allows no energy spread to develop as the electrons are accelerated; energy spread should be stabilizing for the BBU since it independently introduces a spread in the betatron wavelength. Without the sextupole field, Figure 2-16 shows that the amplitude of the beam displacement from the axis would be $\approx 10^8$ cm after 800 gaps; ie. the beam would be catastrophically unstable. With the sextupole field, the beam displacement is limited to ≈ 1 cm, as seen on the figure. The beam displacement

Figure 2-15 Sextupole coil current versus winding radius.

BBU GROWTH AT 800th GAP

NO SEXTUPOLE

WITH SEXTUPOLE
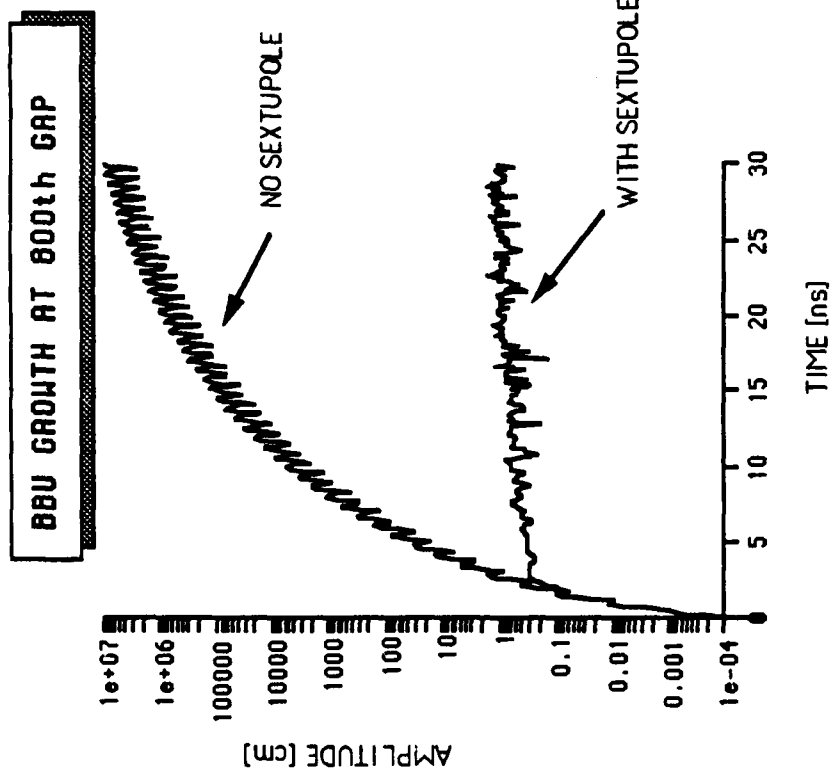
BEAM CURRENT = 10 kA
PULSE LENGTH = 30 ns
INITIAL X = 0.0001 cm
INITIAL ENERGY = 1.0 MeV

No. of GAPS = 800
GAP-TO-GAP = 30 cm
ENERGY GAIN = 0.3 MeV/GAP
DEFLECTING MODE FREQ. = 785 MHz
Q = 4
Z/Q = 10 OHMS

SOLENOIDAL FIELD = 5 kG
QUADRUPOLE FIELD
  AMPLITUDE = 0.3 x SOLENOID
  PITCH LENGTH = 18 cm
SEXTUPOLE FIELD
  AMPLITUDE = 0. & 6. x SOLENOID
  PITCH LENGTH = 18 cm

AMPLITUDE [cm]

1e+07
1e+06
100000
10000
1000
100
10
1
0.1
0.01
0.001
1e-04

TIME [ns]

5 10 15 20 25 30

Figure 2-16 Beam profile at gap 800. (10 kA beam)

saturates at this amplitude before the 400th gap, and remains stable through the 800th gap, which was the final gap in the calculation.

Figure 2-17 shows the same calculation carried out for a 40 kA beam. Again, the sextupole field clamps the BBU growth when the displacement reaches $\approx$ 1 cm amplitude.

Other tests have demonstrated that the saturation of the BBU near amplitudes of 1 cm is insensitive to the initial amplitude. When the initial amplitude in Figure 2-16 is increased from 10^{-4} cm to 0.1 cm, the saturation occurs after fewer gaps, but the saturated amplitude is still $\approx$ 1 cm.

These calculations offer the promise of defeating the BBU with high-order multipole fields, such as sextupoles. The effect of these fields on the beam emittance or on beam stability other than the BBU has not yet been investigated. These studies are on-going at the present time.

Shielded gaps may offer yet another means to control the BBU. In the SLIA conceptual design shielded gaps are used to avoid the low-frequency beam displacement in off-axis pipes due to return-current asymmetries in the feed. No measurable deflection of beams was observed with shielded gaps, within diagnostic resolution, in the experiments of Wilson at NBS and Hasti at SNLA. Miller *et al.* of SNLA have also studied a version of these gaps in the RADLAC development program. The high-frequency character of these gaps is unknown, and must be evaluated in "cold-test" cavity measurements.

Miller *et al.*[59] have used the SOS code, a 3-D code developed at Mission Research Corporation (MRC), to analyze the differences between pillbox cavities of the type used at ATA and the so-called "shielded-gap" configurations which are envisioned for the SLIA. Their model utilized perfectly-conducting structures everywhere (including the feed termination), and therefore does not provide design data. The model is useful, however, in displaying the relative differences between pillbox and shielded-gap configurations. Their conclusion is that a shielded-gap, made by inserting a short length of coaxial transmission line in a pillbox cavity, can substantially reduce the coupling impedance to the BBU instability, provided that the coax is designed so that the lowest TE mode cutoff frequency is greater than the frequency of the TM cavity mode which drives the BBU. More recent calculations at MRC[60] and at LLNL[61] have found that shielded-gap configurations can introduce new, weakly-damped modes which increase the BBU coupling impedance. These calculations have so far not found any shielded-gap design that substantially improves the BBU coupling impedance over that obtainable with a simple radial line. This subject is still under study at SAIC, MRC, and LLNL.

BBU GROWTH AT 800th GAP

BEAM CURRENT = 40 kA
PULSE LENGTH = 30 ns
INITIAL X = 0.0001 cm
INITIAL ENERGY = 1.0 MeV

No. of GAPS = 800
GAP-TO-GAP = 30 cm
ENERGY GAIN = 0.3 MeV/GAP
DEFLECTING MODE FREQ. = 785 MHz
Q = 4
Z/Q = 1 0 OHMS

SOLENOIDAL FIELD = 5 kG
QUADRUPOLE FIELD
    AMPLITUDE = 0.3 x SOLENOID
    PITCH LENGTH = 18 cm
SEXTUPOLE FIELD
    AMPLITUDE = O. & 6. x SOLENOID
    PITCH LENGTH = 18 cm

NO SEXTUPOLE

WITH SEXTUPOLE

AMPLITUDE [cm]

1e+07
1e+06
100000
10000
1000
100
10
1
0.1
0.01
0.001
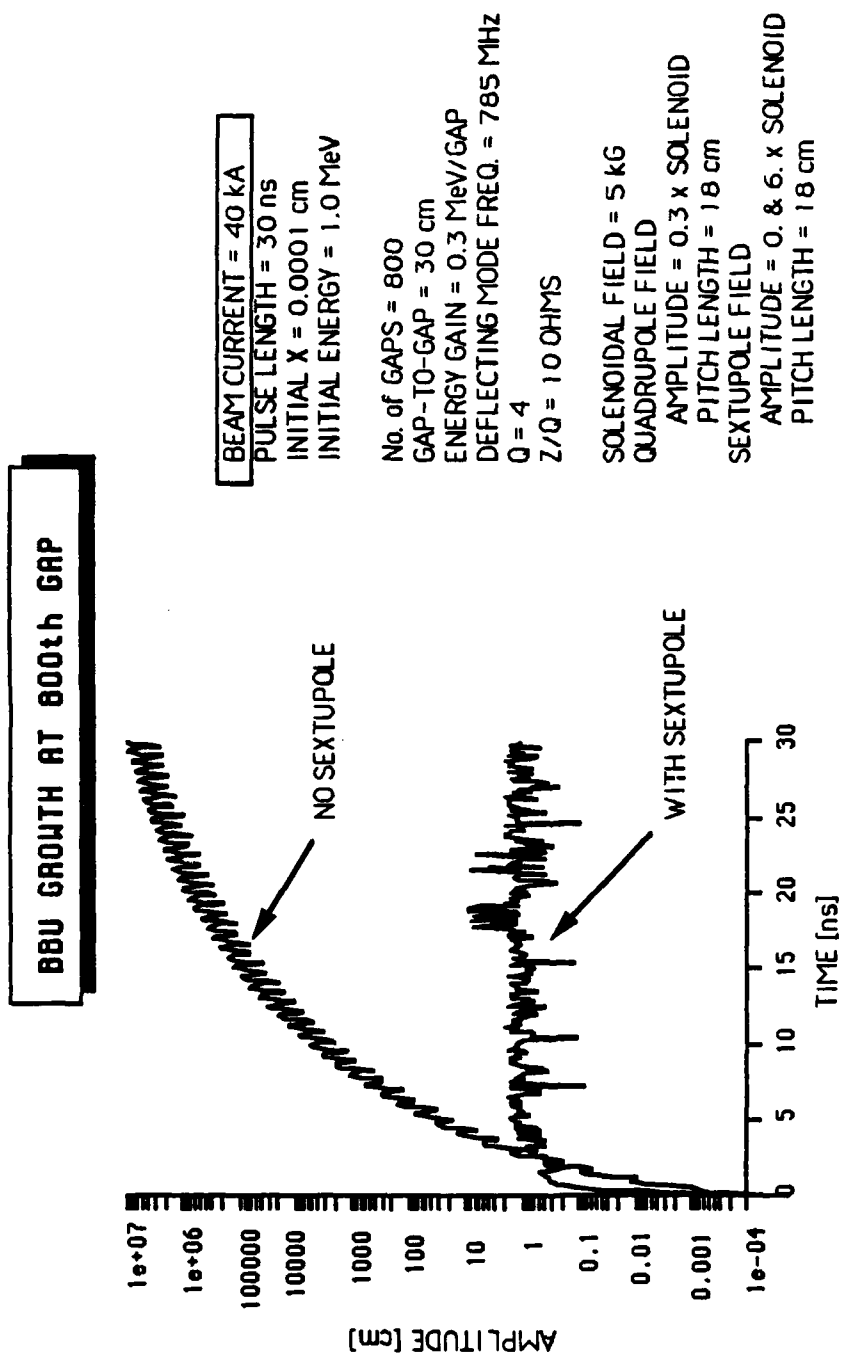1e-04

0   5   10   15   20   25   30
TIME [ns]

Figure 2-17 Beam profile at gap 800. (40 kA beam)

2.3 The Spiral Line Induction Accelerator (SLIA)

Our investigations of the properties of high current, strong focused accelerators led to the joint proposal, in 1985, of what is now called the SLIA, by SAIC and Pulse Sciences, Inc. The SLIA, illustrated in Figure 2-18, consists of a continuous beam line which is recirculated through an induction module multiple times; the number of recirculations depends on the sizes of the beam pipe and the module cores.

The SLIA as proposed has several advantages over closed orbit machines. In particular, injection and ejection become much easier than for a closed orbit device. In addition, the open-ended design of the SLIA allows very long pulse lengths to be envisioned; the pulse length is set by the injector pulse length rather than by the circulation time, as in a closed orbit machine. The magnetic fields used for focusing and bending in the SLIA beam line are effectively static in time, simplifying their design and allowing low field errors to be achieved. It may even be possible to use permanent magnets for some of the fields in the transport line. These advantages come at the cost of added mechanical and electrical complexity, however. The beam transport line design is complicated by the simultaneous presence of many coils and the induction module design is quite novel, requiring careful considerations to reduce asymmetries in the accelerating fields applied to the different gaps. Nonetheless, based on a 1985 proposal by SAIC and PSI, a SLIA experiment was funded and a transport line was built to study the properties of a strong focused recirculator. This experiment is now planned to lead to a 2 module, 3-turn machine producing an 8.5 MeV, 10 kA beam.

The research funded by ONR under this contract contributed and continues to contribute directly to the evolution of the SLIA by its concentration on fundamental issues of beam transport and stability in strong focused systems. The original work by Roberson, Mondelli and Chernin on momentum compaction in the stellatron has been basic to the design of the recirculator. The work performed on beam stability and envelope matching has also facilitated the design of the beam line. One of the most fundamental physics issues for the SLIA, the beam break-up instability, has been extensively studied under ONR sponsorship, resulting in some promising proposals for stabilization by non-linear fields and by energy spread. Work on orbital resonances, while most pertinent to closed orbit devices in which a beam circulates many times, may also find application in the SLIA, or certainly in the induction synchrotron accelerator (ISA) for which it has been proposed to use the SLIA as an injector.

Though a number of important physics and design issues remain to be resolved, the technology represented by the SLIA appears to be a promising direction for future research
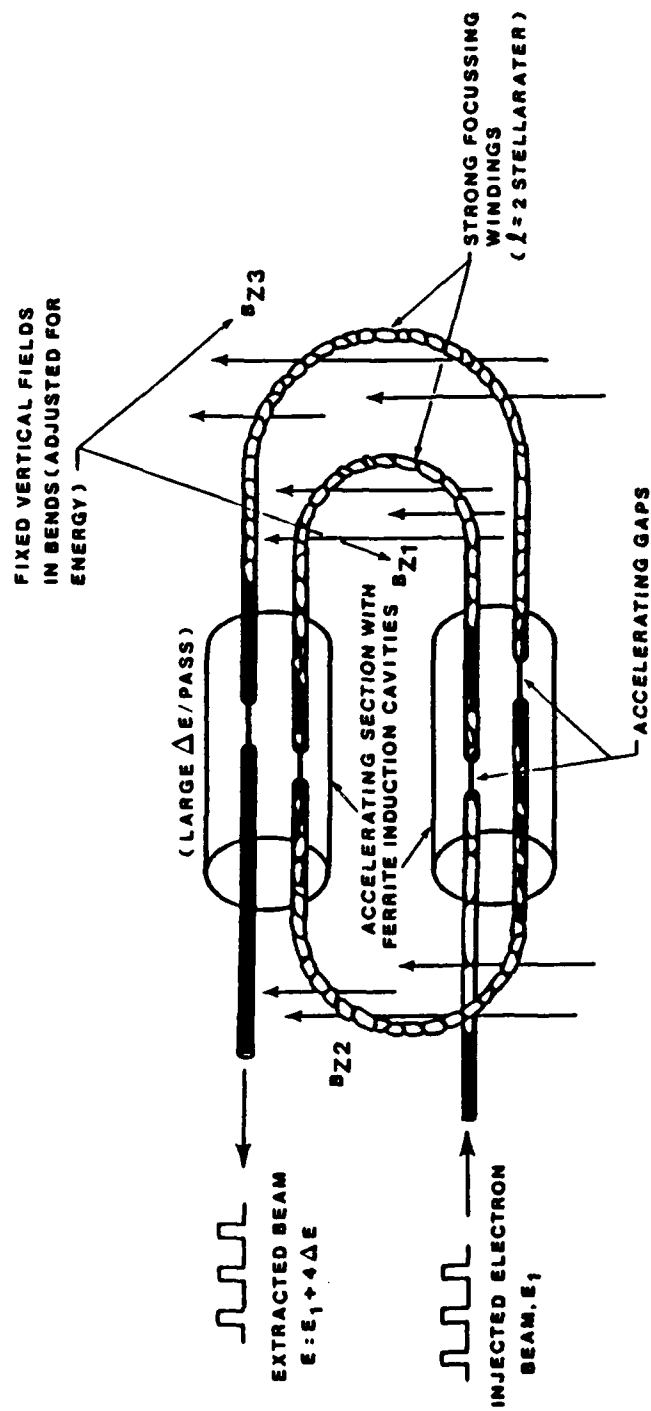
Figure 2-18 Schematic of the Spiral Line Induction Accelerator (SLIA): a two pass ex-
ample.

in high power electron accelerators. ONR sponsorship of the basic physics and scaling of strong focused, compact accelerators has laid important groundwork for on-going research in an area of continuing interest to the Navy.

3.0 Conclusions and Recommendations

Our studies of compact, strong focused, high current electron accelerators have addressed many aspects of beam behavior in these devices. We have found that systems employing $\ell = 2$ stellarator windings can be designed to be stable and robust, with excellent energy bandwidth. Experimental programs at NRL, UC Irvine, and Pulse Sciences, Inc. continue to investigate the properties of these focusing systems.

The criteria for stability, both due to single particle resonances and to collective effects, are reasonably well understood at this point, except, perhaps, for high frequency phenomena like the short wavelength negative mass instability and the electromagnetic three- wave instability. It appears that current limits in closed devices like the betatron/stellatron, are due to tune shifts and to the negative mass instability, while in induction linacs, including SLIA configurations, current is limited by the beam break-up instability. Energy limits are similarly constrained by tune shifts in closed devices if one realizes the condition required to avoid resonanaces is to raise all fields proportionally, in particular, $B_\theta \alpha B_z$; in the SLIA, energy limits will be dictated by induction module technology and by the number of recirculations allowed by pipe and core radii. Finally, beam pulse length limits in a closed device are clearly bounded by the circumference/c while in a SLIA or induction linac, output pulse length is limited only by injector pulse length and the number of volt-seconds that can be supplied to the cores (for a continuous beam). These conclusions, and the analyses that led to them, represent the main results of our work on compact electron accelerators.

There remain several important issues in these devices which require further study. Prominent among these is the stabilization of the beam break-up instability in the SLIA. Many lines of investigation should be followed, especially the potential role of energy spread, including the variation in recirculation time with energy, and the application of non-linear fields. Also, the use of feed-forward stabilization, whereby the kick received by the beam is sensed as it exits a module and a signal is sent across a chord of the device to a point at which a correcting kick is applied, may have practical application in the SLIA. Virtually no work has been done on this question.

The related issues of beam matching and beam quality in these devices also deserve more thorough treatments. Techniques for matching a beam on and off the stellarator field in order to minimize the resulting envelope oscillations, are presently imperfect and much work needs to be done along these lines. Very little also is presently known about required field tolerances and the effect of field errors on beam behavior in general and on beam quality in particular.

Though significant progress has been made in the understanding of compact electron accelerators further work, both theoretical and experimental, is essential to ensure that practical, workable designs can be developed.

References

1. D.W. Kerst, *Phys. Rev.* **58** 841 (1940).

2. D.W. Kerst, *Phys. Rev.* **59** 110 (1941).

3. D.W. Kerst, in *Handbuch der Physik* vol. XLIV (Springer-Verlag, Berlin, 1959).

4. A.I. Pavlovskii, D.G. Kuleshov, A.I. Gerasimov, A.P. Klementev, V.D. Kuzemtsov, V.A. Tananakin and A.D. Turasov, *Sov. Phys. Tech. Phys.* **22** 218 (1977).

5. J.M. Peterson, LBL reprint 15206 (1982); *Proc. 7th Conference on Applications of Accelerators in Research and Industry* (Denton, Texas, 1982).

6. D.W. Kerst, G.D. Adams, H.W. Koch and C.S. Robinson, *Phys. Rev* **78** 297 (1950).

7. G.I. Budker, in *Proc. CERN Symposium on High Energy Accelerators* (1956).

8. L.A. Ferrari and M.S. Zucker, *Particle Accelerators* **2** 121 (1971).

9. K.R. Symon, D.W. Kerst, L.W. Jones, L.J. Laslett and K.M. Terwillinger, *Phys. Rev.* **103** 1837 (1956).

10. E.D. Courant, M.S. Livingston and H.S. Snyder, *Phys. Rev.* **88** 1190 (1952).

11. W. Walkinshaw and K. Wyllie, TRE (Malvern) Maths Memo /58/ww, June 7 (1948). (Unpublished).

12. N. Rostoker, *Particle Accelerators* **5** 93 (1973).

13. G.S. Jones, R.H. Levy, H.A. Bethe and B.T. Feld, *Phys. Rev. Lett.* **145** 925 (1966); J.D. Daugherty, J.E. Eninger and G.S. Janes, *Phys. Fluids* **12** 2677 (1969).

14. N. Rostoker, *Comments on Plasma Physics* **6** 91 (1980).

15. P. Sprangle and C.A. Kapetanakos, *J. Appl. Phys.* **49** 1 (1978).

16. P. Sprangle, C.A. Kapetanakos and S.J. Marsh, in *Proc. International Topical Conf. on High Power Electron and Ion Beam Research and Technology*, Palaiseau, France (1981).

17. G. Barak, D. Chernin, A. Fisher, H. Ishizuka and N. Rostoker, *idem*.

18. W. Clark, P. Korn, A. Mondelli and N. Rostoker, *Phys. Rev. Lett.* **37** 592 (1976).

19. H. Ishizuka, G. Lindley, B. Mandelbaum, A. Fisher and N. Rostoker, *Phys. Rev. Lett.* **53** 266 (1984).

20. F. Mako, J. Golden, L. Floyd, K. McDonald, T. Smith and C.A. Kapetanakos, *IEEE Trans. Nucl. Sci.* **NS-32** 3027 (1985).

21. F. Mako, J. Golden, D. Dialetis, L. Floyd, N. King and C.A. Kapetanakos, in *High Brightness Accelerators*, A.K. Hyder, M.F. Rose and A.H. Guenther, eds., Plenum Press, New York (1988).

22. J. Golden, R. Mako, L. Floyd, T. Smith D. Dialetis, S.J. Marsh and C.A. Kapetanakos, *Proc. IEEE Particle Accelerator Conference*, p. 936 (1987).

23. C.A. Kapetanakos, P. Sprangle, D. Chernin, S.J. Marsh and I. Haber, *Phys. Fluids* **26** 1634 (1983).

24. D. Chernin and P. Sprangle, *Particle Accelerators* **12** 85 (1982).

25. D. Chernin and P. Sprangle, *Particle Accelerators* **12** 101 (1982).

26. P. Sprangle and J.L. Vomvoridis, *Particle Accelerators* **18** 1 (1985).

27. C.A. Kapetanakos, S.J. Marsh and D. Dialetis, NRL Memorandum Report 6214 (1988).

28. A.A. Mondelli and C.W. Roberson, NRL Memorandum Report 5008 (1982) [*Particle Accelerators* **15** 221 (1984).]

29. C.W. Roberson, A.A. Mondelli and D. Chernin, *Phys. Rev. Lett.* **50** 507 (1983).

30. H. Ishizuka, G. Leslie, B. Mandelbaum, A. Fisher and N. Rostoker, *IEEE Trans. Nucl. Sci.* **NS-32** 2727 (1985).

31. E.D. Courant and H.S. Snyder, *Ann. Phys.* **3** 1 (1958).

32. I.M. Kapchinskij and V.V. Vladimirskij, *Proc. International Conf. on High Energy Accelerators*, CERN (1959).

33. A. Mondelli and D. Chernin, APS/DPP Meeting, Boston, MA (1984). [*Bull. Am. Phys. Soc.* **29** 1431 (1984).]

34. R.L. Gluckstern, *Proc. 1979 Linear Accelerator Conference*, p. 245.

35. D. Chernin, *Proc. 1985 Particle Accelerator Conference* [*IEEE Trans. Nucl. Sci.* **NS-32** 2504 (1985).]

36. D. Chernin, *Particle Accelerators* **24** 29 (1988).

37. D. Chernin and A. Mondelli, *Compact Accelerator Workshop*, LLNL (Oct. 1985).

38. D. Chernin and B. Levush, *APS/DPP Meeting*, Baltimore, MD (1986). [*Bull. Am. Phys. Soc.* **31** 1462 (1986).]

39. H. Ishizuka, et al., *Proc. 6th International Conf. on High Power Particle Beams* (Kobe, Japan, 1986).

40. D. Chernin, *Phys. Fluids.* **29** 556 (1986).

41. T.P. Hughes and B.B. Godfrey, *Phys. Fluids* **29** 1698 (1986).

42. M.A.D. Wilson, *IEEE Trans. Nucl. Sci.* **NS-28** 3375 (1981).

43. D. Birx, *Compact Accelerator Workshop*, LLNL (Oct. 1985).

44. A. Mondelli, D. Chernin, S. Putnam and L. Schlitt, *Compact Accelerator Workshop*, LLNL (Oct. 1985).

45. G. Caporaso, *Proc. LINAC '86*, SLAC (1986).

46. A. Mondelli, D. Chernin and J. Petillo, *APS/DPP Meeting*, San Diego, CA (1987). [*Bull. Am. Phys. Soc.* **32** 1912 (1987).]

47. J.D. Lawson, *The Physics of Charged-Particle Beams*, Clarendon Press, Oxford (1978), ch. 4.

48. D. Chernin, "Orbital Resonances and Energy and Current Limits in High Current Cyclic Accelerators," SAIC Report 86/1516 (1986).

49. D. Chernin, *Part. Accel.* **14** 139 (1984).

50. D. Chernin and B. Levush, "Non-Linear Particle Orbits in a Twisted Quadrupole Field," *APS/DPP Meeting*, Baltimore, MD (Nov. 1986).

51. D. Chernin, A. Mondelli and C. Roberson, *Phys. Fluids* **27** 2378 (1984).

52. S. Humphries and D.M. Woodall, *Bull. Am. Phys. Soc.* **28** 1054 (1983).

53. J. Struckmeier and M. Reiser, *Part. Accel.* **14** 227 (1984).

54. B.B. Godfrey and T.P. Hughes, *Phys. Fluids* **28** 669 (1985).

55. V.K. Neil, L.S. Hall, and R.K. Cooper, *Part. Accel.* **9**, 213 (1979).

56. R.J. Briggs, D.L. Birx, G.J. Caporaso, V.K. Neil, and T.C. Genoni, *Part. Accel.* **18**, 41 (1985).

57. B.B. Godfrey, *Transverse Wake Potentials for Wide Radial Lines*, MRC/ABQ-R-1046 (Mission Research Corporations, Albuquerque, 1988)

58. A. Mondelli and D. Chernin, *BAPS* **31**, 1445 (1986).

59. R.B. Miller, B.M. Marder, P.D. Coleman, and R.E. Clark, *The Effect of Accelerating Gap Geometry on the Beam Breakup Instability in Linear Induction Accelerators*, Sandia Report *SAND87-1389J* (Sandia National Laboratories, Albuquerque, NM, 1987).

60. T.P. Hughes and B.B. Godfrey, *Electron Beam Stability in Compact Recirculating Accelerators*, MRC Report *MRC/ABQ-R-1040* (Mission Research Corporation, Albuquerque, NM, 1988).

61. S. Putnam, private communication.

APPENDIX A
Published Papers

1. "The Stellatron Accelerator," C.W. Roberson, A. Mondelli and D. Chernin, *Particle Accelerators* **17** 79 (1985).

2. "Beam Stability in a Stellatron," D. Chernin, *Phys. Fluids* **29** 556 (1986).

3. "Use of Radiation from Betatron Oscillations as an Electron Beam Diagnostic," D. Chernin and B. Levush, *J. Appl. Phys.* **61** 2737 (1987).

4. "The Spiral-Line Induction Accelerator," S. Putnam, V. Bailey, A. Mondelli, D. Chernin and J. Petillo, *J. Def. Res.* (to be published).

5. "Evolution of RMS Beam Envelopes in Transport Systems with Linear X-Y Coupling," D. Chernin, *Particle Accelerators* **24** 29 (1988).

THE STELLATRON ACCELERATOR

C. W. ROBERSON

Office of Naval Research, Arlington, VA 22217 U.S.A.

A. MONDELLI

Science Applications, Inc., McLean, VA 22102 U.S.A.

and

D. CHERNIN†

Berkeley Research Associates, Springfield, VA 22150 U.S.A.

The magnetic field configurations consisting of the combination of a weak-focusing betatron field, toroidal field and either $l = 0$ or $l = 2$ stellarator windings are assessed for their potential as focusing fields for high-current cyclic electron accelerators. These accelerators, named "stellatrons," are shown to have improved tolerance to mismatch between the average beam energy and the equilibrium beam energy that matches the vertical magnetic field compared to devices without the stellarator fields. Both analytical calculations in the paraxial approximation and numerical particle-orbit calculations are presented to substantiate this finding. The problems of orbital resonances and of injection into these devices are discussed. Earlier work in the field, much of it unpublished, is discussed and compared with the stellatron concept.

I. INTRODUCTION

Electron accelerators built to carry out nuclear and high-energy physics experiments typically carry average currents of less than an ampere at kinetic energies as high as 50 GeV. During the past twenty years, significant progress has been made in high-current, low-energy beam generation. These intense-beam accelerators are generally motivated by applications, mostly for radiation source development and for controlled nuclear fusion research. Megampere currents at megavolt energies are now routinely obtained using pulselines charged by Marx capacitor banks, connected to cold cathode (field-emission) diodes.[1]

Multikiloampere electron currents at tens of megavolts have been obtained using linear induction accelerators.[2-6] Recently, there has been considerable interest in extending the current-carrying capabilities of cyclic induction accelerators such as variations of the betatron and linear induction modules in cyclic (racetrack or other) configurations.

---

† Present Address: Science Applications, Inc., McLean, VA 22102 U.S.A.

Conventional betatrons[7,8] are current limited due to the defocusing effects of space charge at injection. Overcoming the space-charge limit requires high-energy injection. By injecting a beam at high energy, approximately 200 A of circulating current has been obtained in a small betatron in which the beam was ultimately accelerated to 100 MeV.[9] In another experiment using a 4-MeV induction linac, approximately 500 A of circulating current has been confined in a conventional betatron configuration.[10] Devices designed to improve the current-carrying capability of betatrons have included fixed-field alternating-gradient (FFAG) betatrons[11] and plasma betatrons.[12] The FFAG uses alternating gradient strong focusing fields[13,14] in addition to a vertical betatron field. In the FFAG, the magnetic fields remain constant in time, while the flux linking the particle orbit is changed to produce an inductive electric field. To avoid single-particle resonances as the energy is increased, the equilibrium radius of the orbit is allowed to vary with energy, keeping the orbits "self-similar". The currents achieved in prototypes[11] have been modest, limited by the tune shift due to space-charge effects.

The plasma betatron employs a toroidal magnetic field in addition to the betatron field. A plasma is injected or created in the device and the applied inductive electric field causes a portion of the electron distribution to gain more energy from the electric field between collisions than it loses during a collision, a phenomenon called electron runaway.[54] In magnetic-fusion devices, runaway currents of hundreds of amperes at energies of several MeV have been obtained.[15,16,39]

The HIPAC[17] device, using only a toroidal magnetic field with a cross-field injection scheme known as inductive charging,[18] has been investigated in connection with an ion-acceleration concept. Average electron densities of $4 \times 10^9 \, cm^{-3}$ have been achieved. The trapped electrons are not accelerated in this device, but are used instead to create a strong potential well for ions.

In another series of experiments,[19] average electron densities of $10^{10} \, cm^{-3}$ have been achieved using inductive charging in toroidal device. A total charge of 100 microcoulombs has been trapped, which if accelerated to relativistic velocities would result in a current of 10 kA. With a time-independent vertical field and a transformer used to produce an inductive electric field, only small electron current (<50 A) is obtained. The results indicate that the electric cloud is not accelerated, but remains trapped in the torus.

Current interest has been focused on high-current nonneutral electron-beam acceleration.[20] Recently, a modified betatron configuration has been suggested[21-23] that employs a conventional weak-focusing betatron field and toroidal magnetic field. The principal advantage offered by the modified betatron is that the toroidal magnetic field reduces the required injection energy by containing the space-charge defocusing forces. Extensive analysis of this configuration has been carried out both analytically and numerically.[24-34]

Recent experiments employing inductive charging in a modified betatron configuration have achieved beam currents of approximately 200 A and energies of approximately 1 MeV using 30-kV injection voltage.[35] In an elongated or "stretched" modified betatron, beam currents of approximately 50 A at energies of 1 MeV have been achieved using 50-kV injection.[34]

Another approach to high-current cyclic accelerators is the use of linear induction modules in a cyclic configuration. One such scheme[3] has used a long-pulse linear induction module with beam recirculation through isolated beam paths for each transit through the induction module.[36] This configuration is essentially a folded induction linac. Yet another approach is to use a long-pulse induction module in a racetrack geometry. High currents can be handled by adding a toroidal magnetic field. This field introduces particle drifts in the bends, however, which can be averaged out by the addition of stellarator windings.[37] For reasonable parameters, the stellarator windings can contain particles with energies up to approximately 1 MeV per kilogauss of stellerator field on a 1-m radius of curvature bend,[38] based on single-particle numerical orbit integrations.

If a time-dependent vertical magnetic field is added to the bends in order to guide the beam, then the stellerator windings provide bandwidth for an energy mismatch between the beam energy and the matched energy in the vertical field. The matched energy in the vertical magnetic field is approximately 30 MeV/kG-m.[38]

The bandwidth can be important, not only because it allows one to handle beams with a significant variation in kinetic energy, but also because it reduces the sensitivity of the system to abrupt changes such as occur at accelerating gaps.

This paper describes an analysis of a configuration consisting of a combination of stellarator and betatron fields, called the stellatron.[40–43] The motivation, in part, has been to increase the allowed mismatch between the beam energy and the betatron field. In both the conventional and modified betatron, the allowed mismatch $\Delta\gamma/\gamma_0$ is given by

$$\frac{\Delta\gamma}{\gamma_0} \leq \tfrac{1}{2}(1-n)\frac{a}{r_0},$$

where n is the betatron field index and a/r_0 is the inverse aspect ratio of the accelerator chamber. Typically $a/r_0 = 0.1$ and so $\Delta\gamma/\gamma_0 \leq 2.5\%$ is the allowed bandwidth for mismatch in the conventional and modified betatron for $n = 1/2$. Since the vertical field at injection in several planned experiments is generally less than 100 G, field errors of a few gauss can cause loss of the beam.

By adding a stellarator field to a cyclic accelerator, a strong-focusing system is obtained that can sustain high currents and large mismatch between particle energy and vertical field. Stellarator fields are most simply characterized by two integers, l and m, these being respectively the number of field periods in the poloidal and toroidal directions in the device [see Eq. (3) and Fig. 3A below]. Two special cases have been treated in some detail. The $l = 2$ stellatron[40,41] is shown in Fig. 1. The stellarator field consists of a toroidal field plus a continuously twisted quadrupole field. The twisted quadrupole configuration is analogous to the alternating-gradient strong-focusing fields that are routinely utilized in modern synchrotrons.

The $l = 0$ stellatron shown in Fig. 2 is similar to a bumpy-torus fusion device with the addition of the betatron field. Here, the varying radial-field component leads to strong focusing. The $l = 1$ configuration has no transverse field gradient at the beam axis, and therefore is only weakly focused. Stellatrons with $l \geq 3$ are

ℓ = 2 SYSTEM — "STELLATRON"
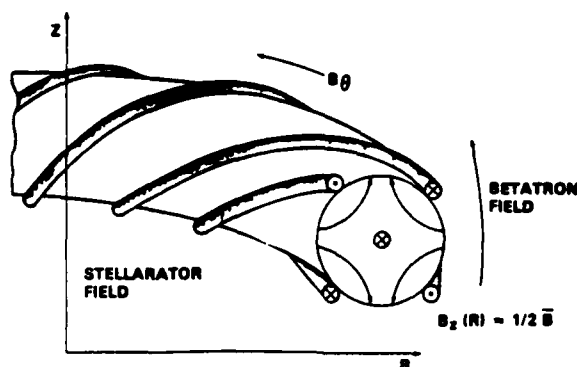
FIGURE 1   The *l* = 2 stellatron.

high-shear devices with low fields near the magnetic axis. The nonlinear proper-
ties of these configurations may be useful in conjunction with *l* = 0 or *l* = 2
focusing fields to provide detuning of orbital resonances.

In Section II, the stability properties of the *l* = 0 and *l* = 2 configurations are
derived, including the effects of the self fields of the beam. The particle tunes are
calculated. In Section III particle orbits for the conventional and modified
betatrons and the *l* = 0 and 2 stellatrons are calculated numerically and compared.
The energy-mismatch bandwidth of the stellatron is calculated as a function of the
focusing strength. The sensitivity of the particle orbits to the betatron field index
in the stellatron is also examined.

In Section IV, integer orbital resonances in the stellatrons are discussed. Integer
orbital resonances occur when the betatron "tune" (the number of betatron
wavelengths around the circumference) is an integer. In Section V, various

l = 0 SYSTEM — "BUMPY TORUS"
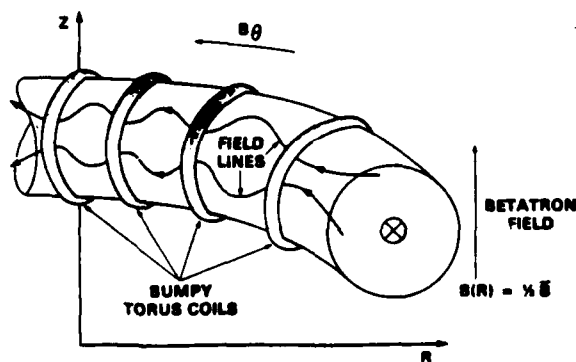
FIGURE 2   The *l* = 0 stellatron.

high-current injection schemes are described and the potential advantages offered by the stellatron are examined. Section VI is a discussion of the available literature (much of it unpublished), and Section VII presents a summary of the results.

II. PARTICLE ORBITS IN THE PARAXIAL APPROXIMATION

A linearized or paraxial analysis of particle orbits, valid for a particle that is "near" a circular design orbit with "nearly" the correct energy to be matched on that orbit, has been carried out to gain some quantitative understanding of particle behavior in the stellatron. Orbits of particles not satisfying these conditions must in general be found numerically, as discussed in the following section. The linearized analysis, however, yields important information about the frequency and the stability of the particle oscillations about the design orbit.

The analysis employs a general magnetic-field configuration which we describe in the coordinates of Fig. 3A. The applied fields consist, in part, of a vertical and radial "betatron" field of the form

$$\mathbf{B}^b \approx -\frac{nz}{r_0} B_{z0}\hat{r} + B_{z0}\left[1 - \frac{n(r-r_0)}{r_0}\right]\hat{z}, \tag{1}$$

where $(r, z) = (r_0, 0)$ is the location of the design orbit (assumed circular), B_{z0} is the vertical field at the design orbit, and n is the betatron field index. A toroidal field,

$$B_{\theta 0}\left[1 - \frac{r-r_0}{r_0}\right]\hat{\theta}, \tag{2}$$

is superimposed on (1), as well as a "stellarator" or multipole field which is written in the cylindrical approximation as the negative gradient of the scalar potential

$$\Phi^s(\rho, \phi, s) = -\frac{B_{s0}}{k} 2^l I_l(k\rho) \sin (l\phi + ks), \tag{3}$$

where $k = m/r_0$ and B_{s0} are constants and l and m, referred to as the poloidal and toroidal field numbers respectively, are taken as integers. In addition, s is defined to be $-r_0\theta$, so that (ρ, ϕ, s) is a righthanded system. The axis of the stellarator field is assumed to be aligned with the symmetry plane of the betatron field, $z = 0$.

Each of the fields (1)–(3) has its own special purpose. The betatron field (1), of course, acts simply to cancel the centrifugal force experienced by a circulating particle. In a stellatron, this field rises with the particle energy so that the betatron condition is (at least approximately) satisfied. The weak-focusing nature of (1), when n is between 0 and 1, which is crucial to the successful operation of betatrons, is of secondary importance to the stellatron. Stable orbits still occur in the stellatron when n is outside of the interval (0, 1). The stellatron configuration therefore has the virtue of being insensitive to errors in the vertical field or its gradient. This insensitivity has beneficial consequences in practical designs.
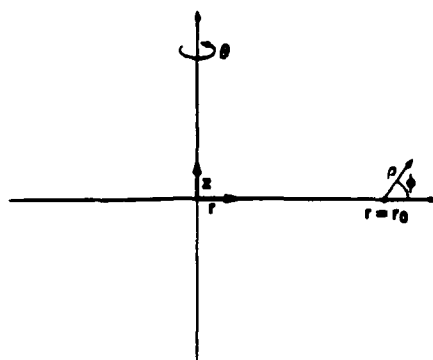
Fig. 3A
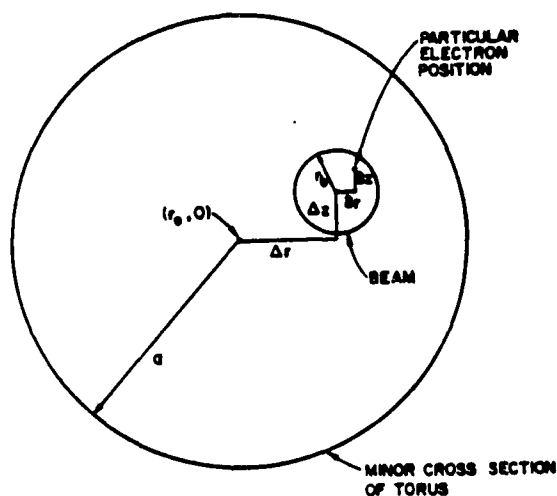
Fig. 3B

FIGURE 3   Geometry and coordinate systems. The origin in Fig. 3A is at the center of a torus of major radius r_0. Fig. 3B illustrates a cut along the minor cross section, showing the beam and individual particle positions.

A toroidal field (2) is added to the conventional betatron in the hope of increasing the contained current. Indeed, it has been found that with only fields (1) and (2) the beam densities which can be contained in equilibrium increase by a factor $(B_\theta/2B_z)^2$, for large B_θ, over those in a conventional betatron, (1). Additionally, the toroidal field acts to control the tune shift due to the effects of space charge. This feature is important when orbital resonances must be avoided.

The stellarator field (3) is added to provide the beneficial effects of alternating-gradient strong focusing. For $l = 0$ or 2, Eq. (3) gives an alternating gradient field component at the design orbit. This field greatly improves the momentum compaction over that of a configuration consisting of (1) and (2) only, and so

greatly relaxes certain design tolerances of the machine. Windings of other l-number may also be useful; in particular fields with $l \geq 3$ may help in controlling orbital resonances, but the analysis must be done numerically. The $l = 1$ field produces an oscillating magnetic field (not a field gradient) on the axis; such a configuration would not possess a circular design orbit and is not expected to possess any noteworthy focusing properties. This paper is concerned only with stellatrons having $l = 0$ (a "bumpy torus") and $l = 2$ (a "twisted quadrupole").

Since the stellatron is intended to carry large currents, it becomes important to consider the effects of the self fields of the beam. In general, this is an extremely hard problem. To make progress analytically, a simple model for these fields is assumed, consisting of a circular beam cross section (minor radius r_b) and uniform density with center located at $(r_0 + \Delta r, \Delta z)$ in a perfectly conducting cylindrical chamber of radius a (Fig. 3B). The self fields in the stellatron at the particle location $(r_0 + \Delta r + \delta r, \Delta z + \delta z)$ are given by

$$E_r = -2\pi n_0 e \left(\delta r + \frac{r_b^2}{a^2} \Delta r \right) \tag{4a}$$

$$E_\theta = 0 \tag{4b}$$

$$E_z = -2\pi n_0 e \left(\delta z + \frac{r_b^2}{a^2} \Delta z \right) \tag{4c}$$

$$B_r = \beta_0 E_z \tag{4d}$$

$$B_\theta = 0 \tag{4e}$$

$$B_z = -\beta_0 E_r \tag{4f}$$

in cgs units, where n_0 is the beam density, $-e$ is the electron charge, and $\beta_0 = v_0/c$ is the velocity of a particle on the design orbit normalized to the speed of light. In Eqs. (4a-f), the first term in each set of parentheses is due to the self field of the beam, while the second term is due to the image of the beam in the perfectly conducting wall. Toroidal corrections to Eqs. (4) may be important in some cases but are ignored here.

$l = 2$ Stellatron

The case $l = 2$ is considered first in detail since this case, rather than $l = 0$, corresponds most closely to a conventional quadrupole strong-focusing system. The $l = 2$ stellarator field near the axis is, from (3)

$$\mathbf{B}^s = kB_{c0}\{[z_1 \cos m\theta - r_1 \sin m\theta]\hat{r} + [r_1 \cos m\theta + z_1 \sin m\theta]\hat{z}\}, \tag{5}$$

where $r_1 = r - r_0$, $z_1 = z$. Taking the fields (1), (2), (4), (5) and using them in the equations of motion gives equations correct to first order in the small quantities r_1/r_0, $\Delta r/r_0$, z_1/r_0, and $\Delta z/r_0$

$$\ddot{r}_1 + \Omega_{z0}^2(1 - n + \mu \cos m\theta)r_1 - \frac{1}{2}\frac{\omega_b^2}{\gamma_0^2}\left(r_1 - \Delta r + \frac{r_b^2}{a^2}\Delta r \right)$$

$$= \Omega_{z0}\gamma_0^2 v_{\theta 1} - (\mu\Omega_{z0}^2 \sin m\theta)z_1 + \Omega_{\theta 0}\dot{z}_1 \tag{6a}$$

$$\ddot{z}_1 + \Omega_{z0}^2(n - \mu \cos m\theta)z_1 - \frac{1}{2}\frac{\omega_b^2}{\gamma_0^2}\left(z_1 - \Delta z + \frac{r_b^2}{a^2}\Delta z\right) = -(\mu \Omega_{z0}^2 \sin m\theta)r_1 - \Omega_{\theta0}\dot{r}_1 \quad (6b)$$

$$\dot{v}_{\theta1} = 0, \quad (6c)$$

where $\Omega_{z0} = eB_{z0}/m_e\gamma_0 c$, $\mu = kr_0 B_{s0}/B_{z0}$, $\omega_b^2 = 4\pi n_0 e^2/m_e\gamma_0$, m_e is the electron mass, and $v_{\theta1} = r_1\dot{\theta}_0 + r_0\dot{\theta}_1$. A subscript, 0, refers to quantities evaluated on the design orbit where $v_0/r_0 = \Omega_{z0}$ and dots denotes time derivatives.

As they stand, Eqs (6a–c) are not straightforward to solve since they involve both the motion of the particle about the beam center and the motion of the beam center about the design orbit. Since $r_1 = \Delta r + \delta r$ and $z_1 = \Delta z + \delta z$, separate solutions are required for (r_1, z_1) and $(\Delta r, \Delta z)$. A self-consistent set of equations for both beam-center motion and for motion of particles about the beam center may be found, however, by averaging (6a–b) over a distribution of particle initial conditions. Details of this averaging procedure are given in the Appendix. The result is that motion of the beam center is governed by the equations

$$\frac{\partial^2}{\partial\theta'^2}\Delta r + \left(1 - n - \frac{r_b^2}{a^2}n_s + \mu \cos m\theta'\right)\Delta r = \frac{c^2}{r_0\Omega_{z0}^2}\frac{\langle\gamma_1\rangle}{\gamma_0} - (\mu \sin m\theta')\Delta z + b\frac{\partial \Delta z}{\partial\theta'} \quad (7a)$$

$$\frac{\partial^2}{\partial\theta'^2}\Delta z + \left(n - \frac{r_b^2}{a^2}n_s - \mu \cos m\theta'\right)\Delta z = -(\mu \sin m\theta')\Delta r - b\frac{\partial \Delta r}{\partial\theta'}, \quad (7b)$$

where we have changed independent variables from (θ, t) to $(\theta', t') \equiv (\theta, t - \theta/\Omega_{z0})$, i.e., Eqs. (7a–b) describe the movement of the beam center as seen by a reference particle moving with angular velocity Ω_{z0}. In Eq. (7), the notation $n_s \equiv \omega_b^2/(2\gamma_0^2\Omega_{z0}^2)$, $b \equiv B_{\theta0}/B_{z0}$, and $\gamma_1 \equiv \beta_0\gamma_0^3\beta_1$ is introduced. In Eq. (7a), the quantity $\langle\gamma_1\rangle$ is just the ensemble average of the difference in energy between a particle and the reference particle, i.e. $\langle\gamma_1\rangle \equiv \langle\gamma - \gamma_0\rangle$. $\langle\gamma_1\rangle$ is independent of time and for a matched beam, $\langle\gamma_1\rangle = 0$. Once Eq. (7) is solved, the solution may be inserted into Eqs. (6a, b) which may then be solved for the location of any individual particle. The method used for solving Eq. (7) is described below, and may be used on Eq. (6) as well.

Equations (7a, b) may be completely solved in the special case $n = 1/2$, a fact which traces its origin to the poloidal symmetry this value of n imposes on the restoring forces experienced by the beam. Although the solution is special in this sense, it is expected to share most of its features with the solution for arbitrary n (which must be obtained numerically) since the particle focusing should be dominated by the quadrupole strength μ and only be weakly affected by the precise value of n. For $n = 1/2$, then, define the complex variable $\xi = (\Delta r + i\Delta z)/r_0$ for which Eqs. (7a, b) give the equation

$$\xi'' + ib\xi' + \left(\frac{1}{2} - \frac{r_b^2}{a^2}n_s\right)\xi + \mu e^{im\theta'}\xi^* = \langle\Delta\rangle \quad (8)$$

where $\langle\Delta\rangle$ is the momentum mismatch $\langle\gamma_1\rangle/(\beta_0^2\gamma_0)$. In Eq. (8), primes denote $\partial/\partial\theta'$ and an asterisk denotes complex conjugate. The further change of variable $\xi =$

$\psi e^{im\theta'/2}$ yields an equation with constant coefficients,

$$\psi'' + i(m+b)\psi' + \left(\frac{1}{2} - \frac{r_b^2}{a^2}n_s - \frac{mb}{2} - \frac{m^2}{4}\right)\psi + \mu\psi^* = \Delta e^{-im\theta'/2}, \tag{9}$$

the solution to which consists of a particular solution plus a sum of exponentials of the form $\psi_0 e^{\pm i\nu_\pm \theta'}$ where ψ_0 is a constant and $\nu_\pm$ are given by

$$\nu_\pm = [\hat{n} + \tfrac{1}{4}\hat{m}^2 \pm (\hat{n}\hat{m}^2 + \mu^2)^{1/2}]^{1/2}, \tag{10}$$

where $\hat{n} = 1/2 - r^2/a^2 n_s + b^2/4$, $\hat{m} = m + b$. A particular solution to Eq. (9) is

$$\psi_p = Ae^{im\theta'/2} + Be^{-im\theta'/2}, \tag{11}$$

where

$$A = \frac{\mu\langle\Delta\rangle}{\left[m^2 + mb - \frac{1}{2} + \frac{r_b^2}{a^2}n_s\right]\left[\frac{1}{2} - \frac{r_b^2}{a^2}n_s\right] + \mu^2} \tag{12}$$

$$B = \frac{\langle\Delta\rangle}{\frac{1}{2} - \frac{r_b^2}{a^2}n_s + \mu^2\left[m^2 + mb - \frac{1}{2} + \frac{r_b^2}{a^2}n_s\right]^{-1}}. \tag{13}$$

Referring back to the definitions of ξ and ψ, it is evident that B gives the "zero-frequency" part of the radial shift due to a beam with momentum mismatch $\langle\Delta\rangle$, that is, $B/\langle\Delta\rangle$ is the momentum compaction factor, which may be made small by choosing μ large. Setting $\mu = 0$ in Eq. (13) recovers the usual result for a conventional betatron or modified betatron. (Addition of a toroidal field to a conventional betatron does not affect momentum compaction.)

The small oscillations of the beam center are stable ($\nu_\pm$ are real) if and only if three conditions are satisfied

$$\hat{n} + \tfrac{1}{4}\hat{m}^2 > 0 \tag{14a}$$

$$(\hat{n} - \tfrac{1}{4}\hat{m}^2)^2 - \mu^2 > 0 \tag{14b}$$

$$\hat{n}\hat{m}^2 + \mu^2 > 0. \tag{14c}$$

These conditions are summarized in Fig. 4, where the stable region of parameter space is illustrated in terms of the auxiliary variables $u = 4\hat{n}/\hat{m}^2$ and $v = |\mu|/\hat{m}^2$. Typically one operates in the stable region with $u < 1$. The orbital stability requirement places strict limits on the size of μ that can be tolerated, i.e., strict limits on the achievable momentum compaction for given b and m. Any experiment must be designed so that u and v remain in the stable region for all time; a sample experimental trajectory is illustrated in the figure. For a low current beam $\hat{n}$ is positive and Eq. (14b) gives the only nontrivial condition

$$|\tfrac{1}{2}m^2 + mb - 1| > |2\mu| \tag{15}$$

The orbital stability criteria for individual particle motion within the beam are of identical form to Eqs. (14a–c) with the replacement, in the definition of $\hat{n}$, of
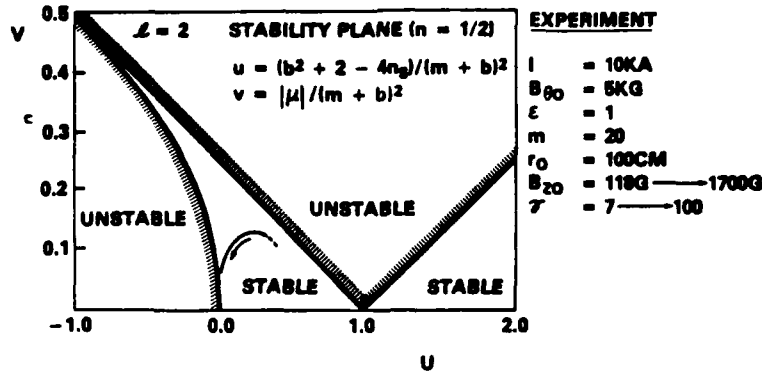
FIGURE 4   The $l = 2$ stability plane. u and v are defined in the text. The arrow indicates a sample experimental trajectory.

$(r_b/a)^2 n_s \to n_s$. That this is so may be seen by an analysis of Eqs. (6a, b) exactly parallel to that carried out for Eqs. (7a, b) considering that now, in Eqs. (6a, b), Δr and Δz are known quantities. With this substitution in Eq. (13), the zero-frequency term in the individual particle motion is obtained as

$$B_p = \frac{\Delta - \langle \Delta \rangle}{\frac{1}{2} - n_s + \mu^2(m^2 + mb - \frac{1}{2} + n_s)^{-1}},$$ (16)

where $\Delta = \gamma_1/\gamma_0 \beta_0^2$ is proportional to the energy difference between the individual electron energy and the matched beam energy. With $\mu = 0$, the results for a conventional betatron and a modified betatron are obtained. This solution with $\mu = 0$ suffers a loss of momentum compaction, i.e., $B_p \to \infty$, when n_s passes through $1/2$. In a conventional betatron, $n_s \leq 1/2$ is required for orbital stability. The modified betatron, however, would typically use $n_s \gg 1/2$ at injection, and would then pass through $n_s = 1/2$ during acceleration, since $n_s \propto \gamma^{-3}$. This transition at $n_s = 1/2$ corresponds to a momentary loss of equilibrium in the modified betatron as the configuration switches from a diamagnetic to a paramagnetic equilibrium.[26,27]

This transition can be avoided in the stellatron by using large $|\mu|$. The stability condition (14b), however, sets an upper limit to $|\mu|$ for a particular choice of m, b and n_s. The requirement on μ^2 may be expressed as

$$(n_s - 1/2)(m^2 + mb + n_s - 1/2) < \mu^2 < (n_s - 1/2 + m^2/4 + mb/2)^2.$$ (17)

For the condition (17) to be meaningful, n_s must satisfy

$$n_s - \frac{1}{2} < \frac{1}{2}\left(\frac{m}{2} + b\right)^2,$$ (18)

which is clearly compatible with $n_s \gg 1/2$. The $l = 2$ stellatron, therefore, can avoid a loss of momentum compaction during acceleration, while retaining the ability to use large n_s at injection.

$l = 0$ Stellatron

The $l = 0$ stellatron has fields given by

$$B_r^s = \tfrac{1}{2}B_{s0}mx \sin m\theta \tag{19a}$$

$$B_\theta^s = B_{s0} \cos m\theta \tag{19b}$$

$$B_z^s = \tfrac{1}{2}B_{s0}my \sin m\theta \tag{19c}$$

in a cylindrical (r, θ, z) coordinate system (Fig. 3), where $x = r_1/r_0$ and $y = z_1/r_0$. Using the procedure described above for linearizing the equations of motion in the displacement from a reference orbit and using the paraxial approximation for the electron motion with $n = 1/2$, the equations of motion for single electrons including beam self-fields may be expressed as

$$\psi'' + \frac{1}{m^2}[2 - 4n_s + b^2(1 + \varepsilon \cos 2\theta_m)^2]\psi = \frac{4}{m^2}\frac{\delta P}{P_0}\exp\left[\frac{ib}{2m}(2\theta_m + \varepsilon \sin 2\theta_m)\right], \tag{20}$$

where $\varepsilon = B_{s0}/B_{\theta 0}$, $\theta_m = m\theta/2$, P_0 is the momentum of a particle which is matched on the reference orbit, δP is the "momentum error", and

$$\psi = (x + iy) \exp\left[\frac{i}{2}\int b(1 + \varepsilon \cos m\theta)\, d\theta\right]. \tag{21}$$

In Eq. (20), n_s will in general depend on θ in a way governed by an envelope equation, thereby making the inclusion of self-field effects more difficult than for the $l = 2$ case in which a constant beam radius can be maintained.[57] Consequently, only single-particle orbits will be considered.

Equation (20) is a Hill equation, for which there are theorems concerning characteristic frequencies and stability.[44] The Floquet solutions to this equation for $n_s = 0$, are of the general form

$$\psi = e^{i\nu\theta m} \sum_{n=-\infty}^{\infty} C_n e^{i2n\theta_m}, \tag{22}$$

which display an infinite set of natural oscillations at the frequencies, $\nu \pm 2n$. The value of ν can be determined numerically for a given set of accelerator parameters, but the dependence of ν on these parameters is not known analytically.

It is possible to determine and display the regions of parameter space where ν is real, i.e., where the motion is stable. Starting with the homogeneous equation,

$$\psi'' + \frac{1}{m^2}[2 + b^2(1 + \varepsilon \cos 2\theta_m)^2]\psi = 0, \tag{23}$$

the solution $\psi(\pi)$, which satisfies $\psi(0) = 1$ and $\psi(0) = 0$ is constructed numerically. The stability condition[44] is $|\psi(\pi)| < 1$, which is illustrated in Fig. 5 for a particular example. The intersections of the unstable regions with the abscissa are given by

$$\frac{1}{m^2}(b^2 + 2) = q^2; \qquad q = 1, 2, \ldots \tag{24}$$

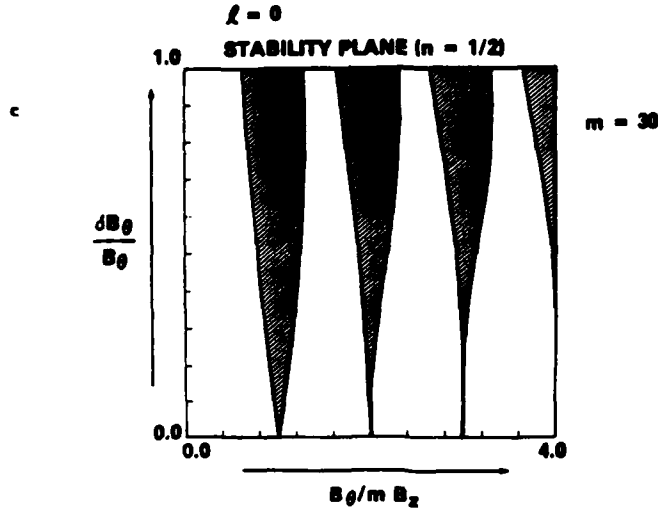which correspond to resonances between the "focusing frequency" which a

FIGURE 5   The $l = 0$ stability plane. The shaded regions are unstable.

particle experiences and its cyclotron frequency in the toroidal field. Under resonant conditions, there is a transfer of energy from longitudinal to transverse motion and the adiabatic invariance of the magnetic moment in the toroidal field is destroyed. During acceleration, if B_z is increased and B_θ is held fixed, the operating point on Fig. 5 will move from right to left. The accelerator should operate in the left-most stable band to avoid crossing unstable bands. At injection, therefore, $m > b$ is required, which implies the need for a large number of field periods. When space-charge effects are taken into account, one finds the stronger requirement, $m > 2b$, to avoid envelope instabilities.[64]

The momentum compaction factor for the $l = 0$ configuration may be calculated, for small values of ε and b/m, directly from Eq. (20). For $n_s = 0$, the result is

$$\frac{\delta x}{(\delta p/p_0)} = 2\left[1 - \left(\frac{\varepsilon b}{2}\right)^2 \frac{1}{1-(b/m)^2}\right] \tag{25}$$

which illustrates the helpful effect of the alternating gradient, as measured by ε, on the tolerance of the $l = 0$ device to momentum mismatch. When ε or b/m is large, numerical integration of the orbit equations is required.

III. NUMERICAL CALCULATION OF SINGLE-PARTICLE ORBITS

A computer code, which integrates the single-particle equations of motion, has been utilized to study nonlinear aspects of the stellatron configuration. The code solves the fully relativistic dynamical equations, without utilizing the paraxial

approximation for the electron motion or an expansion in the particle displacement from a reference orbit. The applied fields in the code include toroidal corrections to first order in the inverse aspect ratio. In addition, the code does not assume the field index to be 1/2.

The total magnetic field used by the code is the superposition of a conventional betatron field B_b and a stellarator field B_s. The conventional betatron field is given in Eq. (1). The stellarator field may be expressed as

$$\mathbf{B}_s = -\nabla \Phi_s \tag{26}$$

where ϕ_s is the magnetic scalar potential for the stellarator field. To first order in the inverse aspect ratio, ϕ_s has been given by Danilkin[45] as

$$
\begin{aligned}
\Phi_s(\rho, \phi, s) = -B_{\theta 0}\Bigg\{ & s + \frac{\varepsilon_l}{\alpha} I_l(x) \sin\left[l\phi - l\alpha s\right] \\
& -\frac{\kappa\varepsilon_l}{4l\alpha^2}\left[x^2 I_l'(x) - x(1+l)I_l(x)\right] \sin\left[(l+1)\phi - l\alpha s\right] \\
& -\frac{\kappa\varepsilon_l}{4l\alpha^2}\left[x^2 I_l'(x) - x(1-l)I_l(x)\right] \sin\left[(l-1)\phi - l\alpha s\right] \\
& +\frac{\kappa\varepsilon_l}{4l\alpha^2}\left[\frac{K_{l+1}(x_0) - x_0 K_{l+1}'(x_0)}{K_l'(x_0)} + x_0^2\right] I_{l+1}(x) \sin\left[(l+1)\phi - l\alpha s\right] \\
& +\frac{\kappa\varepsilon_l}{4l\alpha^2}\left[\frac{K_{l-1}(x_0) - x_0 K_{l-1}'(x_0)}{K_l'(x_0)} + x_0^2\right] I_{l-1}(x) \sin\left[(l-1)\phi - l\alpha s\right]\Bigg\},
\end{aligned} \tag{27}
$$

where $s = r_0\theta$, $x = l\alpha\rho$, $\alpha = 2\pi/L$, L is the helix pitch length, $\kappa = 1/r_0$, $x_0 = l\alpha\rho_c$, $\rho = \rho_c$ is the location of (assumed) wall surface currents, and I, K are the modified Bessel functions. The coordinates. (ρ, ϕ, s) are defined in Fig. 3. More generally, the field may be expressed as a superposition of fields of different l-number. This feature has not been included in the numerical model. In addition, beam image forces may be included in the model, but have not been utilized for any of the results presented in this section. The wave number, $k = m/r_0$, in the preceding analytical model is equivalent to $-l\alpha$.

Figure 6 shows single-particle orbits obtained with this code. The figure is the projection of the orbits onto the minor cross-section. The torus has a $1m$ major radius and $0.1m$ minor radius. The vertical magnetic field is fixed at $B_{z0} = 118$ G. corresponding to a matched particle (at the minor axis) with $\gamma_0 = 7$. The individual frames of Fig. 6 show a comparison of particle orbits in a conventional betatron, a modified betatron, an $l = 0$ stellatron and an $l = 2$ stellatron. Each frame shows two particle trajectories, one with positive mismatch and one with negative mismatch. All the trajectories are initialized on the minor axis with momentum parallel to the minor axis, and with various amounts of energy mismatch, $\Delta\gamma/\gamma_0$, as shown under each frame. The conventional and modified betatron frames demonstrate that these devices cannot tolerate mismatch, $\Delta\gamma/\gamma_0 = \pm 3\%$. In fact, using Eq. (12), we can estimate the tolerance of these devices to energy mismatch.

PARTICLE ORBITS
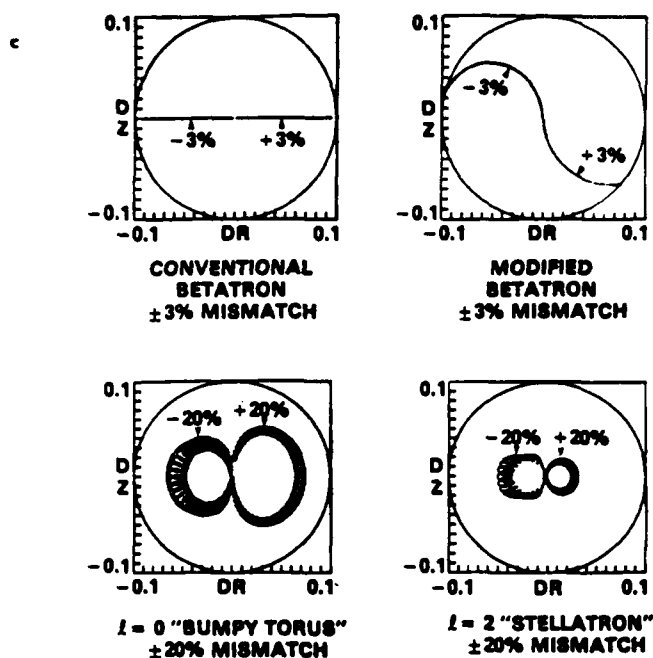
FIGURE 6   Particle orbits in conventional betatron, modified betatron, $l = 0$ stellatron, and $l = 2$ stellatron.

For $n_s(r_b/a)^2 \ll 1/2$, the allowed energy mismatch is given by

$$\frac{\Delta\gamma}{\gamma_0} \leq \frac{1}{4}\frac{a}{r_0}.$$ (28)

For $a/r_0 = 0.1$, we obtain $\Delta\gamma/\gamma_0 \leq 2.5\%$, which is consistent with the figure. The $l = 0$ and $l = 2$ stellatron configurations, on the other hand, can retain particles with more than $\Delta\gamma/\gamma_0 = \pm 20\%$ mismatch, as shown on the lower two frames of Fig. 6.

FIGURE 7   Energy bandwidth as a function of focusing strength ε for the $l = 0$ stellatron. ($n = 1/2$).

FIGURE 8 Energy bandwidth as a function of focusing strength e for the $l = 2$ stellatron. ($n = 1/2$).

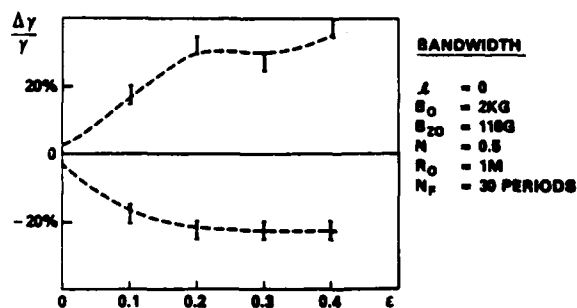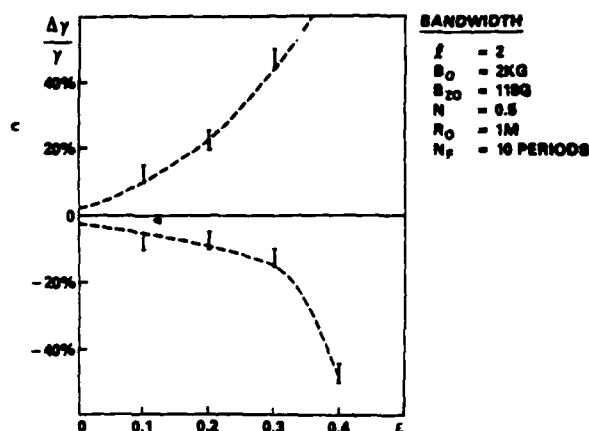The tolerance of the accelerator to mismatch between the average beam energy and the vertical magnetic field can be described as a bandwidth of allowed mismatch. For larger mismatch, the beam excursion from its reference orbit does not fit inside the accelerator aperture. The bandwidth, therefore, is essentially a measure of the momentum compaction of the accelerator. Since a calculation of the bandwidth involves particles with large $\Delta\gamma/\gamma_0$ that make large excursions from the reference orbit, the analytical formalism of the preceding section is inadequate.

By launching particles as shown in Fig. 6, with various $\Delta\gamma/\gamma_0$, the largest $|\Delta\gamma/\gamma_0|$ for which the particle is contained can be found. This bandwidth can be displayed as a function of any parameter of the accelerator. Figures 7 and 8, for example, show the bandwidth for the $i = 0$ and $l = 2$ stellatrons as the amplitude of the
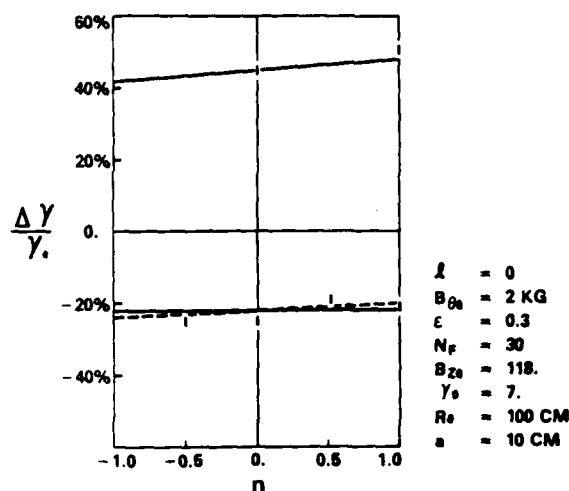

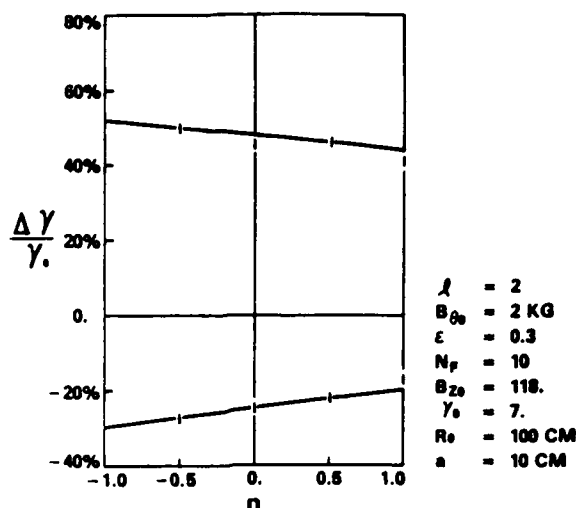FIGURE 9 Energy bandwidth as a function of vertical field index n at $e = 0.3$ for the $l = 0$ stellatron.

FIGURE 10 Energy bandwidth as a function of vertical field index n at $\epsilon = 0.3$ for the $l = 2$ stellatron.

strong focusing field is varied. In both devices, the bandwidth is $\pm 2.5\%$ in the limit where $\epsilon = 0$, and exceeds 20% for $\epsilon > 0.3$. For $l = 2$, the quantity, μ, in the preceding section is given by $\mu = \epsilon mb/2$, where $b = B_{\theta 0}/B_{z0}$.

Figures 9 and 10 show the bandwidth for the $l = 0$ and $l = 2$ stellatrons at $\epsilon = 0.3$ as the vertical field index is varied. The results here demonstrate the relative insensitivity of the stellatron configurations to the field index. The need to maintain good uniformity in the field index for a conventional or modified betatron drives the stored energy and cost for the vertical field coils (or leads to the use of iron) in those accelerators. The stellatron configuration greatly relaxes the need for such uniformity.

IV. ORBITAL RESONANCES IN THE STELLATRON

Until now, the applied fields in the stellatron have been assumed to be "perfect" in the sense that only the fields described analytically above in Eqs. (1-3) are present. In general, of course, a physical magnet system will have some imperfections leading to small field and focusing errors, which can be represented by additional terms in the paraxial equations. Generally these small errors lead to a small response but under certain conditions—when some rational number of particle wavelengths fit around the machine—the particle orbits can be violently disrupted. In this section, these resonance conditions are considered for the $l = 0$ and $l = 2$ stellatrons, and possible ways either to avoid them or to minimize their effects are discussed. It must be said however, that there is no reason why such resonances should be of any less concern in the modified betatron and stellatron class of devices than they are in more conventional cyclic accelerators in which

they are of course, of crucial importance in establishing an operating point. Though some of the high mode-number integer resonances might be successfully passed through, there is considerable reason to believe that major beam disruptions may occur at low-order resonance crossings, if such are attempted. This point is not often sufficiently stressed in the literature promoting the use of devices similar to some of those employed in magnetic-confinement fusion research to accelerate large currents to high energies.

This section will focus on the integer resonances, driven by the Fourier components of an error in the vertical field, though others may also be important. The tune shift due to space charge will also be neglected at first, to consider the resonant response of single particles.

As in the previous section, the $l = 2$ case, for which the tunes may be explicitly calculated [Eq. (10)], is considered first. For single-particle motion, the four possible "betatron" frequencies are $m/2 \pm \nu_\pm$ where $\nu_\pm$ satisfies the biquadratic,

$$\nu^4 - (\tfrac{1}{2}m^2 + mb + b^2 + 1)\nu^2 + \tfrac{1}{4}(\tfrac{1}{2}m^2 + mb - 1)^2 - \mu^2 = 0. \tag{29}$$

The most general resonance condition is written

$$n_1\left(\frac{m}{2} + \nu_+\right) + n_2\left(\frac{m}{2} - \nu_+\right) + n_3\left(\frac{m}{2} + \nu_-\right) + n_4\left(\frac{m}{2} - \nu_-\right) = p, \tag{30}$$

where $n_1, \ldots, n_4$, p are all integers; this condition applies to all types of resonant driving terms. Integer resonances occur when all n_j except one, n_k, vanish and $p/n_k = n$ is itself an integer, the Fourier mode number of the field error. When an integer resonance occurs, the displacements which a particle undergoes on successive encounters with a field "bump" add in phase and the result can be loss of the particle from the machine.

Figure 11 shows the integer resonance contours $1, 2, \ldots, 10$ in the $b - \mu$ plane for $m = 20$. (The n and $m - n$ contours coincide.) The resonance contours are all hyperbolae, from Eq. (29); the stability boundary coincides with the degenerate case $n = m/2$. Ideally, an accelerator should be designed to avoid all resonance contours, a design which may clearly be realized by holding b and μ fixed during acceleration (neglecting the tune shift due to space charge, which may, in fact, limit the current in this as in other cyclic devices). If b and μ are allowed to change during acceleration, it may be possible to pass through at least some of the integer resonances, though this is only speculation based on a few computer studies. The possibility of passing through resonances in the stellatron is discussed further below.

The resonance situation in the bumpy torus is somewhat less straightforward to analyze. In the presence of an error in the vertical field having Fourier mode number k, a term of the form

$$(\text{const}) \cdot \exp\left[2ik\theta_m/m + (ib/2m)(2\theta_m + \varepsilon \sin 2\theta_m)\right] \tag{31}$$

is added to the right-hand side of Eq. (23), where the multiplicative constant is proportional to the magnitude of the field error. One may employ the Green's function constructed from the Floquet solutions to Eq. (23) to deduce that a

L=2 PLANE
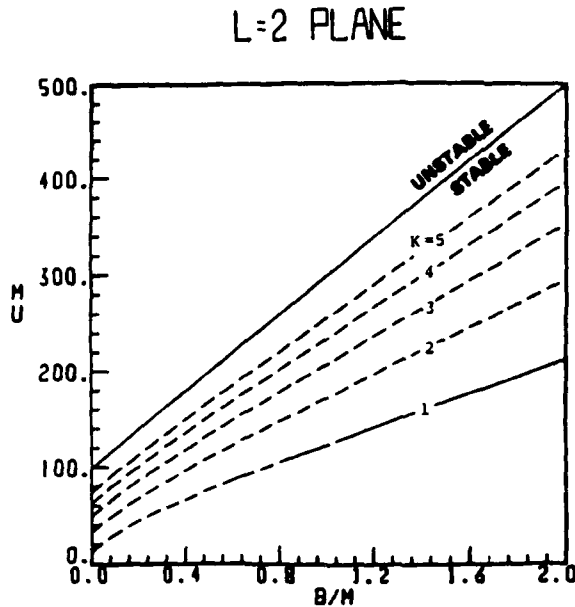
FIGURE 11   Integer-resonance contours in the $b/m - \mu$ plane for the $l = 2$ ste... .-:.

secular term, proportional to θ_m, will occur in the particular solution if

$$\cos \pi\left(\frac{b+2k}{m}\right) = \psi_1(\pi), \tag{32}$$

where ψ_1 is the solution to the homogeneous equation satisfying $\psi_1(0) = 1$, $\psi_1'(0) = 0$. Contours along which Eq. (32) is satisfied may be generated numerically for each k in the $b/m - \varepsilon$ plane; an example is shown in Fig. 12. Note the behavior of the $k = 0$ resonance line, which crosses other k-lines at $b/m = 2 - k/m$ in the second stable band. A $k = 0$ field error is equivalent to a momentum error, so one expects momentum compaction to be poor near the $k = 0$ contour. It is unlikely, however, that one would try to operate in the second stable band.

It is clear that the "stable" regions of Fig. 12 are in fact criss-crossed with potentially dangerous resonance lines which must either be avoided or crossed somehow during the course of an experiment. The operating point of an accelerator may be held fixed in the plane, of course, by raising all fields in synchronism, i.e., by keeping $\varepsilon = \delta B_\theta/B_{\theta 0}$ and $b = B_{\theta 0}/B_{z0}$ fixed for all time. It is worth considering the feasibility of crossing these resonances, however, since increasing all the fields together has definite large costs in terms of field energy. It might be desirable, for instance, to accelerate while keeping $B_{\theta 0}$ and $\delta B_{\theta 0}$ fixed in time, allowing the tunes to change as b does. The immediate question is, "can resonances be passed through without major disruption of the beam?"

Since resonances occur when the number of betatron wavelengths completed in one major revolution (i.e., the "tune") is an integer, half-integer, or other rational
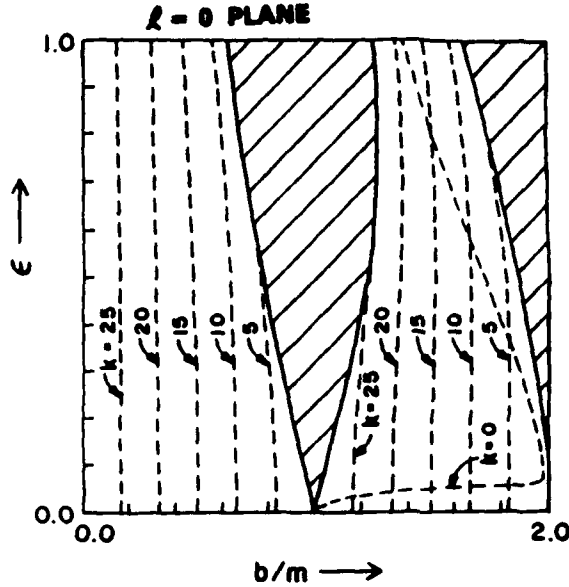
FIGURE 12 Integer-resonance contours in the $b/m - \varepsilon$ plane for the $l = 0$ stellatron.

number, a possible solution may consisting of setting constant tune by allowing the particle reference orbit to have a variable major radius (i.e., to be noncircular). The FFAG accelerator works in this fashion, and achieves constant tunes by forcing "self-similar" orbits during acceleration. A conventional betatron is the special case where the self-similar orbits also have constant radius. With addition of a toroidal field which varies as r^{-1}, however, there is no nonsynchronous field solution with constant tune, as shown below.

The single-particle tunes ($n_s = 0$) in a stellatron depend on the poloidal and toroidal field numbers (l and m), which are assumed fixed, as well as on the field ratios, $b = B_{\theta 0}/B_{z0}$ and $\varepsilon = B_{s0}/B_{\theta 0}$, at the reference orbit. In a modified betatron, the tunes depend only on b. The B_θ and B_z fields have the assumed dependence

$$B_\theta = B_{\theta 0}(t)\frac{r_0}{r} \tag{33a}$$

$$B_z = B_{z0}(t)\left(\frac{r_0}{r}\right)^n. \tag{33b}$$

At $t = 0$, the particle is assumed to be matched at $r = r_0$; hence (for a relativistic particle)

$$r_0 = \frac{mc^2}{e}\frac{\gamma(0)}{B_{z0}(0)}.$$

During acceleration, the particle is allowed to move its matched radius to $r(t)$,

satisfying

$$r(t) = \frac{mc^2}{e} \frac{\gamma(t)}{B_z(r(t), t)}$$

$$= \frac{mc^2}{e} \frac{\gamma(t)}{B_{z0}(t)} \left[\frac{r(t)}{r_0} \right]^n,$$ (35)

or solving for $r(t)$,

$$r(t) = r_0 \left[\frac{mc^2}{er_0} \frac{\gamma(t)}{B_{z0}(t)} \right]^{1/(1-n)}.$$ (36)

If b = constant at $r = r(t)$ is required to fix the tune,

$$b = \frac{B_{\theta0}(t)}{B_{z0}(t)} \left(\frac{r_0}{r(t)} \right)^{1-n}$$

$$= \frac{er_0}{mc^2} \frac{B_{\theta0}(t)}{\gamma(t)} = \text{constant},$$ (37)

which implies that $B_{\theta0}$ must increase synchronously with γ during acceleration. In the stellatron, the requirement for fixed tunes is that both b and ε be fixed separately. This demonstration that b cannot be fixed if the toroidal field is asynchronous with γ, therefore, applies to both the stellatron and the modified betatron. It is therefore not possible to fix the tunes in a modified betatron or stellatron with an asynchronous toroidal field that varies as r^{-1}.

Another possibility for controlling the growth of single-particle resonances may be to use nonlinear focusing fields to de-tune the resonance by making the tunes a function of the amplitude of the particle displacement. The Bessel functions which describe the $l = 0$ or $l = 2$ transverse fields, of course, already provide such a nonlinearity. The use of $l = 3$ fields in conjunction with a modified betatron or $l = 0, 2$ stellatron provides a high-shear nonlinear field which may be of benefit for the control of resonances.

Rapid acceleration of the beam may also provide a means of avoiding damage due to resonances by rapidly accelerating through them. Since the betatron wavelength depends on the particle energy, a stellatron with sufficient energy gain per pass will traverse a resonance before the beam can respond. This possibility has been addressed in the numerical calculation shown in Fig. 13. The first frame shows a stable electron orbit with $\gamma = 49$ and with no field error. In the next frame, a 2% integer field error ($n = 1$) is superimposed on the stellatron fields, and the unaccelerated electron trajectory is rapidly lost to the wall. The lower two frames show the effects of high-gain acceleration through the resonance. At a gain of 3 MeV/pass, the particle motion is essentially contained.

This result suggests that a high-gain stellatron accelerator, with rapidly varying fields, may be desirable. Such a device will not only be beneficial for the control of single-particle resonances, but also will have a shorter acceleration time than conventional betatrons, and will therefore be less sensitive to several collective instabilities. Resistive-wall instabilities, for example, are ineffective if the acceleration time is $\leqslant 100 \mu\text{sec}$.
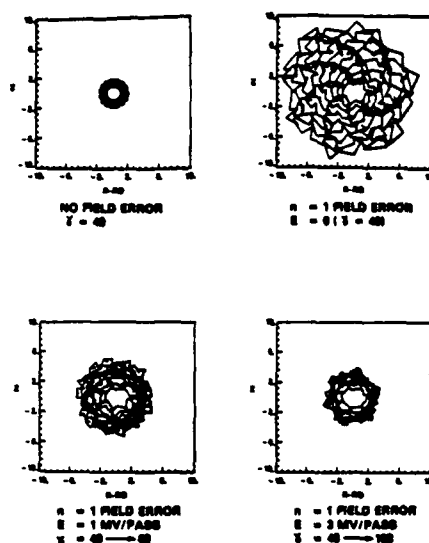
RESONANT ORBITS IN THE STELLATRON

FIGURE 13 Effect of acceleration through a resonance on transverse particle motion.

To allow field penetration in a fast stellatron, the vessel will have to be slotted, and acceleration will then occur primarily at the slots or gaps. The particles will therefore be unavoidably mismatched as they move between slots. The stellatron focusing can tolerate this mismatch, and is therefore compatible with this type of device.

V. INJECTION

Injection into a high-current cyclic accelerator is a challenge. The toroidal field lines that contain the space charge of the beam must be crossed or perturbed to get the beam in. A number of experiments have been carried out in similar geometries using inductive charging,[18,19,35] magnetic diverters,[46,47] and drift injection.[48] A self-synchronous scheme, using the current in the cathode shank to make a magnetic diverter, has been used to inject 50 percent of a 500-kV 20-kA 50-μsec beam into a racetrack torus.[47] These experiments by Gilad et al. and Benford et al. involve injecting the beam into neutral gas. A 450-keV 16-kA 25-μsec beam has been injected into a toroidal magnetic field in a hard vacuum[49] to obtain a trapped beam current of 300 A and a quiescent equilibrium for 20 μsec, which is approximately 3000 revolutions around the torus.

Recent experiments[50] have been carried out in which the torus is filled using a plasma gun. The spatial plasma-density profile is controlled by adjusting the direction of plasma injection or the timing between the gun firing and the

application of the pulse to the cathode. The plasma makes contact with both the cathode and the chamber wall. When the cathode is pulsed negatively, a double-layer plasma sheath appears, and the electrons of the cathode plasma are accelerated in the sheath and ejected into the plasma. With a 1.2-MV 80-μsec pulse, a current of 50 to 80 kA can be injected into the plasma. When the ring radius is held constant, the 40-kA ring decays to approximately half of its value in 400 μsec. When the ring is compressed, the 25-kA ring current increases to 50 kA and is contained for about 4 msec.[57]

Recently an axial pinch scheme has been proposed for injecting electrons across magnetic field lines into the NRL modified betatron.[52]

None of the prior experience has established a widely accepted solution to the injection problem. There are, nevertheless, several features of the stellatron field configuration that may be important from the standpoint of designing an injection scheme. The present discussion will be limited to the $l = 2$ stellatron.

The stellatron field has a separatrix within which the magnetic surfaces are closed and beyond which field lines run to the outside world. Injection along magnetic field line: can be used to place a beam just outside the separatrix. A fast-rising coil may be used locally to slip the separatrix over the beam, thus trapping it. Since the separatrix is a null field, it can be moved through the beam.

The rotational transform of the particle orbits due to the helical fields can be utilized to move the beam electrons away from an internal injector. Electrons can be forced to miss the injector for many revolutions of the accelerator. Figure 14 shows a beam injected at $\Delta r = 8$ cm, $\Delta z = 0$ moving in the toroidal direction with no transverse motion. The beam is injected with $I = 10$ kA, $\gamma = 7$ into fields,
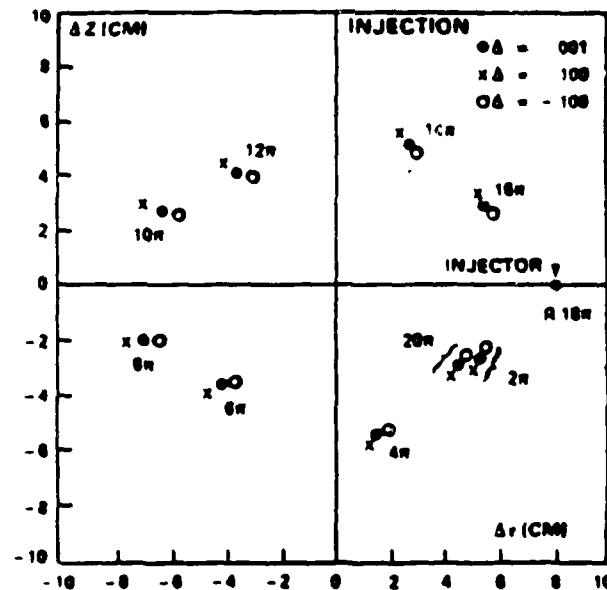

FIGURE 14   Location of beam center after injection.

$B_{\theta 0} = 5$ kG, $\varepsilon = 0.5$, $B_{z0} = 118$ G, $n = 0.5$. The analytical formalism developed in Section 2 is used to track the beam center around the torus. The points marked 2π, 4π, 6π, ... on the figure represent the location of the beam center after completing $\frac{1}{c}$, 2, 3, ... transits of the torus. Approximately nine revolutions (200 μsec) are required to bring the beam electrons back to the vicinity of the injector. The open circles, filled circles and x's on the figure represent the injection of beams having $\Delta\gamma/\gamma_0 = 0.1\%$ mismatch, and $\pm 10\%$ mismatch. The injection dynamics are very insensitive to this mismatch. During the approximately 200ns required for the beam to return to the injector, the focusing fields must be changed to trap the electrons. A small change of the helical field (e.g., variation of ε) during injection may be effective in trapping the beam.

VI. DISCUSSION OF EARLIER WORK

During the course of this work, a number of people have pointed out related unpublished work. In particular, a report on a plasma betatron that has tested a field configuration similar to the $l = 2$ stellatron has been recently brought to our attention.[53] The device consists of a betatron field together with toroidal, helical, and multipole field capability to study plasma containment configurations. The addition of a betatron field to the system is motivated by the production of runaway electrons observ d in the ORMAK tokamak.[15] Acceleration is obtained by changing the flux in a central solenoid. The field at the equilibrium orbit from this solenoid is nulled to zero by compensating coils. A separate set of programmable vertical-field coils is used to provide the equilibrium. One of the reasons given for driving the vertical field coils separately is that the 2-to-1 flux rule is not valid for currents comparable to the Alfven current,[53] due to self-field effects.

The equilibrium beam production in a plasma betatron is complex. The energetic beam is composed f runaway[54] electrons. The current due to those electrons that do not run away is generally an order of magnitude higher than the runaways. The vertical field is set to provide an equilibrium for the plasma currents. The interpretation of the limiting energy of the plasma betatron in terms of the work presented in this paper is as follows. The plasma currents provide a rotational tranform that contains the high-energy particles. This transform can be converted into an effective energy bandwidth. As the energy of the particles increases, the mismatch between the parallel energy and vertical field increases. Since the vertical field must be programmed to maintain the plasma-current equilibrium, this mismatch will grow until the beam orbit size exceeds the dimensions of the chamber. Hence, the maximum energy in a plasma betatron will be the bandwidth provided by the plasma current and the energy of the equilibrium orbit due to the vertical field. Runaway electrons with energies of a few megavolts are not unusual in tokamaks, and a 1.5-MeV beam has been produced in a plasma betatron. In the Livermore plasma-betatron experiment, the beam energy is several hundred kilovolts and the beam current is about 10 A. The plasma current is 10 kA.

The complexity of forming a beam from runaways makes the interpretation of

the Livermore results ambiguous. With the helical field, the observed runaway production is approximately 10 times more intense and occurs at a much lower pressure, indicating that the helical field configuration confines single particles, but that an azimuthal current is necessary to continue the runaways in the absence of a helical field. Without the helical field, the x-ray burst from the beam hitting the wall occurs at approximately 200 μsec. With the helical field, the x-ray burst occurs at 800 μsec. The observed energy is only 200 keV, however, which is only a fraction of what should be obtained if acceleration occurs throughout the pulse.

R. Moir has sent results from interesting work that used an $\mathbf{E} \times \mathbf{B}$ injector in a racetrack geometry.[56] The trajectories of an $l = 2$ helical field combined with a vertical field on one of the bends of a racetrack geometry is studied at low energies. Resonant and nonresonant diffusion of very low current electron beams has been studied. The beam makes 100 transits when the stellerator winding is on, which is about a factor of 5 better than without the stellarator windings.

The stability plane for continuously rotated magnetic quadrupoles in a linear transport system has been obtained previously.[57] A stability plane similar to Fig. 4 results.

In a series of early experiments[58] at the Naval Research Laboratory, D.C., de Packh has combined a betatron and solenoidal lens fields. The excessive currents required to raise the solenoid lens synchronously so as not to cross resonances causes excessive heating. He has also tested a combination betatron and air-core quadrupole system that can be programmed so that no resonance are crossed. With a 55 keV injection voltage he has injected and accelerated a 1/2 amp beam to 2 MeV.

J. D. Lawson has pointed out some early work on particle orbits in a betatron with a toroidal magnetic field.[59] The coupling between the radial and vertical betatron oscillations due to the toroidal field is examined. This work has been motivated by some experiments in which the addition of an 8 gauss toroidal magnetic field to a conventional betatron reduces the output by 75%, largely because the injected electrons follow the toroidal field lines and intercepted the injector structure after one revolution.

In recent experiments at Cornell University[60] an electron ring, confined in a cold, partially ionized hydrogen plasma has been transported into a modified betatron field configuration and accelerated. The energy of the beam is increased from 1.1 to 3.3 MeV. Although there is no direct evidence of instabilities, the ring current decreases from 3 kA to 1.5 kA during the acceleration.

Recently, a periodic magnetic-focusing system for a high-current cyclic system has been suggested.[61] The toroidal field consists of a series of magnetic cusps. The paraxial equation for this configuration may be obtained from Eq. (20) taking $b \rightarrow \infty$ and $\varepsilon \rightarrow 0$ with $b\varepsilon$ fixed. Injection can take place on the open field lines and the nonlinear focusing of the cusp may give a sufficient tune shift to detune the single-particle resonances.

VII. SUMMARY

The addition of continuous strong focusing fields to a betatron or modified betatron leads to a new configuration that has a large tolerance to mismatch

between the particle energy and the vertical magnetic field, thereby relaxing both mechanical and electrical design requirements on the accelerator and the injector. The allowed mismatch bandwidth obtained by strong focusing is especially attractive for $_c$ high-current accelerators, and is compatible with operation at high energy gain per pass.

Strong focusing also offers the advantage of introducing a threshold, γ_T, for the onset of the negative mass instability. For $\gamma < \gamma_T$, there is no negative-mass instability. The threshold is $\gamma_T \approx 13$ for typical stellatron parameters.[40,41] The addition of stellarator windings to a betatron has not yet been analyzed in detail for its effect on collective instabilities. Other issues which are as yet unresolved include the evaluation of methods for avoiding orbital resonances and the demonstration of a beam injection technique.

The strong focusing associated with the stellatron allows a configuration to be designed with $n_s \gg 1/2$ at injection which will operate without passing through a disruptive diamagnetic-to-paramagnetic equilibrium transition[26,27] during acceleration. The modified betatron, on the other hand, suffers an instantaneous loss of momentum compaction as n_s passes through the value, 1/2, during acceleration.

Of the various l-number stellatrons, only the $l = 0$ and $l = 2$ configurations provide a finite transverse field gradient at the beam axis. Both configurations allow a large mismatch between the average beam energy and the equilibrium beam energy for the applied vertical field. Both are also relatively insensitive to the vertical field index. The $l = 0$ system appears easier to construct, but stability during acceleration requires the use of a large number of field periods, i.e. $m \geq b$. The $l = 2$ configuration, on the other hand, requires a more complicated (quadrupole) field, but does not require a large number of field periods for stable operation; the field can be generated using modular coils.[62,63]

An objective of this study has been to describe a multi-kiloampere cyclic electron accelerator concept which is compatible with injectors based on Marx pulseline technology. Such injectors are limited to electron energy of a few MeV, and the accelerator must therefore tolerate significant beam self-fields at injection. These fields can lead to substantial beam emittance as well as beam mismatch with the vertical magnetic field. In addition, the Marx pulseline technology itself is limited in the voltage ripple and the shot-to-shot voltage reproducibility that can be achieved at reasonable cost. The accelerator must be able to tolerate such uncertainties in the injected beam parameters on each shot. The stellatron configurations described here have a large tolerance both to beam emittance and to beam mismatch, which makes this concept attractive for handling high currents and for mating to a Marx pulseline injector.

As this paper was being completed, encouraging experimental results from a group at the University of California at Irvine were reported to us.[66] A 200-A beam has been accelerated to 2 MeV in a small $l = 2$ stellatron device; smaller currents have been accelerated to 4 MeV in the same experiment.

VIII. ACKNOWLEDGEMENTS

Accelerator Project in the NRL Plasma Physics Division. We particularly appreciate the encouragement of T. Coffey.

REFERENCES

1. K. R. Prestwich, D. E. Hasti, R. B. Miller and A. W. Sharpe, *IEEE Trans. Nucl. Sci.* **NS-30**, 3155 (1983).
2. G. J. Caporaso *et al.*, Proc. 5th Intl. Top. Conf. on High-Energy Electron and Ion Beam Research and Technology (San Francisco, CA, 1983).
3. J. E. Leiss, N. J. Norris and M. A. Wilson, *Part. Accel.* **10**, 223 (1980).
4. B. Kulke, D. S. Ravenscroft and G. E. Vogtlin, *IEEE Trans. Nucl. Sci.* **NS-28**, 2882 (1982).
5. R. B. Miller *et al.*, *IEEE Trans. Nucl. Sci.* **NS-28**, 3343 (1981).
6. R. Avery *et al.*, *IEEE Trans. Nucl. Sci.* **NS-18**, 479 (1971).
7. D. W. Kerst, *Phys. Rev.* **58**, 841 (1940).
8. D. W. Kerst, G. D. Adams, H. W. Koch and C. S. Robinson, *Phys. Rev.* **78**, 297 (1950).
9. A. I. Pavlovskii, D. G. Kuleshov, A. I. Gerasimov, A. P. Klementev, V. D. Kuzemtsov, V. A. Tananakin and A. D. Turasov, *Sov. Phys. Tech. Phys.* **22**, 218 (1977).
10. J. M. Peterson, "Betatrons with Kiloampere Beams," LBL reprint, LBL 15206 (1982); Proc. 7th Conf. on Applications of Accelerators in Research and Industry (Denton, Texas, 1982).
11. K. R. Symon, D. W. Kerst, L. W. Jones, L. J. Laslett and K. M. Terwilliger, *Phys. Rev.* **103**, 1837 (1956).
12. L. A. Ferrari and K. C. Rogers, *Phys. Fluids* **10**, 1319 (1967); J. G. Linhart, Proc. 4th Intl. Conf. on Ionized Phenomena in Gases (North Holland Publ. Co., 1960), p. 981.
13. N. C. Christofilos, unpublished, (1950).
14. E. Courant, N. S. Livingston and H. Snyder, *Phys. Rev.* **88**, 1190 (1952).
15. D. A. Spong, J. F. Clarke and J. A. Rome, "Relativistic Electron Production in the Ormak Device", ORNL-TM-4120 (1973).
16. W. Bernstein, F. F. Chen, M. A. Head and A. Z. Kramz, *Phys. Fluids* **5**, 430 (1958).
17. G. S. Janes, R. H. Levy, H. A. Bethe, and B. T. Feld, *Phys. Rev. Lett.* **145**, 925 (1966), J. D. Daugherty, J. E. Eninger and G. S. Janes, *Phys. Fluids* **12**, 2677 (1969).
18. G. S. Janes, *Phys. Rev. Lett.* **15**, 135 (1965).
19. W. Clark, P. Korn, A. Mondelli and N. Rostoker, *Phys. Rev. Lett.* **37**, 592 (1976).
20. N. Rostoker, *Part. Accel.* **5**, 93 (1973).
21. P. Sprangle and C. A. Kapetanakos, *J. Appl. Phys.* **49**, 1 (1978).
22. N. Rostoker, *Comments Plasma Phys. Controlled Fusion* **6**, 91 (1980).
23. P. Sprangle, C. A. Kapetanakos, and S. J. Marsh, in Proceedings of the International Topical Conference on High-Power Electron and Ion Beam Research and Technology, Palaiseau, France, 1981, p. 803.
24. C. A. Kapetanakos, P. Sprangle and S. J. March, *Phys. Rev. Lett.* **49**, 741 (1982); C. A. Kapetanakos, P. Sprangle, D. P. Chernin, S. J. Marsh and I. Haber, *Phys. Fluids* **26**, 1634 (1983).
25. P. Sprangle and J. Vomvoridis, Naval Research Laboratory Report 4688 (1982).
26. D. P. Chernin and P. Sprangle, *Part. Accel.* **12**, 85 (1982); *Part. Accel.* **12**, 101 (1982).
27. John M. Finn and Wallace M. Manheimer, *Phys. Fluids* **26**, 3400 (1983); Wallace M. Manheimer and John M. Finn, *Part. Accel.* **14**, 29 (1983).
28. Wallace M. Manheimer, *Part. Accel.* **13**, 209 (1983).
29. R. C. Davidson and H. S. Uhm, *Phys. Fluids* **25**, 2089 (1982).
30. T. P. Hughes, M. M. Campbell and B. B. Godfrey, *IEEE Trans. Nucl. Sci.* **NS-30**, 2528 (1983).
31. G. Barak, D. Chernin, A. Fisher, H. Ishizuka and N. Rostoker, "High Current Betatron," Proc. of

the 4th Int'l. Conf. on High-Power Electron and Ion Beam Research and Technology (Palaiseau, France, June 29–July 3 1981) Vol. II, pp. 795ff.

32. G. Barak and N. Rostoker, *Phys. Fluids* **26**, 856 (1983).

33. G. Roberts and N. Rostoker "Analysis of Modified Betatron with Adiabatic Particle Dynamics," Proc. of the 5th Intl. Conf. on High Power Electron and Ion Beam Research and Technology (San Francisco, California, 1983).

34. N. Rostoker, "High Current Betatron Experiments and Theory," Proc. of the 5th Intl. Conf. on High Power Electron and Ion Beam Research and Technology (San Francisco, California, 1983).

35. B. Mandelbaum, H. Ishizuka, A. Fisher and N. Rostoker, "Behavior of Electron Beam in a High Current Betatron," Proc. of the 5th Intl. Conf. on High Power Electron and Ion Beam Research and Technology, (San Francisco, California, 1983).

36. M. A. D. Wilson, *IEEE Trans. on Nucl. Sci.* **NS-28**, 3340 (1981).

37. C. W. Roberson, *IEEE Trans. on Nucl. Sci.* **NS-28**, 3433 (1981).

38. A. A. Mondelli and C. W. Roberson, "Energy Scaling Laws for the Racetrack Induction Accelerator," NRL Memorandum Report No. 5008 (1982), to be published in Particle Accelerators; "A High-Current Induction Accelerator" *IEEE Trans. on Nucl. Sci.* **NS-30**, 3212 (1983).

39. K. M. Young, *Plasma Physics* **16**, 119 (1974).

40. C. W. Roberson, A. A. Mondelli and D. Chernin; *Phys. Rev. Lett.* **50**, 507 (1983).

41. C. W. Roberson, A. A. Mondelli and D. Chernin; "The Stellatron—A Strong Focusing High Current Betatron" *IEEE Trans. Nucl.* **NS-30**, 3162 (1983).

42. A. A. Mondelli, D. Chernin and C. W. Roberson, "The Stellatron Accelerator," Proc. of the 5th Intl. Conf. on High Power Electron and Ion Beam Research and Technology (San Francisco, California, 1983).

43. D. Chernin, A. A. Mondelli and C. W. Roberson, *Phys. Fluids* **27**, 2378 (1984).

44. W. Magnus and S. Winkler, *Hill's Equation*, Dover Publications, Inc., New York, 1979.

45. I. S. Danilkin, in *Stellarators*; Proc. of the P. N. Lebedev Physics Inst., D. V. Skobel'tsyn, ed. (Consultants Bureau, New York, 1979), Vol. 65, pp. 23 ff.

46. D. F. Brower, B. R. Kusse and G. D. Meixel, Jr., *IEEE Trans. on Plasma Sci.* **PS-2**, 193 (1974).

47. P. Gilad, B. R. Kusse and T. R. Lockner, *Phys. Rev. Lett.* **33**, 1275 (1974).

48. J. Benford *et al.*, *Phys. Rev. Lett.* **31**, 346 (1973). J. Benford, J. Guillory and C. Stallings, *J. Appl. Phys.* **45**, 1657 (1974); J. Benford, B. Ecker and V. Bailey, *Phys. Rev. Lett.* **33**, 574 (1975).

49. A. Mohri, M. Masuzaki, T. Tsuzuki and K. Ikuta, *Phys. Rev. Lett.* **34**, 574 (1975).

50. A. Mohri, K. Narihara, Y. Tomita, T. Tsuzuki, M. Hasegawa and K. Ikuta, Plasma Physics and Controlled Nuclear Fusion Research (Proc. 8th Int. Conf. Brussels, 1980) Vol. 1, IAEA, Vienna (1981) 511.

51. A. Mohri, K. Narihara, Y. Tomita, M. Hasegawa, T. Tsuzuki and T. Kobata, "REB Injected Toroidal Plasma," International Conference on Plasma Physics, Goteborg, Sweden, (1982).

52. F. Mako, W. Manheimer, C. A. Kapetanakos, D. Chernin and F. Sandel, "External Injection into a High Current Modified Betatron Accelertaor," NRL Memorandum Report 5196 (1983).

53. T. J. Fessenden, C. W. Hartman and R. H. Munger, "Preliminary Study of the Acceleration of Electrons in a Plasma Betatron," UCRL-78016 (1976).

54. H. Dreicer, *Phys. Rev.* **117**, 329 (1960).

55. J. Dress and W. Paul, *Z. Phys.* **180**, 380 (1964).

56. Ralph W. Moir, "Experimental Investigations of Nonadiabatic Scattering of Charged Particles in a Toroidal Magnetic Field," Ph.D. Thesis, Massachusetts Institute of Technology (1967).

57. R. L. Gluckstern, Proc. of Linear Accelerator Conference, 245 (1979).

58. D. C. dePackh, NRL Quarterly on Nuc. Sci. and Tech, 31 (1958); NRL Quarterly on Nuc. Sci. and Tech., 32 (1961); Bulletin of the American Physical Society, Series II, 5: 225 (1960).

59. W. Walkinshaw and K. Wyllie, TRE (Malvern) Maths Memo/58/WW, June 7 (1948). (Unpublished).

60. D. P. Taggart, M. R. Parker, H. J. Hopman and H. H. Fleishmann, "Betatron Acceleration of Kiloampere Electron Rings in RECE-Christa" *IEEE Trans. Nucl. Sci.* **NS-30**, 3165 (1983).

61. S. Humphries, Jr. and D. M. Woodall, *Bull. Am. Phys. Soc.* **28**, 1054 (1983).

62. M. A. Ivanorskii et al., 'The Tor-2 Stellarator" in Stellarators, Proc. of the P. N. Lebedev Physics Inst., D. V. Skobeltsyn, editor (Consultants Bureau, New York, c. 1974), vol. 65, pp. 61 ff.

63. T. K. Chu et al., "Modular Coils: A Promising Toroidal Reactor Coil System", Princeton Plasma Physics Laboratory Report PPPL-1796 (April, 1981).

64. M. Reiser, Part. Accel. 8, 167 (1978).

65. Yu. L. Klimontovich, Zhur. Eksptl. Teoret. Fiz. 33, 982 (1957) [Sov. Phys. JETP 6, 753 (1958)]. See also. e.g. S. Ichimaru Basic Principles of Plasma Physics: A Statistical Approach (W. A. Benjamin; Reading, MA.; 1973).

66. N. Rostoker, private communication.

APPENDIX

This Appendix discusses the method of averaging Eqs. (6a–6c) over particle initial conditions so as to find separate equations for the particle position $(r_1(t), z_1(t))$— "Lagrangian" variables, dependent on the individual particle's initial position and momentum, and for the location of the beam center, $(\Delta r(\theta, t), \Delta z(\theta, t))$— "Eulerian" or field variables dependent only on time t and the observation point θ. The radial coordinate is treated here; identical expressions hold for z.

The distribution function may be defined in complete generality in "Klimontovich" form[65]

$$f(r, \theta, z, p_r, p_\theta, p_z; t) = \int d^3 r^{(0)} \, d^3 p^{(0)} f^{(0)}(\mathbf{r}^{(0)}, \mathbf{p}^{(0)})$$

$$\cdot \, \delta^{(3)}(\mathbf{r} - \bar{\mathbf{r}}(\mathbf{r}^{(0)}, \mathbf{p}^{(0)}, t))$$

$$\cdot \, \delta^{(3)}(\mathbf{p} - \bar{\mathbf{p}}(\mathbf{r}^{(0)}, \mathbf{p}^{(0)}, t)), \tag{A-1}$$

where $\mathbf{r}^{(0)}$ and $\mathbf{p}^{(0)}$ are the initial position and momentum of a particle, $\bar{\mathbf{r}}$ and $\bar{\mathbf{p}}$ are the solutions to the equations of motion for a particle of given initial position and momentum, and the integral extends over all initial conditions. At a given azimuth θ, then

$$\Delta r(\theta, t) = \frac{\int r \, dr \, dz \, d^3 p (r - r_0) f(r, \theta, z, p_r, p_\theta, p_z; t)}{\int r \, dr \, dz \, d^3 p f(r, \theta, z, p_r, p_\theta, p_z; t)}$$

$$= \frac{\int d^3 r^{(0)} \, d^3 p^{(0)} f^{(0)}(\mathbf{r}^{(0)}, \mathbf{p}^{(0)}) r_1 \, \delta(\theta - \bar{\theta})}{\int d^3 r^{(0)} \, d^3 p^{(0)} f^{(0)}(\mathbf{r}^{(0)}, \mathbf{p}^{(0)}) \, \delta(\theta - \bar{\theta})}$$

$$\equiv \langle r_1 \rangle, \tag{A-2}$$

where $r_1 = \bar{r} - r_0$ and the arguments of r_1 and $\bar{\theta}$ have been suppressed. Next consider the quantity $\langle \dot{r}_1 \rangle$ and relate it to derivatives of $\Delta r(\theta, t)$. Defining for convenience the operator $\hat{f}$ as

$$\hat{f}\phi = \int d^3 r^{(0)} \, d^3 p^{(0)} f^{(0)}(\mathbf{r}^{(0)}, \mathbf{p}^{(0)}) \phi(\mathbf{r}^{(0)}, \mathbf{p}^{(0)})$$

one finds

$$\langle \dot{r}_1 \rangle = \frac{\hat{f} \cdot \dfrac{\partial r_1}{\partial t} \delta(\theta - \bar{\theta})}{\hat{f} \cdot \delta(\theta - \bar{\theta})}$$

$$= \frac{\dfrac{\partial}{\partial t}(\hat{f} \cdot r_1 \delta(\theta - \bar{\theta})) - \hat{f} \cdot r_1 \dfrac{\partial}{\partial t}\delta(\theta - \bar{\theta})}{\hat{f} \cdot \delta(\theta - \bar{\theta})}$$

$$= \frac{\dfrac{\partial}{\partial t}(\hat{f} \cdot r_1 \delta(\theta - \bar{\theta})) + \dfrac{\partial}{\partial \theta}(\hat{f} \cdot r_1 \dot{\theta}\delta(\theta - \bar{\theta}))}{\hat{f} \cdot \delta(\theta - \bar{\theta})} \qquad \text{(A-3)}$$

$$= \frac{\partial}{\partial t}\left[\frac{\hat{f} \cdot r_1 \delta(\theta - \bar{\theta})}{\hat{f} \cdot \delta(\theta - \bar{\theta})}\right] + \frac{\partial}{\partial \theta}\left[\frac{\hat{f} \cdot r_1 \dot{\theta}\delta(\theta - \bar{\theta})}{\hat{f} \cdot \delta(\theta - \bar{\theta})}\right]$$

$$- \frac{[(\hat{f} \cdot r_1 \delta(\theta - \bar{\theta})) \cdot \dfrac{\partial}{\partial \theta}\hat{f} \cdot \dot{\theta}\delta(\theta - \bar{\theta}) - (\hat{f} \cdot r_1 \dot{\theta}\delta(\theta - \bar{\theta})) \cdot \dfrac{\partial}{\partial \theta}\hat{f} \cdot \delta(\theta - \bar{\theta})}{[\hat{f} \cdot \delta(\theta - \bar{\theta})]^2}$$

To this point, the expression for $\langle \dot{r}_1 \rangle$ is formally exact. To make further progress the linearization approximation is utilized in order to make the replacement $\dot{\bar{\theta}}_0 \approx \dot{\theta}_0 \equiv \Omega_{z0}$. To linear order, then, from (A-3)

$$\langle \dot{r}_1 \rangle = \left(\frac{\partial}{\partial t} + \Omega_{z0}\frac{\partial}{\partial \theta}\right)\Delta r(\theta, t) \qquad \text{(A-4)}$$

Similarly one may show, to the same order of approximation,

$$\langle \ddot{r}_1 \rangle = \left(\frac{\partial}{\partial t} + \Omega_{z0}\frac{\partial}{\partial \theta}\right)^2 \Delta r(\theta, t). \qquad \text{(A-5)}$$

Equations (A-4, 5) and the corresponding equations for $\langle \dot{z}_1 \rangle$ and $\langle \ddot{z}_1 \rangle$ are used in the text to obtain (7a, b) from (6a, b).

Beam stability in a stellatron

D. Chernin

Science Applications International Corporation, 1710 Goodridge Drive, McLean, Virginia 22102

Collective effects in the $l = 2$ stellatron [Phys. Rev. Lett. **50**, 507 (1983)], a high-current electron accelerator, are studied. A thin-beam model is employed, and only long-wavelength, low-frequency modes are considered. The eigenvalue problem is formulated in general and solved analytically in the smooth approximation; comparison with a numerical solution of the eigenvalue problem is excellent. It is found that the dispersion relation in the smooth approximation is identical in form to that for the modified betatron, under a simple substitution. An analytical expression for the transition energy, obtained earlier by a simple dynamical argument, is confirmed. The stellarator field is found to reduce the growth rate of the negative mass instability.

I. INTRODUCTION

The $l = 2$ stellatron, a betatron with an added $l = 2$ stellarator winding, was originally proposed[1] in order to improve the tolerance of a betatron or modified betatron[2] to a mismatch between the average beam energy and the vertical magnetic field. Such a tolerance would be a desirable feature of any high-current accelerator, since injectors inevitably produce a beam with measurable energy spread as well as a variable average energy. Though the original analysis included space-charge effects in a simple, non-self-consistent way, the argument for improved momentum compaction can be based on single particle orbit considerations alone.

Treatment of space-charge effects in the stellatron is complicated by the lack of symmetry in the fields. Self-consistent, monoenergetic, KV-like[3] equilibria can be constructed,[4] however, and these give explicit relations among the beam radii (the beam is elliptical, in general), emittance, current, energy, and externally applied fields; the shifts in the betatron frequencies due to space charge are also obtained from these equilibrium studies.

In the present paper the stability of a beam confined in a stellatron is considered. This work was motivated, in part, by certain experimental results on the $l = 2$ stellatron at the University of California at Irvine.[5] Though beam currents have been increased in that experiment by the addition of the $l = 2$ windings, currents are still not as large as one might expect from the amount of injected charge. An instability of some kind may be responsible for the current loss. An attempt to discover possible current limiting mechanisms in the stellatron initiated the work presented here.

The present stability calculation makes the following approximations: All first-order fields are treated in the long-wavelength ($\lambda \gg a \equiv$ minor radius of toroidal chamber), low-frequency ($\omega \ll c/a$) limit; toroidal corrections to the first-order fields are neglected. We note in particular that the long-wavelength approximation may omit the potentially interesting case $\lambda \sim 2\pi r_0/m$, where r_0 is the major radius of the torus and m is the number of stellarator field periods around the device. The beam is treated as a structureless, thin, threadlike charge distribution so that the effects of betatron oscillations and energy spread on the equilibrium are ignored; the magnitude of these effects can be roughly estimated, however.[6] The beam environment, which has a critical

effect on beam stability, is treated simply: the beam is assumed to be contained in a perfectly conducting toroidal chamber. Only the longitudinal, or negative mass mode is unstable in these circumstances. Several comments are made below, however, regarding the effects of walls of arbitrary impedance on both longitudinal and transverse modes.

Under the above approximations we have the following findings to present: (1) the eigenvalue problem governing the longitudinal and transverse modes of a beam in a stellatron; (2) a dispersion relation, obtained from an approximate solution to the eigenvalue problem, which is identical in form to that obtained for the modified betatron,[7] with the redefinition of a certain symbol; (3) confirmation of an analytical expression,[8] obtained by a simple dynamical argument, for the so-called transition energy, below which the longitudinal mode is stable (in the absence of dissipative effects); (4) a quite favorable numerical comparison between the solution to the eigenvalue problem of (1) and the dispersion relation of (2) for the longitudinal mode.

This paper is organized as follows. Section II describes the derivation of the linearized equations of motion, assuming the applied fields are given near the axis of the torus. Section III outlines the derivation of the first-order charge and current densities in terms of the single particle variables using a summation over initial conditions. In Sec. IV the approximate solution to Maxwell's equations is obtained, and the total first-order fields to be used in the equations of motion are derived. In Sec. V the eigenvalue problem is formulated and is shown to reproduce the modified betatron dispersion relation in the absence of the twisted quadrupole field. An approximate solution based on a two-time scale analysis is presented and some comments are made on the form of the resulting dispersion relation. Finally, in Sec. VI, a numerical solution to the full eigenvalue problem is presented and compared to results from the dispersion relation of Sec. V.

Section VII summarizes these results and makes a few additional remarks.

II. EQUATIONS OF MOTION

We shall use a standard (r, θ, z) cylindrical coordinate system. In the unperturbed state we have a thin beam enclosed in a perfectly conducting torus of major radius r_0 and

minor radius a. The position of an electron which, in the absence of ac excitation would be at $(r_0, \theta_0(t), 0)$ is, in the presence of the excitation, at

$$\mathbf{r} = (r_0 + \xi)\hat{r}_0 + \eta\hat{\theta}_0 + \chi\hat{z}_0, \tag{1}$$

where ξ, η, and χ, known as polarization variables,[9,10,11] are functions of θ_0 and t and where the unit vectors in (1) refer to the unperturbed position of the particle at time t. The applied fields seen by a particle at $(r_0 + r_1, \theta, z_1)$ are taken to be

$$B_r^a \simeq -nB_{z0}z_1/r_0 + k_s B_s(z_1 \cos m\theta - r_1 \sin m\theta), \tag{2a}$$

$$B_\theta^a \simeq B_{\theta 0}, \tag{2b}$$

$$B_z^a \simeq B_{z0}(1 - nr_1/r_0) + k_s B_s(r_1 \cos m\theta + z_1 \sin m\theta), \tag{2c}$$

where B_{z0}, $B_{\theta 0}$, and $k_s B_s$ are constants, n is the betatron field index, and m is an integer, the number of quadrupole field periods around the device. If the rf fields (as yet unknown) caused by the perturbation are denoted by a superscript, the linearized equations of motion become

$$\ddot{\xi} + \omega_0^2(1 - n - \gamma_0^2 + \mu \cos m\theta_0)\xi - \omega_0\gamma_0^2\dot{\eta}$$
$$\quad - \Omega_{\theta 0}\dot{\chi} + \mu\omega_0^2 \sin m\theta_0\chi$$
$$\quad = -(e/m_e\gamma_0)(E_{r_e}^{(rf)} + \beta_0 B_{z_e}^{(rf)}), \tag{3a}$$

$$\ddot{\eta} + \omega_0\dot{\xi} = -(e/m_e\gamma_0^3)E_{\theta_e}^{(rf)}, \tag{3b}$$

$$\ddot{\chi} + \omega_0^2(n - \mu \cos m\theta_0)\chi + \Omega_{\theta 0}\dot{\xi} + \mu\omega_0^2 \sin m\theta_0\xi$$
$$\quad = -(e/m_e\gamma_0)(E_{z_e}^{(rf)} - \beta_0 B_{r_e}^{(rf)}), \tag{3c}$$

where a dot denotes $\partial/\partial t + \omega_0 \partial/\partial\theta_0$, $\omega_0 = eB_{z0}/m_e\gamma_0 c$, $\Omega_{\theta 0} = eB_{\theta 0}/m_e\gamma_0 c$, $-e$ and m_e are the charge and mass of the electron, β_0 and γ_0 are the usual relativistic factors, and $\mu \equiv k_s r_0 B_s/B_{z0}$ is a dimensionless quadrupole strength. In the absence of rf fields we integrate (3b) once and substitute in (3a) to obtain the usual equations[1] for betatron oscillations. To complete the calculation it is only necessary to obtain expressions for the rf fields in terms of ξ, η, and χ.

III. SOURCES FOR MAXWELL'S EQUATIONS

To express the first-order charge and current densities in terms of the polarization variables we begin with the formal Klimontovich expression for the total charge density at the point $\mathbf{r}$ at time t

$$\rho(\mathbf{r}, t) = -e \int d^3\bar{r}_0 \, d^3\bar{p}_0 \, F(\bar{r}_0, \bar{p}_0)\delta^{(3)}(\mathbf{r} - \bar{r}), \tag{4}$$

where F is a distribution of zero-order positions and momenta and $\bar{r}$ is the actual (zero + first-order) trajectory $\bar{r} = \bar{r}_0 + \xi\hat{r}_0 + \eta\hat{\theta}_0 + \chi\hat{z}_0$. Expanding the delta function in (4), one finds for the first-order charge density

$$\delta\rho(\mathbf{r}, t) = -\frac{\xi}{r}\frac{\partial}{\partial r}r\rho_0 - \frac{1}{r}\frac{\partial\eta}{\partial\theta}\rho_0 - \chi\frac{\partial\rho_0}{\partial z}, \tag{5}$$

where ξ, η, and χ are evaluated at θ and t, and ρ_0 is the zero-order density. A similar treatment for the current density yields

$$\delta\mathbf{J}(\mathbf{r}, t)$$
$$= \dot{\xi}\rho_0\hat{r} + \left(-\xi\omega_0\frac{\partial}{\partial r}r\rho_0 + \frac{\partial\eta}{\partial t}\rho_0 - \chi r\omega_0\frac{\partial\rho_0}{\partial z}\right)\hat{\theta}$$
$$+ \dot{\chi}\rho_0\hat{z}. \tag{6}$$

The perturbed line-charge density, which will be needed below, is obtained by integrating (5) over the beam cross section:

$$\delta\lambda = \lambda_0\left(\frac{-\xi}{r_0} - \frac{1}{r_0}\frac{\partial\eta}{\partial\theta}\right), \tag{7}$$

where λ_0 is the zero-order line-charge density. In (7) the first term is due to radial expansion of the ring while the second term is due to azimuthal bunching of charge.

IV. SOLUTION TO MAXWELL'S EQUATIONS

As described in the Introduction we will confine our attention to the long-wavelength, low-frequency modes. In particular we shall assume

$$a \ll |\gamma_{ph}/k_\parallel|, \tag{8}$$

where γ_{ph} is the relativistic factor corresponding to the wave-phase velocity and $k_\parallel$ is the wavenumber in the direction parallel to the beam velocity. This inequality allows us to replace the wave operator $\nabla^2 + \omega^2/c^2$ by just $\nabla_\perp^2$ and so to calculate transverse fields from statics. The longitudinal field, $E_{\theta_e}^{(rf)}$, required in (3b), is then calculated from Faraday's law, in this approximation.

It is convenient to think of a general density perturbation as a superposition of two types: (1) the beam does not move transversely but suffers a change in density; and (2) the beam retains its zero-order density but moves transversely. Even though we will be mainly interested in the longitudinal mode, we include perturbations of type (2), since for certain transverse modes the quasistatic approximation still holds and these are not difficult to retain in the analysis. The transverse modes, however, will be stable in the absence of wall resistivity or other real impedance.

In solving Maxwell's equations for either type of perturbations one encounters a difficulty in treating an infinitesimally thin beam, since such a beam produces infinite fields on its surface. We will, consequently, in this section think of the beam as having some small, but finite radius r_b. Our results will depend only very weakly on the value of r_b.

A perturbation of type (1) is represented by the middle term of (5) and the middle term of the $\hat{\theta}$ component of (6). Calculation of the transverse fields for such a perturbation, for perfectly conducting wall boundary conditions is elementary. Use of the transverse fields in Faradays's law gives $E_{\theta_e}^{(rf)}$ at the center of the beam as

$$E_{\theta_e}^{(rf)} = \frac{2\lambda_0}{r_0^2}\left(\frac{1}{2} + \ln\frac{a}{r_0}\right)\left(\frac{\partial^2}{\partial\theta^2} + \frac{\omega^2 r_0^2}{c^2}\right)\eta, \tag{9}$$

where we have assumed an $e^{-i\omega t}$ time dependence and have retained only the second term of (7), in the spirit of the cylindrical approximation. All transverse fields vanish at the center of the beam for perturbation type (1).

The dipole perturbation, type (2), produces nonzero transverse rf electric and magnetic fields at the beam center

but no additional contribution to $(\cdot)$ since transverse motion of the beam simply compresses, but does not change, the flux between the beam center and the wall. The transverse fields due to this perturbation, represented by the first and third terms of (5) and the first and third terms of the $\hat{\theta}$ component of (6), are straightforward to find, again using statics

$$E_{r_0} = -2\pi\rho_0\xi(1 - r_b^2/a^2), \tag{10a}$$

$$E_{z_0} = -2\pi\rho_0\chi(1 - r_b^2/a^2), \tag{10b}$$

$$B_{r_0} = \beta_0 E_{z_0}, \tag{10c}$$

$$B_{z_0} = -\beta_0 E_{r_0}. \tag{10d}$$

The fields in (10a)–(10d), however, are not the only first-order fields. There is another contribution as may be seen from the following argument: Any field component $F(x)$ may be written $F_0(x) + F_1(x)$, where F_0 is the zero-order field and F_1 is the first-order field due to the first-order sources defined at the observation point x. In the equations of motion all fields are evaluated at the location of the beam $x_0 + x_1$. Consequently, the correct first-order fields to be used in (3a)–(3c) are sums of the form

$$\frac{\partial F_0}{\partial x}\bigg|_{x=x_0} x_1 + F_1(x_0), \tag{11}$$

where F_1 is given by (10). We find then that

$$E_{r_0}^{(r)} = 2(\lambda_0/a^2)\xi, \tag{12a}$$

$$E_{z_0}^{(r)} = 2(\lambda_0/a^2)\chi, \tag{12b}$$

while (10c) and (10d) still hold.

V. THE EIGENVALUE PROBLEM

Substitution of the fields in (9), (12a), (12b), (10c), and (10d) in the linearized equations (3a)–(3c) gives

$$D^2\xi + (1 - n - n_{sb} - \gamma_0^2 + \mu\cos m\theta)\xi - \gamma_0^2 D\eta - b D\chi$$
$$+ \mu\sin m\theta\chi = 0, \tag{13a}$$

$$(1-\alpha)\frac{\partial^2}{\partial\theta^2}\eta - 2i\bar{\omega}\frac{\partial}{\partial\theta}\eta - \bar{\omega}^2(1 + \alpha\beta_0^2)\eta + D\xi = 0, \tag{13b}$$

$$D^2\chi + (n - n_{sb} - \mu\cos m\theta)\chi + b D\xi + \mu\sin m\theta\xi = 0, \tag{13c}$$

where $D = \partial/\partial\theta - i\bar{\omega}, \bar{\omega} = \omega/\omega_0, n_{sb} = 2\nu r_0^2/(\gamma_0^3\beta_0^2 a^2), \nu$ is Budker's parameter, $\nu = -e\lambda_0/m_e c^2, \alpha = 2\nu(\frac{1}{2} + \ln a/r_b)/(\gamma_0^3\beta_0^2), b = B_{\theta 0}/B_{z 0}$, and we have dropped the subscript 0 on θ. If we define ψ to be a column vector with components $\xi, \xi', \eta, \eta', \chi, \chi'$, where a prime denotes $\partial/\partial\theta$, the eigenvalue condition determining $\bar{\omega}$ is

$$\psi(\theta + 2\pi) = \psi(\theta). \tag{14}$$

In the case $\mu = 0$ the condition for (14) to be satisfied is most easily obtained by assuming for ψ the dependence $e^{il\theta}$, where l is an integer, the azimuthal mode number. For this case (13) reduces to the evaluation of a 3×3 determinant for the eigenvalue condition, with the result

$$\frac{\nu_\parallel^2}{\beta_0^2\bar{\Omega}^2}\left(\frac{1}{\gamma_0^2} + \frac{\bar{\Omega}^2 - \nu_z^2}{(\bar{\Omega}^2 - \nu_z^2)(\bar{\Omega}^2 - \nu_r^2) - b^2\bar{\Omega}^2}\right) = 1, \tag{15}$$

where $\nu_\parallel^2 = 2l^2(\nu/\gamma_0)(\frac{1}{2} + \ln a/r_b)/\gamma_{ph}^2, \gamma_{ph}^{-2} = 1 - \omega^2 r_0^2/(l^2 c^2), \bar{\Omega} = \bar{\omega} - l, \nu_r^2 = 1 - n - n_{sb}$, and $\nu_z^2 = n - n_{sb}$. Equation (15) agrees with the result of Ref. 7, where the dispersion relation for the modified betatron is obtained under assumptions similar to those employed here. The solutions to (15) are thoroughly analyzed, in the approximation $\gamma_{ph} = \gamma_0$, in Ref. 7, where resistive wall effects are also considered; the effects of a more general wall impedance are examined in Ref. 6.

Let us now return to the eigenvalue problem for the case $\mu \neq 0$. For long-wavelength modes, one expects each of ξ, η, and χ to be composed of a main, slowly varying part and a much smaller, rapidly oscillating piece, this latter part due to the rapidly oscillating quadrupole focusing. This suggests that we write $\xi = \xi_s + \xi_f$, and similarly for η and χ, where the subscripts denote slow and fast variation. It should be said here that we anticipate that $|m| \gg 1$ in typical applications; the UC Irvine experiment, for example, uses $m = 12$. Substituting for ξ, η, and χ in (13a)–(13c) and performing an average over the fast scale, $2\pi/m$, gives the equations

$$D^2\xi_s + (1 - n - n_{sb} - \gamma_0^2)\xi_s + \mu\langle\cos m\theta\xi_f\rangle$$
$$- \gamma_0^2 D\eta_s - b D\chi_s + \mu\langle\sin m\theta\chi_f\rangle = 0, \tag{16a}$$

$$(1-\alpha)\frac{\partial^2}{\partial\theta^2}\eta_s$$
$$- 2i\bar{\omega}\frac{\partial}{\partial\theta}\eta_s - \bar{\omega}^2(1 + \alpha\beta_0^2)\eta_s + D\xi_s = 0, \tag{16b}$$

$$D^2\chi_s + (n - n_{sb})\chi_s - \mu\langle\cos m\theta\chi_f\rangle + b D\xi_s$$
$$+ \mu\langle\sin m\theta\xi_f\rangle = 0, \tag{16c}$$

where the angular brackets, $\langle\cdots\rangle$, denote an average over the fast scale, and we have assumed $\langle\xi_s\rangle = \xi_s, \langle\xi_f\rangle = 0 = \langle\xi'_f\rangle = \langle\xi''_f\rangle$, etc. If we now subtract (16a)–(16c) from the unaveraged equations (13a)–(13c), use $|\xi_f| \ll |\xi_s|$, keep all derivatives acting on fast quantities, and ignore quantities of the form $\cos m\theta\xi_f - \langle\cos m\theta\xi_f\rangle$, we arrive at equations for the fast variables:

$$\frac{\partial^2}{\partial\theta^2}\xi_f - b\frac{\partial}{\partial\theta}\chi_f = -\mu\cos m\theta\xi_s - \mu\sin m\theta\chi_s, \tag{17a}$$

$$\frac{\partial^2}{\partial\theta^2}\chi_f + b\frac{\partial}{\partial\theta}\xi_f = -\mu\sin m\theta\xi_s + \mu\cos m\theta\chi_s, \tag{17b}$$

which are easily solved to give

$$\xi_f = [\mu/m(m+b)](\cos m\theta\xi_s + \sin m\theta\chi_s), \tag{18a}$$

$$\chi_f = [\mu/m(m+b)](\sin m\theta\xi_s - \cos m\theta\chi_s). \tag{18b}$$

Finally, substitution of (18a) and (18b) into (16a)–(16c), using $\langle\cos^2 m\theta\rangle = \langle\sin^2 m\theta\rangle = \frac{1}{2}$, gives the equations for the slow components:

$$D^2\xi_s + \{1 - n - n_{sb} + [\mu^2/m(m+b)] - \gamma_0^2\}\xi_s$$
$$- \gamma_0^2 D\eta_s - b D\chi_s = 0, \tag{19a}$$

$$(1-\alpha)\frac{\partial^2}{\partial\theta^2}\eta_s - 2i\bar{\omega}\frac{\partial}{\partial\theta}\eta_s - \bar{\omega}^2(1 + \alpha\beta_0^2)\eta_s$$
$$+ D\xi_s = 0, \tag{19b}$$

$$D^2\chi_s + \{n - n_{sb} + [\mu^2/m(m+b)]\}\chi_s + b D\xi_s = 0. \tag{19c}$$

Equations (19a)–(19c) are differential equations with constant coefficients and are in fact precisely of the form of (13a)–(13c) if μ is set to zero in (13a)–(13c) and if n_{sb} is replaced by

$$n_{sb} \rightarrow n_{sb} - [\mu^2/m(m+b)].\qquad(20)$$

It is seen that the focusing effect of the twisted quadrupole has been replaced by a smoothed, effective focusing term. It follows, consequently, from (19a)–(19c) that the dispersion relation for the stellatron for long-wavelength modes is just that for the modified betatron, Eq. (15), under the replacement (20). This is the basic result of this paper.

A further result may be obtained by examination of (15). If we approximate $\gamma_{ph}^2 \approx \gamma_0^2$ and assume $|\bar{\Omega}^2| \ll v_r^2, v_z^2$ for the longitudinal mode, then solving the resulting quadratic equation gives the result that the longitudinal mode is stable below a transition energy given by

$$\gamma_{tr} = v_r = \{1 - n - n_{sb} + [\mu^2/m(m+b)]\}^{1/2},\qquad(21)$$

which agrees with an earlier estimate.[8]

For the special case[4] $m + b = 0$, the analysis leading to (20) and (21) no longer applies. In this case one may show, by reconsideration of (17a) and (17b) ff, that the stellatron dispersion relation is again (15) but now under the replacement $b\bar{\Omega} \rightarrow b\bar{\Omega} - \mu^2/bl$. A transition energy, as defined in (21), no longer exists; one is always above transition.

VI. NUMERICAL ANALYSIS

In order to test the analysis leading to the dispersion relation described in the previous section, a numerical solution to the eigenvalue problem for (13a)–(13c) has been carried out. The solution is based on the following construction. We define a 6×6 matrix $\Psi(\theta)$ which has, as columns, solution vectors ψ satisfying (13a)–(13c). Furthermore, we define Ψ to satisfy the initial condition $\Psi(0) = I$, the identity matrix. Since the coefficients in (13a)–(13c) are periodic with period $2\pi/m \equiv \theta_m$ it follows that $\Psi(\theta + \theta_m)$ must also be a solution to (13) and so the columns of $\Psi(\theta + \theta_m)$ must each be expressible as a linear combination of the columns of $\Psi(\theta)$. Considering the initial condition on Ψ, we have that

$$\Psi(\theta + \theta_m) = \Psi(\theta)\Psi(\theta_m),\qquad(22)$$

from which it follows, by induction

$$\Psi(\theta + k\theta_m) = \Psi(\theta)\Psi^k(\theta_m)\qquad(23)$$

for any non-negative integer k.

Suppose we find the matrix U which diagonalizes $\Psi(\theta_m)$,

$$\Psi(\theta_m)U = U\Lambda,\qquad(24)$$

where Λ is a diagonal matrix, containing the eigenvalues of $\Psi(\theta_m)$. The columns of $\Psi(\theta)U$ are then the Floquet solutions, satisfying

$$\Psi(\theta + \theta_m)U = \Psi(\theta)U\Lambda.\qquad(25)$$

It follows from (25), then, that

$$\Psi(\theta + 2\pi)U = \Psi(\theta)U\Lambda^m.\qquad(26)$$

The eigenvalue problem for (13a)–(13c) may now be stated

succinctly as follows: One must find $\bar{\omega}$ such that (at least) one of the eigenvalues of $\Psi(\theta_m)$ is one of the m roots of unity.

A FORTRAN program has been written to solve this problem. Starting with an initial guess for $\bar{\omega}$, the matrix $\Psi(\theta_m)$ is evaluated and its eigenvalues computed; an adjustment to $\bar{\omega}$ is then made using a simple secant method. Convergence typically takes three or four iterations.

For comparison purposes the smooth approximation dispersion relation (15), (20) was also solved numerically using the same first guess. This was a matter of finding the appropriate root of a sixth-order polynomial [the approximations employed to obtain (21) were not made here] and is very fast computationally. In fact the data for the plots shown below, of the longitudinal mode growth rate versus various parameters, originally took ~40 min each to generate on a VAX 11-780 by the first method. Each took less than 3 sec using the smooth approximation dispersion relation. For all cases tried, the two methods agree to at least three significant figures and give plots indistinguishable on the scales used below.

Three plots are shown here. All were made using values typical of the device at UC Irvine, i.e., $a/r_0 = 0.1$, $r_b/a = 0.2$, $n = 0.5$, $m = 12$, and $b = 40$. In the first plot, Fig. 1, $Im(\bar{\omega})$ is plotted versus current for a beam energy of 2 MeV and $\mu = 50$. The dependence follows quite closely to the classical square root law. In Fig. 2, the growth rate is plotted versus energy for a current of 200 A and $\mu = 50$. The value of the transition energy predicted by (21) is ≈ 0.52 MeV and is seen to agree quite well with the numerical value. Finally in Fig. 3 the growth rate is plotted versus μ for a beam energy of 2 MeV and a beam current of 200 A. The stabilizing effect of the quadrupole field can be seen quite clearly. This is to be expected of any field which inhibits transverse motion. In all cases shown $Re(\bar{\omega}) \approx 1$.

VII. DISCUSSION AND SUMMARY

The features and various limiting cases of the dispersion relation for the modified betatron have been extensively dis-
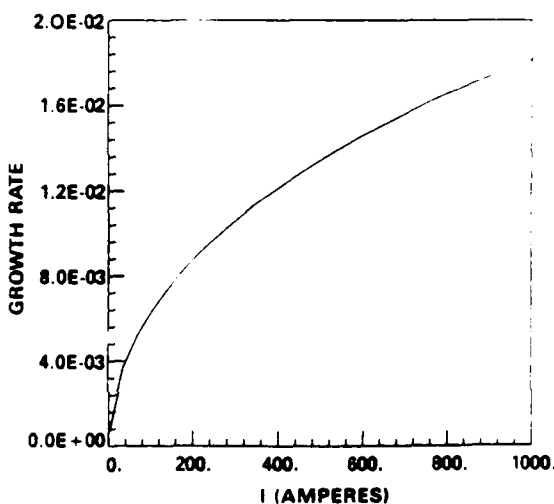

FIG. 1. Normalized growth rate for the longitudinal mode versus current. Beam energy is 2 MeV. Here $\mu = 50$. (Other parameters given in text.)
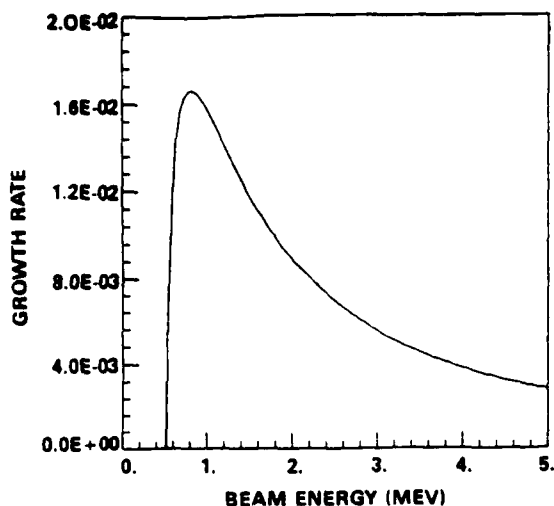
FIG. 2. Normalized growth rate for the longitudinal mode versus energy. Beam current is 200 A. Here $\mu = 50$. The theoretical value for the transition energy is 0.52 MeV.
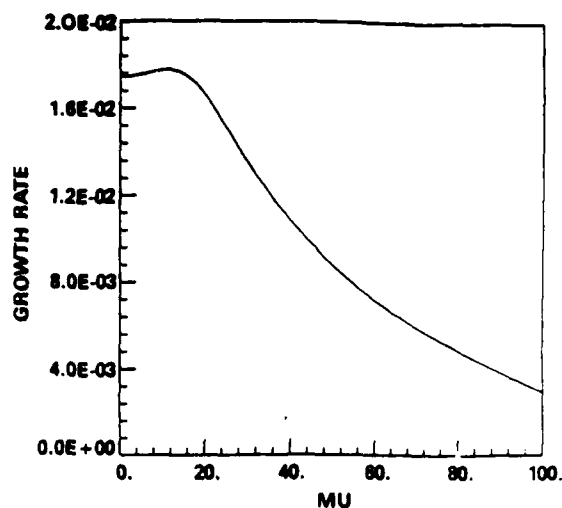

FIG. 3. Normalized growth rate for the longitudinal mode versus quadrupole strength. Beam energy is 2 MeV; beam current is 200 A.

cussed in Refs. 6 and 7. Toroidal corrections and a careful comparison with the results of particle simulations have been carried out by Godfrey and Hughes.[12] We have shown that, under the substitution (20), virtually all of the analyses already carried out on the long-wavelength stability of the modified betatron may be carried over to the stellatron. In the long-wavelength, quasistatic limit the net effect of the addition of stellarator windings to a modified betatron, we have found, is to add a smooth, transverse focusing term which can be large compared to the weak-focusing or space-charge defocusing terms. Stellarator fields enhance stability in this sense. Other proposed stellaratorlike focusing schemes may be treated in a similar manner. There are two resulting, related effects on the dispersion relation. One is the introduction of a finite transition energy, given by (21), below which the longitudinal mode growth vanishes altogether and the second is a simple shift (increase) of the transverse frequencies, v_r and v_z. Of course, below the transition energy, dissipative effects (a resistive wall, for example) will cause both longitudinal and transverse modes to grow,[7,13,14] but at a growth rate which is smaller the larger the quadrupole focusing. Such modes would then presumably be more easily stabilized by effects neglected here, especially azimuthal velocity spread.

The smooth approximation of Sec. V, above, will break down for $l > m/2$. Also, the solution to Maxwell's equations obtained in Sec. IV becomes unreliable for $l > r_0/a$, which is typically of the order of m. Consequently, short-wavelength modes must be studied by entirely different methods from those employed here. In fact, there is some evidence[15] from

particle simulations for strong interactions of the beam with certain electromagnetic modes of the toroidal cavity, under certain conditions. These interactions are an important topic for further study.

ACKNOWLEDGMENTS

[1]C. W. Roberson, A. Mondelli, and D. Chernin, Phys. Rev. Lett. 50, 507 (1983).

[2]P. Sprangle and C. A. Kapetanakos, J. Appl. Phys. 49, 1 (1978); N. Rostoker, Comments Plasma Phys. 6, 91 (1980).

[3]I. M. Kapchinskij and V. V. Vladimirskij, Proceedings of the International Conference on High Energy Accelerators (CERN, Geneva, Switzerland, 1959), p. 274.

[4]D. Chernin, IEEE Trans. Nucl. Sci. NS32, 2504 (1985).

[5]H. Ishizuka, G. Leslie, B. Mandelbaum, A. Fisher, and N. Rostoker, Ref. 4, p. 2727.

[6]P. Sprangle and D. Chernin, Part. Accel. 15, 35 (1984).

[7]P. Sprangle, L. Vomvoridis (private communication); see also Ref. 6, Eq. (1).

[8]C. W. Roberson, A. Mondelli, and D. Chernin, IEEE Trans. Nucl. Sci. NS30, 3162 (1983).

[9]D. L. Bobroff, IRE Trans. Electron Devices ED-6, 68 (1959).

[10]V. K. Neil and W. Heckrotte, J. Appl. Phys. 36, 2761 (1965).

[11]R. J. Briggs and V. K. Neil, J. Nucl. Energy C9, 209 (1967).

[12]B. B. Godfrey and T. P. Hughes, Phys. Fluids 28, 669 (1985).

[13]V. K. Neil and A. M. Sessler, Rev. Sci. Instrum. 36, 429 (1965).

[14]L. J. Laslett, V. K. Neil, and A. M. Sessler, Rev. Sci. Instrum. 36, 436 (1965).

[15]T. Hughes (private communication).

Use of radiation from betatron oscillations as an electron-beam diagnostic

D. Chernin
Science Applications International Corporation, 1710 Goodridge Drive, McLean, Virginia 22102

B. Levush
University of Maryland, Laboratory for Plasma and Fusion Energy Studies, College Park, Maryland 20742

It is generally difficult to diagnose the energy of an electron beam propagating in a focusing channel. Here we suggest observation of the Doppler-shifted radiation due to the electrons' betatron motion in the channel as a sensitive, nonperturbing diagnostic. Sample spectra have been calculated for a specific type of channel used in a cyclic electron accelerator and their features are discussed.

I. INTRODUCTION

For some recently proposed high-current electron accelerators it would be desirable to have a passive diagnostic of the various beam parameters. Beam current measurements may be made by a variety of means, but passive measurements of beam density and energy are less easy. One might consider observation of ordinary synchrotron radiation in cyclic devices as an energy diagnostic, but this is effective only at moderately high energies; at the lower energies attained so far in these devices the metallic chamber acts very effectively as a shield for this long wavelength radiation. Higher-frequency radiation, significantly above cutoff of the beam tube, is emitted by the electrons as they execute betatron oscillations. This radiation is Doppler shifted in the forward direction by a factor proportional to the square of the energy (for $\beta \to 1$); hence, it is a good candidate for an energy diagnostic.

This paper presents an analysis of the radiation from betatron oscillations for a particular device, the stellatron[1] (a strong-focused betatron), one of which has been built and operated at the University of California at Irvine.[2] We will, however, make a number of general comments applicable to many similar machines.

This paper is organized as follows: In Sec. II, we describe the magnetic field configuration of the stellatron, write down the paraxial equations of motion, and write down their solution, giving the expressions for the four betatron frequencies; this section is brief since the results are given elsewhere.[1,3] It is mainly included to introduce some notation. Next, we examine the standard expression[4] for radiated intensity for prescribed particle motion, and make some comments on what one expects to observe. We then give some specific examples of spectra and discuss their features, including the effect of "geometric line broadening," an inhomogeneous broadening mechanism due to orbit curvature. The final section draws conclusions and makes a few additional remarks.

II. PARTICLE ORBITS IN THE STELLATRON

The stellatron is a betatron with superposed strong focusing in the form of an $l = 2$ stellarator (twisted quadrupole) field; we take the accelerator to be in the form of a torus of major radius r_0 and a minor radius a. The magnetic fields near the null line (taken to be a circle of radius r_0) of the quadrupole are, in cylindrical coordinates (r, θ, z),

$$B_r \simeq -nB_{z0}y + k_w B_s r_0(y \cos k_w s - x \sin k_w s), \quad (1a)$$

$$B_\theta \simeq B_{\theta 0}, \quad (1b)$$

$$B_z \simeq B_{z0}(1 - nx) + k_w B_s r_0(x \cos k_w s + y \sin k_w s), \quad (1c)$$

where B_{z0}, B_s, and $B_{\theta 0}$ are constants, n is the betatron field index, k_w is $2\pi/(\text{period of quadrupole twist})$, and x and y are normalized radial and vertical displacements, respectively: $x = (r - r_0)/r_0$, $y = z/r_0$. If an electron has energy $mc^2\gamma_0$ then its first-order equations of motion are

$$x'' + [(1 - n)/r_0^2 + k_q^2 \cos k_w s]x$$
$$= -yk_q^2 \sin k_w s + k_b y', \quad (2a)$$

$$y'' + [n/r_0^2 - k_q^2 \cos k_w s]y = -xk_q^2 \sin k_w s - k_b x', \quad (2b)$$

where $k_q^2 = k_w B_s/r_0 B_{z0}$, $k_b = B_{\theta 0}/r_0 B_{z0}$, and a prime denotes d/ds. Note that in the cylindrical limit $r_0 \to \infty$, k_q, k_w, and k_b all remain fixed. Only the focusing terms due to curvature in the vertical field, represented by the $1 - n$ and n terms in (2a) and (2b), vanish.

The Floquet solutions of (2a) and (2b) generally contain an infinite number of terms but in the special case $n = \frac{1}{2}$, a symmetry exists in (2a) and (2b) and one may find the general solution as a sum of four oscillating terms:

$$x + iy = e^{ik_w s/2}(A_+ e^{ik_+ s} + \sigma_+ A_+^* e^{-ik_+ s}$$
$$+ A_- e^{ik_- s} + \sigma_- A_-^* e^{-ik_- s}), \quad (3)$$

where

$$k_\pm^2 = \frac{1}{2r_0^2} + \frac{k_b^2}{4} + \frac{(k_w + k_b)^2}{4}$$
$$\pm \left[\left(\frac{1}{2r_0^2} + \frac{k_b^2}{4} \right)(k_w + k_b)^2 + k_q^4 \right]^{1/2} \quad (3a)$$

and

$$\sigma_\pm = k_q^2 / [(k_\pm - (k_w + k_b)/2)^2 - 1/2r_0^2 - k_b^2/4].$$

In (3) the complex constants $A_\pm$ depend on the four initial conditions. The solution (3) is stable if $|\frac{1}{2}k_w^2 + k_w k_b - 1/r_0^2| > |2k_q^2|$, which sets the limit on the quadrupole strength.

In the experimentally interesting limit of large k_b (large

toroidal field) the betatron frequencies take the forms

$$\omega_1 \equiv (\tfrac{1}{2}k_w + k_+)\beta_0 c \approx (k_b + k_w)\beta_0 c, \tag{4a}$$

$$\omega_2 \equiv (\tfrac{1}{2}k_w - k_+)\beta_0 c \approx -k_b \beta_0 c, \tag{4b}$$

$$\omega_3 \equiv (\tfrac{1}{2}k_w + k_-)\beta_0 c \approx k_w \beta_0 c, \tag{4c}$$

$$\omega_4 \equiv (\tfrac{1}{2}k_w - k_-)\beta_0 c \approx \beta_0 c/(2r_0^2 k_b). \tag{4d}$$

Note that $k_b \beta_0 c$ is just the electron cyclotron frequency in the toroidal field, $eB_{\theta 0}/m\gamma_0 c$. Of the four modes, only the first two typically emit radiation at frequencies significantly above the beam tube cutoff, $\sim c/a$.

In the opposite limit $k_b \to 0$ (no longitudinal magnetic field), we obtain the forms of the betatron frequencies in the cylindrical limit as[3]

$$[k_w/2 \pm (\tfrac{1}{4}k_w^2 \pm k_q^2)^{1/2}]\beta_0 c. \tag{5}$$

Of course since the betatron frequencies depend on many parameters (magnetic fields, field gradients, etc.) one may consider a measurement of a betatron frequency as a measurement of any of these parameters; most of these, however, are most easily and directly measured in other ways. An exception is a measurement of beam density. Although we have not included beam self-field effects in our evaluation of the betatron frequencies one may do so[1]; if this is done, however, one finds that only the lowest betatron frequency is at all sensitive to beam density for typical values of other parameters. This lowest-frequency mode is typically far below cutoff of the beam tube and so is most efficiently observed by simple electrostatic probes.

III. RADIATION SPECTRA

The energy radiated per unit solid angle per unit frequency by a single electron moving along a specified trajectory in free space is given by[4]

$$\frac{dI(\omega)}{d\Omega} = \frac{1}{c}\left(\frac{e\omega}{2\pi}\right)^2 \left|\int dt\, \hat{n} \times (\hat{n} \times \boldsymbol{\beta}) e^{i\omega[t - \hat{n}\cdot\mathbf{r}(t)/c]}\right|^2, \tag{6}$$

where $\hat{n}$ is a unit vector pointing from the electron to a distant observer and the integral extends over times during which $\boldsymbol{\beta}$ is changing. Equation (16) is applicable to the radiation from electron orbits in the stellatron for frequencies far above the beam pipe cutoff; it also assumes that collective effects—electron bunching on a scale of a radiation wavelength—may be neglected. In order to calculate the spectrum of radiation emitted by an electron circulating in the stellatron, it is possible, if rather tedious, to substitute (3) into (6), expand the exponentials in terms of Bessel functions, and perform the integral over time. The result one sees involves spectral peaks at the frequencies

$$n_0\omega_0 + n_1\omega_2 + n_2\omega_2 + n_3\omega_3 + n_4\omega_4, \tag{7}$$

where ω_0 is the basic "cyclotron" frequency $= \beta_0 c/r_0$ and $n_0,...,n_4$ are integers. The amplitude of the radiation for any given set of n's depends on the energy of the electron and on its initial conditions.

Rather than write out the explicit but nontransparent mathematical results for the integral in (6), let us discuss what one expects to see. Consider, first of all, a particle moving not in a torus but along the axis of a cylinder with veloc-

ity $\beta_0 c$, executing a betatron oscillation at a frequency ω_β about the axis. An observer stationed on the axis, with the electron moving toward him, will see radiation at the Doppler-shifted value $\omega_\beta/(1 - \beta_0)$. If the observer is located at some angle θ off the axis of the cylinder, he sees a smaller Doppler shift $\omega_\beta/(1 - \beta_0 \cos \theta)$. Therefore, a detector centered on the axis with a small finite angular acceptance $\Delta\theta$ will see a spread in radiation frequencies of the order of

$$\beta_0(\Delta\theta)^2\omega_\beta/\{2(1 - \beta_0)[1 - \beta_0 + \beta_0(\Delta\theta)^2/2]\}.$$

In addition, as the observer moves off the axis he begins to see energy radiated in harmonics of the Doppler-shifted fundamental.

This "geometric line broadening" is illustrated in Fig. 1 and 2 for an electron moving along the axis of a cylinder in which focusing is provided by both a twisted quadrupole and longitudinal magnetic fields. Figure 1 shows the spectrum as seen by an observer located exactly on the cylinder axis (i.e., $\theta = \Delta\theta = 0$). Three peaks are seen; a fourth is actually present but at indistinguishable amplitude on this scale. The four peaks precisely correspond to the four Doppler-shifted betatron frequencies $\omega_1,...,\omega_4$ for this case. The finite line widths are solely due to the fact that we numerically integrate (6) only over a finite time; the widths are seen to shrink as we increase the time of integration. For a real cylinder of finite length, of course, the radiated linewidth is nonzero. No harmonics of the fundamentals are present.

Figure 2 shows the result of an integration of (6) over an angular range $\gamma\theta$ from 0 to 0.6 (i.e., $\Delta\theta \doteq 0.6/\gamma = 0.06$). Line broadening and the appearance of energy radiated in harmonics is evident in this case. The fundamental peaks, however, are still identifiable.

The situation in a torus is such that it automatically presents any observer with a range of Doppler-shifted frequencies, as well as with many harmonics of the betatron and
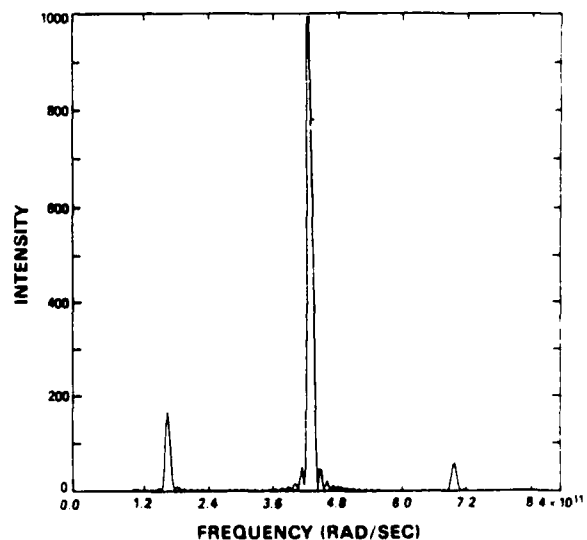
FIG. 1. Radiation emitted in forward direction by an electron moving along a cylindrical focusing channel. $\gamma = 10$, $k_w = 0.1$ cm^{-1}, $k_q B_s = 34$ G/cm $B_{\theta 0} = 0$.

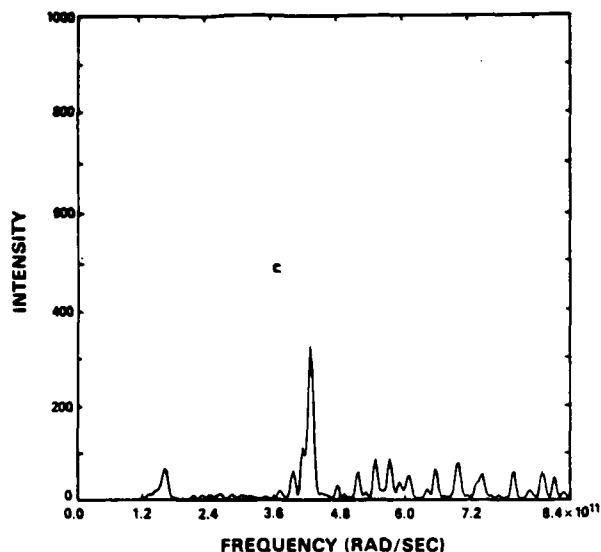FIG. 2. Integrated radiation spectrum over an angular range $\gamma\theta = 0 \to 0.6$.

FIG. 4. Radiation emitted by electron moving in a torus with $r_0 = 41 \times 10^2$ cm.

cyclotron frequencies. A distant observer "sees" an electron moving toward and away from him in a periodic fashion, therefore one expects radiation in the range $\omega_\beta / (1 - \beta_0)$ to $\omega_\beta / (1 + \beta_0)$. The intensity, though, at the Doppler up-shifted value is much larger than at the down-shifted value since relativistic effects tend to cause the most radiation to be emitted in the forward direction. As a practical matter, when trying to observe radiation from high-frequency betatron oscillations, one may expect interference from very high harmonics of the cyclotron frequency ω_0. This may be minimized by limiting observation to radiation polarized normal to the plane of the torus.

In Figs. 3–5, we show a series of spectra for an electron moving in the fields of a stellatron for different torus major
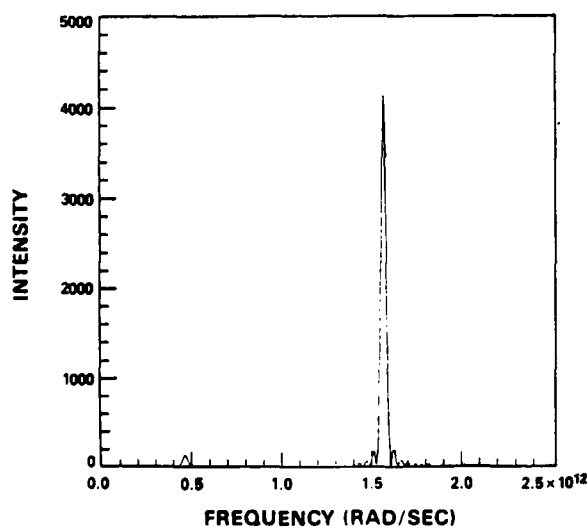
radii. In all cases, the integration time interval is held fixed. All cases share the values $B_{\theta 0} = 8.6$ kG, $k_w B_s = 247$ G/cm, $k_w = 0.293$ cm^{-1}, $\gamma_0 = 5.23$, which are typical of the UC Irvine device. The values for the four Doppler up-shifted betatron frequencies, for $r_0 = 41$ cm, are $\omega_1,...,\omega_4 = 2.03 \times 10^{12}$, -1.57×10^{12}, 4.62×10^{11}, and 3.91×10^9 rad/s.

Figure 3 shows the result for $r_0 = 41 \times 10^6$ cm; as expected, the spectrum is quite clean, consisting of narrow lines at $-\omega_2$ and ω_3. (The other two peaks are extremely weak for the particle initial conditions we chose.)

When the radius is reduced to 41×10^2 cm, the spectrum in Fig. 4 results. The expected line broadening is beginning

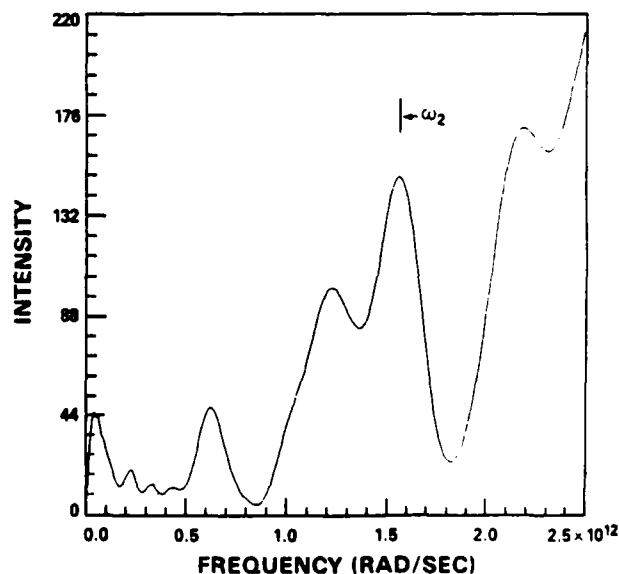FIG. 3. Radiation emitted by electron moving in a torus with $r_0 = 41 \times 10^6$ cm.

FIG. 5. Radiation emitted by electron moving in a torus with $r_0 = 41$ cm.
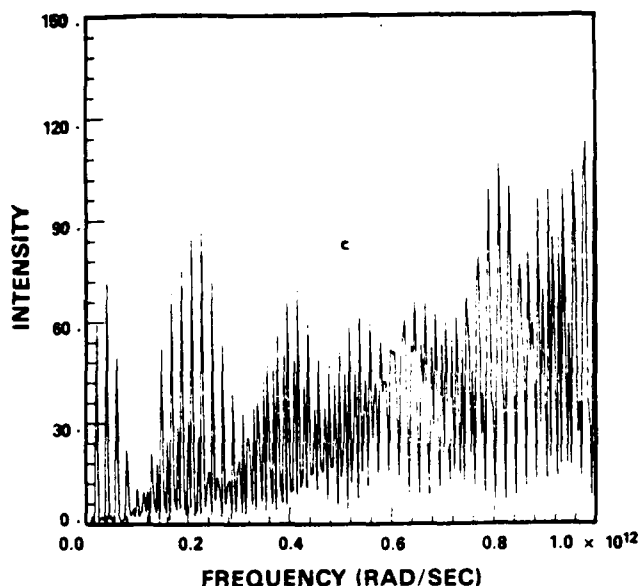
FIG. 6. As in Fig. 5, but with finer frequency resolution.

to become evident at this radius.

Finally, for $r_0 = 41$ cm, the spectrum is dramatically more complicated as illustrated in Fig. 5. The lines have become quite broad, although the dominant one at $-\omega_2$ is still identifiable, and significant amounts of energy are now being observed at harmonics and beats of the betatron frequencies. A calculation done at finer frequency resolution (Fig. 6) shows the complicated structure of the spectrum for this case.

IV. DISCUSSION AND CONCLUSIONS

In a straight section, we have found that radiation emitted by the betatron motion of electrons may provide a useful energy diagnostic by measurement of the forward Doppler shift. In a torus, however, geometrical effects greatly complicate the form of the spectrum and interpretation of the spectral peaks. The widths of the peaks will depend both on geometric effects and on the actual energy spread in the beam. Still, it may be possible to identify the various peaks in the toroidal case with careful study. We have also considered the possibility that radiation from betatron oscillations might provide a useful diagnostic for other quantities. Though this may be the case for various field gradients and field strengths, it does not seem to be useful as a beam density measurement, since only the betatron frequencies below the beam tube cutoff are at all sensitive to the value of the density.

ACKNOWLEDGMENTS

[1] C. W. Roberson, A. Mondelli, and D. Chernin, Phys. Rev. Lett. 50, 507 (1983); Part. Accel. 17, 79 (1985).
[2] H. Ishizuka, G. Leslie, B. Mandelbaum, A. Fisher, and N. Rostoker, IEEE Trans. NS-32, 2727 (1985).
[3] B. Levush, T. Antonsen, and W. Manheimer, J. Appl. Phys. 60, 1584 (1986).
[4] J. D. Jackson, Classical Electrodynamics (Wiley, New York, 1962), Eq. (14.67).

2740   J. Appl. Phys., Vol. 61, No. 8, 15 April 1987

D. Chernin and B. Levush   2740

"The Spiral-Line Induction Accelerator"

by:

S. Putnam, V. Bailey, A. Mondelli, D. Chernin and J. Petillo

(In press; classified.)

c

EVOLUTION OF RMS BEAM ENVELOPES IN TRANSPORT SYSTEMS WITH LINEAR $X - Y$ COUPLING†

D. CHERNIN

Science Applications International Corp., 1710 Goodridge Drive, McLean, Virginia 22102

Beam transport systems in which the two transverse degrees of freedom of particle motion (x and y) are coupled are often used to transport high-current, low-energy beams. Consideration of the matching problem for such systems requires a formalism for the description of the evolution of the beam envelope, including the effect of space charge. By defining a 4×4 beam covariance matrix, it is possible to give a simple prescription for following the rms beam ellipse through an arbitrary linear transport system, allowing the length of the axes of the ellipse and its angle of tilt to vary; the prescription trivially reproduces the usual K-V envelope equations in the decoupled case. The matching condition for the general coupled system is given, and the stability problem for the matched solution in the presence of space charge is formulated in general and discussed in a particular example.

1. INTRODUCTION

The familiar K-V envelope equations[1] are applicable to beams confined by focusing systems that do not couple the two transverse degrees of freedom of particle motion, x and y. The beam ellipse remains upright in these systems, and the axes merely vary in length along the direction of beam propagation. Certain focusing systems used for the transport of high-current, low-energy beams, however, do couple the x and y motion. In some simple cases with azimuthal symmetry, e.g. a solenoid, a transformation to a rotating frame decouples the two transverse degrees of freedom, but in the general case the problem is most directly treated in the coupled, "laboratory-frame" variables. Systems to which the following analysis may be applied include the modified betatron[2] (for all stable values of field index), the bumpy torus,[3] the reversing solenoid lens,[4] and the stellarator-focused betatron, or stellatron.[5] For this last case, matched beam solutions have been constructed,[6,7] but the stability of these solutions in the presence of space charge remains to be studied. The formalism outlined here allows such an analysis to be carried through this is done, as an example, below.

The stability of K-V distributions in quadrupole and solenoid systems has been analyzed by Hofmann, Laslett, Smith, and Haber[8] and by Struckmeier and Reiser.[9] Hofmann. *et al.* carried out a thorough analysis of the electrostatic

---

discussed here in Section 4.] No assumption is made here, of course, about the exact form of the distribution of particle initial conditions. Using Eq. (1) it follows that the matrix Σ obeys the equation

$$\Sigma'(s) = M\Sigma + (M\Sigma)^T, \tag{3}$$

where ^{T} denotes transpose.

The matrix M generally consists of two parts, one due to applied, extenal fields and another due to self, space-charge fields. For magnetic focusing with $\mathbf{B} = (B_x, B_y, B_z)$,

$$M^{ext}(s) = \begin{bmatrix} 0 & 1 & 0 & 0 \\ \bar{B}_{yx} & 0 & \bar{B}_{yy} & -\bar{B}_z \\ 0 & 0 & 0 & 1 \\ -\bar{B}_{xx} & \bar{B}_z & -\bar{B}_{xy} & 0 \end{bmatrix}, \tag{4}$$

where $\bar{B}_{ab} \equiv -q(\partial B_a/\partial b)/pc$, $\bar{B}_z \equiv -qB_z/pc$, q is the particle charge, p is its momentum, c is the speed of light, and cgs units are used.

The space-charge contribution ot $M(s)$ will depend on the spatial elements of Σ, viz., $\Sigma_{11} \equiv \sigma_{xx}$, $\Sigma_{33} \equiv \sigma_{yy}$, and $\Sigma_{13} \equiv \Sigma_{31} \equiv \sigma_{xy}$, that is, on the size and orientation of the beam ellipse. The space-charge forces are linear, of course, only when the ellipse is uniformly populated, as for the K–V distribution, which here takes the form

$$f(v^T W v) = \frac{|W|^{1/2}}{\pi^2} \delta[v^T(s_0)W(s_0)v(s_0) - 1], \tag{5}$$

where W is a positive definite, real symmetric matrix. If we define $V(s \mid s_0)$ as that 4×4 matrix solution to the single-particle equations of motion satisfying $V(s_0 \mid s_0) = 1$, the identity matrix, then

$$W(s) = V^{-1T}(s \mid s_0)W(s_0)V^{-1}(s \mid s_0) \tag{6}$$

and[10]

$$\Sigma(s) = \frac{1}{4} W^{-1}(s) = V(s \mid s_0)\Sigma(s_0)V^T(s \mid s_0). \tag{7}$$

The space-charge part of M is evaluated in terms of σ_{xx}, σ_{yy}, and σ_{xy} for the K–V distribution in the Appendix. The result may be expressed as

$$M^{sc}(s) = \frac{\bar{I}}{(\beta\gamma)^3} \begin{bmatrix} 0 & 0 & 0 & 0 \\ q_{xx} & 0 & q_{xy} & 0 \\ 0 & 0 & 0 & 0 \\ q_{xy} & 0 & q_{yy} & 0 \end{bmatrix}, \tag{8}$$

where $\bar{I}$ = beam current in $\hat{s}$ direction/(mc^3/q), m is the particle mass, β and γ are the usual relativistic factors, $q_{xx} = S_y/D$, $q_{yy} = S_x/D$, $q_{xy} = -\sigma_{xy}/D$, $D = S_0(S_x + S_y)$, $S_x = S_0 + \sigma_{xx}$, $S_y = S_0 + \sigma_{yy}$, and $S_0 = (\sigma_{xx}\sigma_{yy} - \sigma_{xy}^2)^{1/2}$.

With $M(s)$ given by the sum of Eqs. (4) and (8), Eq. (3) describes the evolution

of the x-y coupled K–V beam envelope in the presence of space charge. In the decoupled system, with M^{ext} in 2×2 block diagonal form ($\bar{B}_{xx} = \bar{B}_{yy} = 0 = \bar{B}_z$) and $\sigma_{xy} = 0$, some algebra shows that Eq. (3) reproduces the usual K–V envelope equations, for the radii $r_x = 2\sigma_{xx}^{1/2}$ and $r_y = 2\sigma_{yy}^{1/2}$. For $\sigma_{xy} \neq 0$, the K–V beam radii ($r_\pm$) and the angle (α) that the major beam axis makes with the x-axis are given by

$$\tfrac{1}{2}r_\pm^2 = \sigma_{xx} + \sigma_{yy} \pm \sigma_0 \tag{9a}$$

$$\sin 2\alpha = 2\sigma_{xy}/\sigma_0 \tag{9b}$$

$$\cos 2\alpha = (\sigma_{xx} - \sigma_{yy})/\sigma_0, \tag{9c}$$

where $\sigma_0 = [(\sigma_{xx} - \sigma_{yy})^2 + 4\sigma_{xy}^2]^{1/2}$.

In the decoupled case, the quantities $\sigma_{xx}\sigma_{x'x'} - \sigma_{xx'}^2 \equiv \varepsilon_{x\,rms}^2$ and $\sigma_{yy}\sigma_{y'y'} - \sigma_{yy'}^2 \equiv \varepsilon_{y\,rms}^2$ are conserved, in the absence of acceleration. When coupling is present it follows from Eq. (7) or, more generally, from Eq. (3) that the determinant of Σ is conserved. In the decoupled case, $|\Sigma| = \varepsilon_{x\,rms}^2 \varepsilon_{y\,rms}^2$, which suggests that the quantity

$$\varepsilon_{xy\,rms} \equiv |\Sigma|^{1/4} \tag{10}$$

may be a useful definition of beam quality in the coupled case; such a quantity is easily calculated by particle-tracking codes.

3. MATCHED SOLUTIONS AND THEIR STABILITY

We consider the simplest definition of a matched solution to Eq. (3) in a periodic focusing system with period L; for all s

$$\Sigma(s + L) = \Sigma(s). \tag{11}$$

A slightly more general definition, which specifies that the beam ellipse rotates by some 'e θ every period, is possible but greatly complicates the analysis in the gen̩ e. This more general definition is important to consider for focusing by a lc ̣nal field; in that case one can find matched solutions that rotate at the Larm... ̣requency. We will assume here, however, that the beam ellipse returns to its initial shape and orientation every period, as specified by Eq. (11). If Eq. (7) is used, the matching condition for any distribution of the form $f(Q)$, where $Q = v^T W v$, is

$$\Sigma_0 = V_0 \Sigma_0 V_0^T, \tag{12}$$

where $\Sigma_0 = \Sigma(s_0)$ and $V_0 = V(s_0 + L \mid s_0)$. The solution of Eq. (12) for Σ_0 gives the matched launching condition for the beam matrix.

The eigenvalues of V_0 all have complex modulus 1 (since, by assumption, the single-particle motion is stable) and occur in conjugate pairs. When the eigenvalues are all distinct the eigenvectors of V_0 are complete, which we assume to be the case. If we define a matrix U that has, as columns, the normalized eigenvectors of V_0, then any 4×4 matrix, in particular Σ_0, may be written

$$\Sigma_0 = UDU^T \tag{13}$$

for some matrix of coefficients D. Substituting Eq. (13) into Eq. (12) and ordering the eigenvalues of V_0 such that $\lambda_1\lambda_2 = \lambda_3\lambda_4 = 1$, one obtains the result that only the elements D_{12}, D_{21}, D_{34}, and D_{43} of D are non-vanishing. Requiring that Σ_0 be symmetric and real means that D is symmetric and real; that is, the matched solution Σ_0 depends on just two arbitrary real parameters, D_{12} and D_{34}. In the decoupled case, of course, these parameters are related to the x and y emittances.

For $s > s_0$ the matched solution, from Eq. (7), is

$$\Sigma_0(s) = F(s)DF^T(s), \tag{14}$$

where $F(s) \equiv V(s \mid s_0)U$ is the matrix containing the four Floquet solutions of Eq. (1); F satisfies

$$F(s_0 + L) = F(s_0)\Lambda, \tag{15}$$

where Λ is diagonal and contains the eigenvalues of V_0.

In the presence of the K–V space-charge term, Eq. (8), one cannot calculate V_0 from Eq. (1) before knowing the matched solution for Σ, and an iterative solution is necessary; the most direct technique is to neglect space charge at first, calculate V_0 and the matched solution for Σ, then recalculate V_0, and so on. This method is used successfully in the example treated in Section 4.

Once a matched solution is obtained one may ask whether it is stable; that is, if a beam is launched with a distribution that is close to being matched, does it remain close to the matched solution for $s > s_0$? This is an important question for highly artificial distributions such as the K–V distribution that are never exactly (but that may be approximately) realized in practice.

In the absence of space charge the matched solution is clearly stable with respect to slight variations in Σ_0; replacing Σ_0 by $\Sigma_0 + \delta\Sigma_0$ in Eq. (7) clearly does not affect the stability of $\Sigma(s)$ since the single-particle solutions $V(s \mid s_0)$ are assumed to be stable.

In the presence of space charge one examines stability by linearizing Eq. (3). Writing $\Sigma(s) = \Sigma_0(s) + \Sigma_1(s)$ and $M(s) = M_0(s) + M_1(s)$, where a subscript 1 denotes the perturbation, one obtains the linearized equation for Σ_1:

$$\Sigma_1'(s) = M_0\Sigma_1 + (M_0\Sigma_1)^T + M_1\Sigma_0 + (M_1\Sigma_0)^T. \tag{16}$$

Only the space-charge part of M, Eq. (8), contributes to M_1 in Eq. (16). The actual linearization of M^{sc} is completely straightforward, if a bit tedious. The nine quantities needed are

$$\frac{1}{q_{xx}}\frac{\partial q_{xx}}{\partial \sigma_{xx}} = \frac{\sigma_{yy}}{2S_0S_y} - d_{xx} \tag{17a}$$

$$\frac{1}{q_{xx}}\frac{\partial q_{xx}}{\partial \sigma_{yy}} = \frac{1 + \sigma_{xx}/2S_0}{S_y} - d_{yy} \tag{17b}$$

$$\frac{1}{q_{xx}}\frac{\partial q_{xx}}{\partial \sigma_{xy}} = \frac{-\sigma_{xy}}{S_0S_y} - d_{xy} \tag{17c}$$

$$\frac{1}{q_{yy}}\frac{\partial q_{yy}}{\partial \sigma_{xx}} = \frac{1 + \sigma_{yy}/2S_0}{S_x} - d_{xx} \tag{17d}$$

$$\frac{1}{q_{yy}}\frac{\partial q_{yy}}{\partial \sigma_{yy}} = \frac{\sigma_{xx}}{2S_0S_x} - d_{yy} \tag{17e}$$

$$\frac{1}{q_{yy}}\frac{\partial q_{yy}}{\partial \sigma_{xy}} = \frac{-\sigma_{xy}}{S_0S_x} - d_{xy} \tag{17f}$$

$$\frac{1}{q_{xy}}\frac{\partial q_{xy}}{\partial \sigma_{xx}} = -d_{xx} \tag{17g}$$

$$\frac{1}{q_{xy}}\frac{\partial q_{xy}}{\partial \sigma_{yy}} = -d_{yy} \tag{17h}$$

$$\frac{1}{q_{xy}}\frac{\partial q_{xy}}{\partial \sigma_{xy}} = \frac{1}{\sigma_{xy}} - d_{xy}, \tag{17i}$$

where

$$d_{xx} = \frac{\sigma_{yy}}{2S_0^2} + q_{xx} \tag{18a}$$

$$d_{yy} = \frac{\sigma_{xx}}{2S_0^2} + q_{yy} \tag{18b}$$

$$d_{xy} = \frac{-\sigma_{xy}}{S_0^2} + 2q_{xy}. \tag{18c}$$

Equation (16) represents ten coupled linear equations with periodic coefficients; the ten quantities are the distinct elements of the 4×4 symmetric matrix Σ_1. By reassembling the ten quantities into a column vector w, Eq. (16) may be formally written

$$w'(s) = N(s)w(s), \tag{19}$$

where $N(s)$ is a 10×10 matrix with period L. In the usual way, one now defines another 10×10 matrix $T(s \mid s_0)$, each column of which satisfies Eq. (19); T is defined to satisfy the initial condition $T(s_0 \mid s_0) = 1$, the identity matrix. The eigenvalues of $T(s_0 + L \mid s_0)$ then determine the stability of the system; an envelope mode is (stable, unstable) if the modulus of the corresponding eigenvalue is (less than or equal to, seems greater than) 1. There are ten eigenvalues of $T(s_0 + L \mid s_0)$, the product of which may be shown to be 1. If λ is an eigenvalue then so is λ^*; $1/\lambda$ is *not* also necessarily an eigenvalue, as it is in the decoupled case.[9] The ten eigenvalues are accounted for as follows: In the decoupled system, Eqs. (3) and (16) both reduce to two 2×2 matrix equations, one each for x and y. Each 2×2 submatrix of Σ is symmetric so there are $2 \times 3 = 6$ independent variables, giving 6 eigenvalues in the decoupled case. (Struckmeier and Reiser restrict perturbations to those that do not change the emittances ε_x and ε_y, and so find $6 - 2 = 4$ eigenvalues.) The remaining four eigenvalues are attributable to the $x - y$ coupling.

4. AN EXAMPLE: BEAM TRANSPORT IN AN $l = 2$ STELLARATOR FIELD

It has been suggested that an $l = 2$ stellarator field may have some advantages for the transport of high-current, relativistic electron beams.[5] Such a field consists of a continuously twisted magnetic quadrupole superimposed on a constant longitudinal field. The analysis of the form of the matched K–V beam in the continuous quadrupole case has been treated by Gluckstern;[6] inclusion of a longitudinal field requires only a redefinition of certain quantities in his analysis. Here we sketch out the solution in our own notation[7] and go on to study the envelope stability problem.

The quadrupole field takes the form

$$B_x(x, y, s) \approx kB_0(-x \sin 2ks + y \cos 2ks) \tag{20}$$

$$B_y(x, y, s) \approx kB_0(x \cos 2ks + y \sin 2ks), \tag{21}$$

where k and B_0 are constants. In the presence of the space-charge fields Eqs. (A-1, -2) the paraxial equations for a particle near the axis may be written compactly as

$$\xi'' + ib_1\xi' - n_{s1}\xi + \left(\mu_1 e^{2iks} + n_{s1}\frac{a-b}{a+b}e^{2i\alpha}\right)\xi^* = 0, \tag{22}$$

where $\xi = x + iy$, $b_1 = -eB_s/pc$, $\mu_1 = -kB_0e/pc$, $n_{s1} = (\omega_b/\beta\gamma c)^2/2$, ω_b = beam-plasma frequency, $-e$ and p are the electron charge and momentum, and a, b, and α are the radii and orientation angle of the ellipse (see Appendix).

The matched beam consists of an ellipse of fixed radii that rotates with the quadrupole field; that is, a and b are constants, and $\alpha = ks$. The substitution $\xi = \psi e^{iks}$ then allows the following solution to Eq. (22):

$$\psi = A_+e^{i\kappa_+s} + \sigma_+A_+^*e^{-i\kappa_+s} + A_-e^{i\kappa_-s} + \sigma_-A_-^*e^{-i\kappa_-s}, \tag{23}$$

where $A_\pm$ are arbitrary complex numbers,

$$\kappa_\pm^2 = -k_2^2 + \frac{1}{2}b_2^2 \pm \left[b_2^2\left(\frac{1}{4}b_2^2 - k_2^2\right) + \mu_2^2\right]^{1/2}, \tag{24}$$

$$\sigma_\pm = \frac{\kappa_\pm^2 + b_2\kappa_\pm + k_2^2}{\mu_2} = \frac{\mu_2}{\kappa_\pm^2 - b_2\kappa_\pm + k_2^2}, \tag{25}$$

where $k_2^2 = k^2 + kb_1 + n_{s1}$, $b_2 = b_1 + 2k$, and $\mu_2 = \mu_1 + n_{s1}(a - b)/(a + b)$. In the interesting special case where $b_2 = 0$, corresponding to the situation in which the period of the quadrupole field equals the electron cyclotron wavelength,[7] one finds $\sigma_\pm = \pm\mathrm{sgn}\,(\mu_2)$.

The betatron oscillations are stable ($\kappa_\pm$ are real) when

$$b_2^2\left(\frac{1}{4}b_2^2 - k_2^2\right) + \mu_2^2 > 0 \tag{26a}$$

$$\frac{1}{2}b_2^2 - k_2^2 > 0 \tag{26b}$$
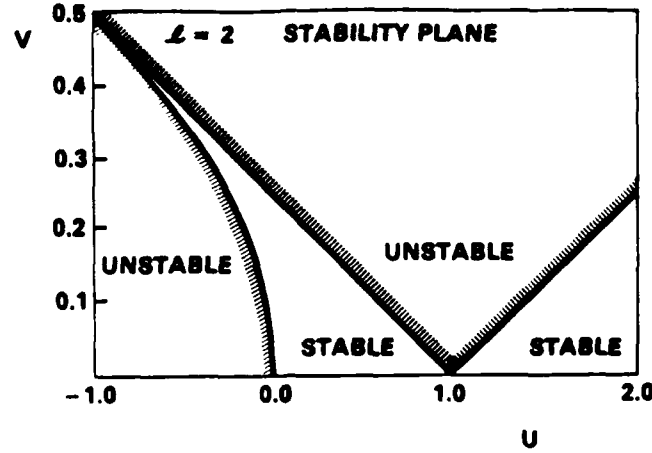
$$|k_2^2| - |\mu_2| > 0. \tag{26c}$$

FIGURE 1 Stellarator stability plane. The quantities u and v are defined in the text following Eq. (26c).

These conditions may be illustrated using the auxiliary quantities

$$u = 1 - 4k_2^2/b_2^2, \qquad v = |\mu_2|/b_2^2,$$

as shown in Fig. 1. In the absence of space charge, only Eq. (26c) represents a nontrivial constraint.

We construct a K–V distribution that is independent of the phases of $A_\pm$:

$$f = f_0\delta(f_+ |A_+|^2 + f_- |A_-|^2 - 1),\tag{27}$$

where f_0, $f_\pm$ are constants. The amplitudes may be expressed as functions of the real and imaginary parts of ψ:

$$|A_+|^2 = \frac{1}{D_1^2}[\kappa_-(1 - \sigma_-)\psi_r - (1 + \sigma_-)\psi_i']^2 + \frac{1}{D_2^2}[\kappa_-(1 + \sigma_-)\psi_i + (1 - \sigma_-)\psi_r']^2 \tag{28a}$$

$$|A_-|^2 = \frac{1}{D_1^2}[\kappa_+(1 - \sigma_+)\psi_r - (1 + \sigma_+)\psi_i']^2 + \frac{1}{D_2^2}[\kappa_+(1 + \sigma_+)\psi_i + (1 - \sigma_+)\psi_r']^2, \tag{28b}$$

where $D_1 = -\kappa_+(1 - \sigma_+)(1 + \sigma_-) + \kappa_-(1 + \sigma_+)(1 - \sigma_-)$, and $D_2 = \kappa_+(1 + \sigma_+) \times (1 - \sigma_-) - \kappa_-(1 - \sigma_+)(1 + \sigma_-)$. One may alternately[6] express the amplitudes in terms of ψ_r, ψ_i, and the canonical momenta $P_r = \psi_r' - \frac{1}{2}b_2\psi_i$, and $P_i = \psi_i' + \frac{1}{2}b_2\psi_r$.

Using Eqs. (28) in Eq. (27) and integrating over ψ_r' and ψ_i' one finds that the beam radii in the real and imaginary directions are

$$a^2 = \frac{(1 + \sigma_+)^2}{f_+} + \frac{(1 + \sigma_-)^2}{f_-} \tag{29a}$$

$$b^2 = \frac{(1 - \sigma_+)^2}{f_+} + \frac{(1 - \sigma_-)^2}{f_-}. \tag{29b}$$

Similarly, one may calculate the emittances in the real and imaginary directions by integrating Eq. (27) over (ψ_r, ψ_r') and (ψ_i, ψ_i'):

$$\varepsilon_r^2 = a^2 \left[\frac{\kappa_+^2(1+\sigma_+)^2}{f_+} + \frac{\kappa_-^2(1+\sigma_-)^2}{f_-} \right] \tag{30a}$$

$$\varepsilon_i^2 = b^2 \left[\frac{\kappa_+^2(1-\sigma_+)^2}{f_+} + \frac{\kappa_-^2(1-\sigma_-)^2}{f_-} \right]. \tag{30b}$$

In the quadrupole-only case, Gluckstern has defined the emittances as areas in the $P_r - \psi_r$ and $P_i - \psi_i$ planes instead. For the present problem these are given by

$$\varepsilon_{Gr}^2 = a^2 \left(\frac{c_+^2}{f_+} + \frac{c_-^2}{f_-} \right) \tag{31a}$$

$$\varepsilon_{Gi}^2 = b^2 \left(\frac{d_+^2}{f_+} + \frac{d_-^2}{f_-} \right), \tag{31a}$$

where $c_+ = \kappa_+(1+\sigma_+) + \frac{1}{2}b_2(1-\sigma_+)$, $c_- = \kappa_-(1+\sigma_-) + \frac{1}{2}b_2(1-\sigma_-)$, $d_+ = \kappa_+(1-\sigma_+) + \frac{1}{2}b_2(1+\sigma_+)$, and $d_- = \kappa_-(1-\sigma_-) + \frac{1}{2}b_2(1+\sigma_-)$.

Using the definitions of Σ and ψ and Eqs. (27) and (28), the value of the matched Σ matrix may now be calculated. The nonzero elements at $s = 0$ are

$$\Sigma_{11} = \frac{1}{4} a^2$$

$$\Sigma_{14} = \Sigma_{41} = \frac{1+\sigma_+}{f_+} [k(1+\sigma_+) + \kappa_+(1-\sigma_+)] + (+ \rightarrow -)$$

$$\Sigma_{22} = \frac{1}{f_+} [k(1-\sigma_+) + \kappa_+(1+\sigma_+)]^2 + (+ \rightarrow -)$$

$$\Sigma_{23} = \Sigma_{32} = -\frac{1-\sigma_+}{f_+} [k(1-\sigma_+) + \kappa_+(1+\sigma_+)] + (+ \rightarrow -) \tag{32}$$

$$\Sigma_{33} = \frac{1}{4} b^2$$

$$\Sigma_{44} = \frac{1}{f_+} [k(1+\sigma_+) + \kappa_+(1-\sigma_+)]^2 + (+ \rightarrow -),$$

where the notation $+ (+ \rightarrow -)$ means add the previous term with all $+$ subscripts replaced by $-$. The matched Σ matrix is clearly divided into a sum of two contributions, one from the fast $(+)$ betatron oscillation mode and one from the slow $(-)$ mode, corresponding to the decomposition in Eq. (13). The determinant of Σ, a constant of motion, is given by

$$|\Sigma| = \left(\frac{D_1 D_2}{16 f_+ f_-} \right)^2. \tag{33}$$

The specification of Σ depends on the two unspecified constants $f_\pm$, which may be determined in a variety of ways. One reasonable choice would seem to be to

D. CHERNIN

specify a value for $|\Sigma|$ and to require that $\varepsilon_r = \varepsilon_i$ in Eq. (30). This choice, however, gives the unsatisfactory result that the matched beam radii are *decreasing* functions of beam current unless the operating point is in the "second stable region" of Fig. 1, where $u > 1$. Curiously, instead of specifying $\varepsilon_r = \varepsilon_i$, the choice $\varepsilon_{Gr} = \varepsilon_{Gi}$, from Eq. (31), avoids this problem, leading to beam radii that are increasing functions of current; we make this choice in the numerical example, below. The corresponding condition on $f_\pm$ is, using Eq. (31),

$$|1 - \sigma_-^2|f_+ = |1 - \sigma_+^2|f_-, \tag{34}$$

except in the special case[7] $b_2 = 0$, for which $\sigma_\pm = \pm \operatorname{sgn}(\mu_2)$; in that case Eq. (34) is replaced by the condition $\kappa_- f_+ = \kappa_+ f_-$.

Figures 2a, 3a, 4a, and 5a illustrate the dependence of beam radii on beam current, beam energy, longitudinal field strength, and quadrupole field strength, respectively. All cases have $k = -2\pi/18\,\mathrm{cm}^{-1}$ and $\beta\gamma\,|\Sigma|^{1/4} = 2.78 \times 10^{-3}\,\mathrm{rad\text{-}cm}$, which correspond to typical values for a beam-transport experiment presently being carried out.[11] Each point on the plots, except those for zero current, requires an iterative procedure to obtain because the betatron wavenumbers $\kappa_\pm$ depend on current density, that is on the beam radii, which makes Eqs. (29) implicit relations for the beam radii, for nonzero current. Once the beam radii are found, the elements of the matched Σ matrix at $s = 0$ follow from Eq. (32).

One may study the stability of the matched solution, using Eq. (16). One might expect that since the matched solution is a constant in the frame rotating with the stellarator field, one could carry through the stability analysis to calculate oscillation frequencies and growth rates analytically for this example. Actually, even in the rotating frame [the frame of the ψ-variable of Eq. (23)] the two degrees of freedom, ψ_r and ψ_i, are coupled, requiring the calculation of the eigenvectors of a full 4×4 matrix to find the matched solution. Note however that in the special case where $b_2 = 0$, described following Eq. (25), the coupling in the rotating frame vanishes, and the formalism described here may be shown to reproduce the K-V envelope equations, with constant focusing terms, in the rotating frame; in this case the envelope oscillation frequencies are easily calculated[9] analytically, and agree with those obtained numerically from Eq. (16). To study the linear stability problem in the coupled case, Eq. (16) must be integrated simultaneously with Eq. (3) for the matched solution, using Eq. (32) as the initial condition. One then forms the matrix $T(L \mid 0)$, defined following Eq. (19) and finds its eigenvalues λ_j, $j = 1, 2, \ldots, 10$. We define the growth rate per period as

$$\Gamma_j = \ln|\lambda_j|. \tag{35}$$

Figures 2b–5b show plots of the growth rates for the unstable ($\Gamma_j > 0$) envelope modes as functions of system parameters. One sees that, depending on parameter values, the dominant mode has a fairly large peak growth rate, which suggests the probability of large emittance growth for a real system at this point. The growth-rate curves of Figs. 2b–5b are typical of an instability due to a system resonance, which is detuned when system parameters are varied slightly; in fact, this is an example of a "confluent resonance" for the stellarator system.[9] We note that calculation of linear growth rates for the K-V beam, although not
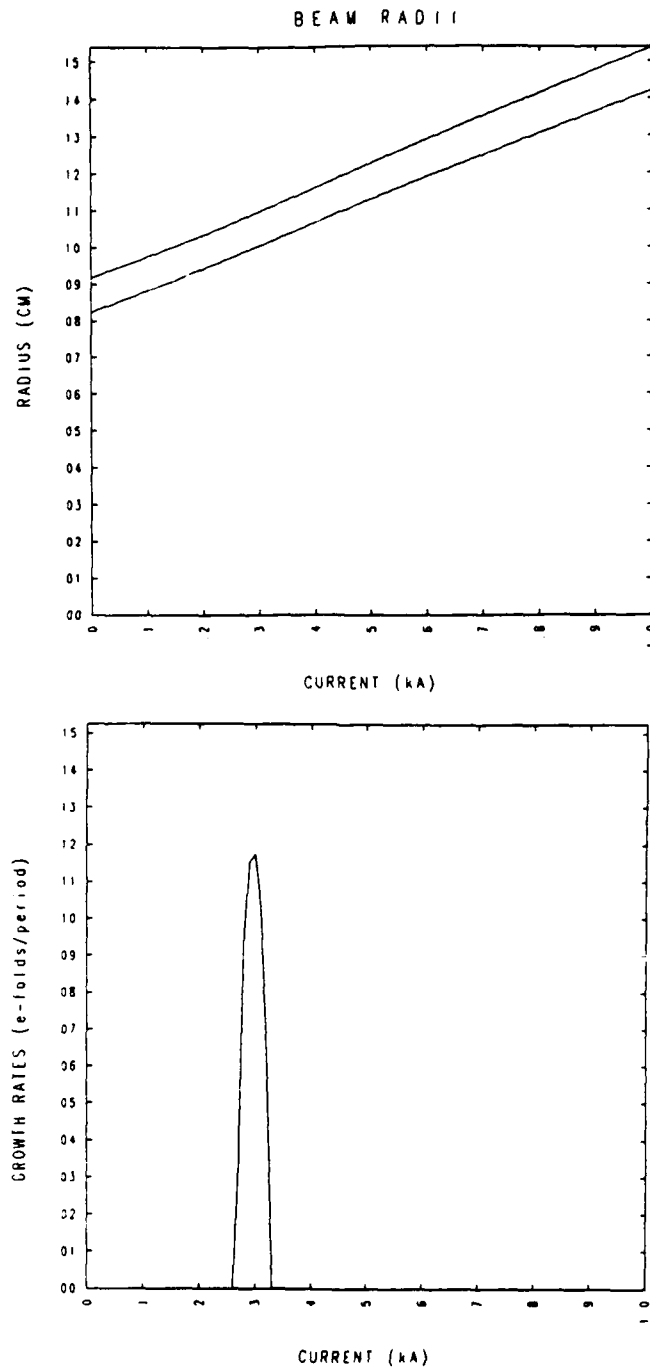
BEAM RADII

CURRENT (kA)

CURRENT (kA)

FIGURE 2   Equilibrium beam radii and growth rates for unstable envelope modes versus current for $E_{beam} = 1$ MeV, $B_t = 5$ kG, and $kB_0 = 500$ G/cm.
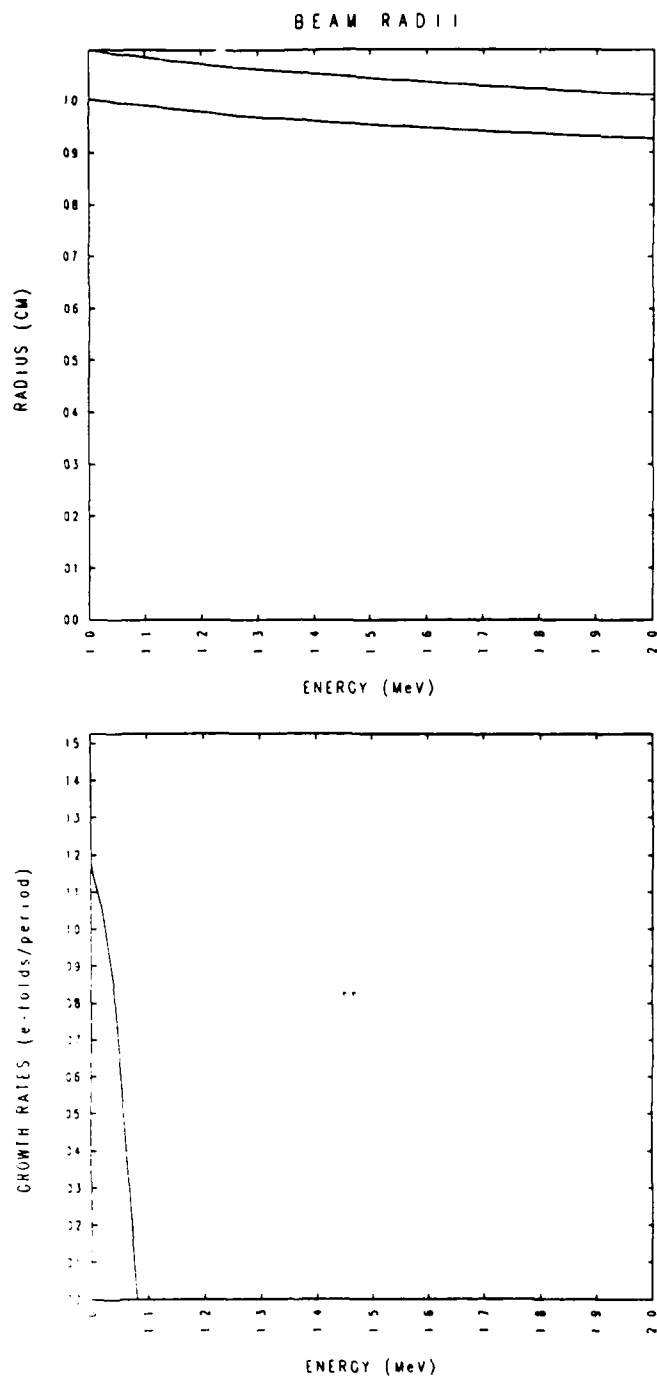
D. CHERNIN

BEAM RADII

FIGURE 3 Equilibrium beam radii and growth rates for unstable envelope modes versus beam energy for I_{beam} = 300 A, B_r = 5 kG, and kB_0 = 500 G/cm.
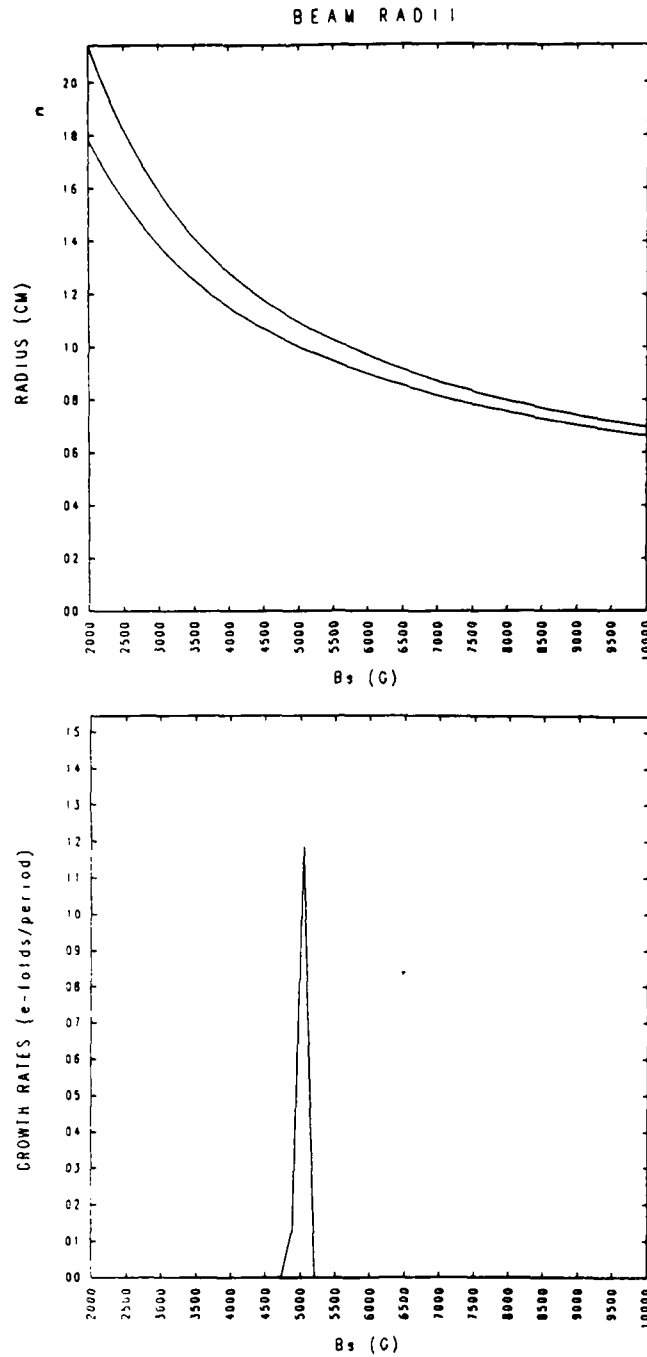
BEAM   RADII

Bs (G)

Bs (G)

FIGURE 4 Equilibrium beam radii and growth rates for unstable envelope modes versus longitudinal field strength for $I_{beam} = 300$ A, $E_{beam} = 1$ MeV, and $kB_0 = 500$ G/cm.
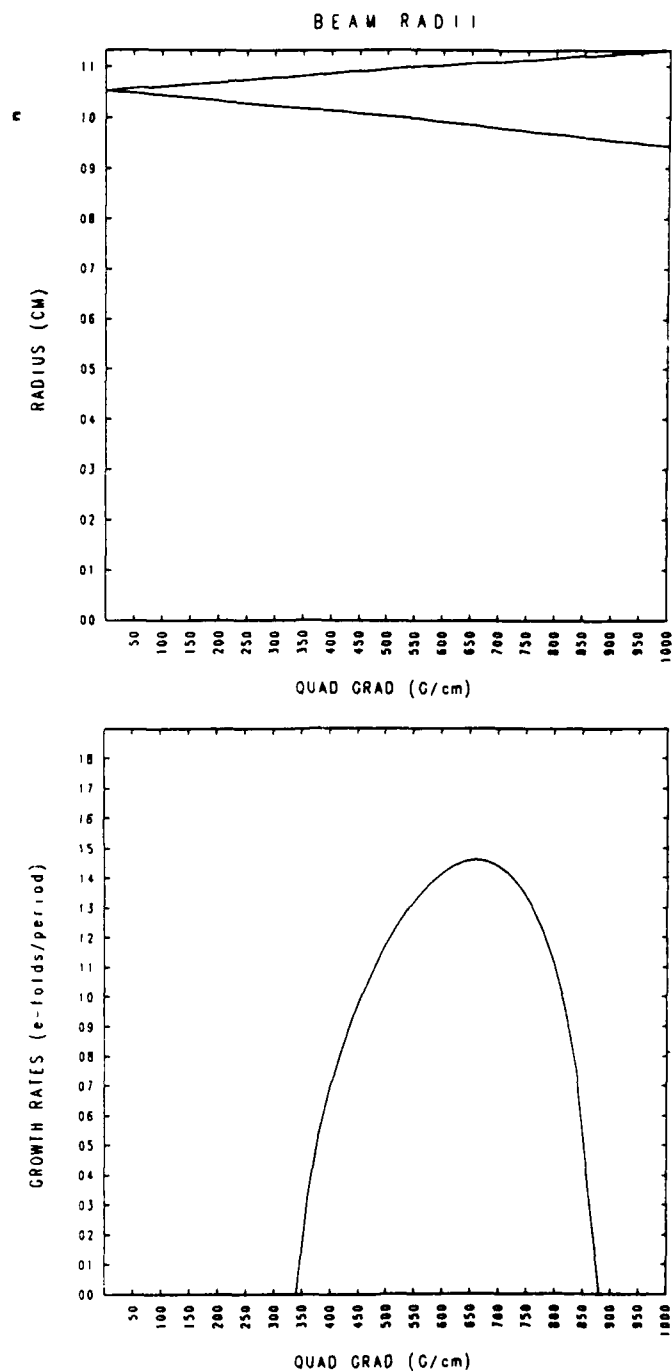
BEAM RADII

QUAD GRAD (G/cm)

QUAD GRAD (G/cm)

FIGURE 5 Equilibrium beam radii and growth rates for unstable envelope modes versus quadrupole field strength for $I_{beam} = 300$ A, $E_{beam} = 1$ MeV, and $B_s = 5$ kG.

quantitatively important for real beams, may suggest values of parameters (external field strengths, beam currents and energies, etc.) required to avoid significant emittance growth in real beams. Numerical simulations need to be done to test this conjecture for the stellarator system, though simulations in the decoupled case show that emittance growth is observed in simulations of beams with realistic profiles when the growth rates for corresponding K–V beams are large.[8,9]

ACKNOWLEDGMENT

I thank A. Mondelli, J. Petillo, and M. Tiefenback for several helpful discussions.

APPENDIX

Space-Charge Contribution to Matrix M for K–V Distribution

We consider the self-fields of an elliptical beam of axes a and b; axis a is tilted at an angle α to the x-axis. The electro- and magneto-static potentials are simply obtained by rotation of coordinates:

$$\phi(x, y) = -\frac{\lambda}{2}(q_{xx}x^2 + 2q_{xy}xy + q_{yy}y^2) \tag{A-1}$$

$$\mathbf{A}(x, y) = \beta\phi\hat{s}, \tag{A-2}$$

where λ is the line-charge density and

$$q_{xx} = \frac{4}{a+b}\left(\frac{\cos^2\alpha}{a} + \frac{\sin^2\alpha}{b}\right) \tag{A-3a}$$

$$q_{yy} = \frac{4}{a+b}\left(\frac{\cos^2\alpha}{b} + \frac{\sin^2\alpha}{a}\right) \tag{A-3b}$$

$$q_{xy} = \frac{4}{a+b}\sin\alpha\cos\alpha\left(\frac{1}{a} - \frac{1}{b}\right). \tag{A-3c}$$

The values of the spatial σ's for a uniformly populated ellipse are

$$\sigma_{xx} = \frac{1}{4}(a^2\cos^2\alpha + b^2\sin^2\alpha) \tag{A-4a}$$

$$\sigma_{yy} = \frac{1}{4}(b^2\cos^2\alpha + a^2\sin^2\alpha) \tag{A-4b}$$

$$\sigma_{xy} = \frac{1}{4}(a^2 - b^2)\sin\alpha\cos\alpha. \tag{A-4c}$$

It is now simply a matter of algebra to eliminate a, b, and α from Eqs. (A-3) in

favor of σ_{xx}, σ_{yy}, and σ_{xy}, using Eqs. (A-4). The intermediate results

$$ab = 4(\sigma_{xx}\sigma_{yy} - \sigma_{xy}^2)^{1/2}, \tag{A-5}$$

$$a^2 + b^2 = 4(\sigma_{xx} + \sigma_{yy}) \tag{A-6}$$

are useful for this exercise. The results for q_{xx}, q_{yy}, and q_{xy}, cited in the text, follow.

REFERENCES

1. I. M. Kapchinskij and V. V. Vladimirskij, *Proc. International Conf. on High Energy Accelerators*, CERN (1959).
2. P. Sprangle and C. A. Kapetanakos, *J. Appl. Phys.* **49**, 1 (1978): N. Rostoker, *Comments on Plasma Phys.* **6**, 91 (1980).
3. D. Chernin, A. Mondelli, and C. Roberson, *Phys. Fluids* **27**, 2378 (1984).
4. S. Humphries, Jr., and D. M. Woodall, *Bull. Amer. Phys. Soc.* **28**, 1054 (1983).
5. C. W. Roberson, A. Mondelli, and D. Chernin, *Phys. Rev. Lett.* **50**, 507 (1983).
6. R. L. Gluckstern, *Proc. 1979 Linear Accelerator Conf.*, pp. 245–248.
7. D. Chernin, Proc. 1985 Particle Accelerator Conf. [*IEEE Trans. Nucl. Sci.* **NS-32**, 2504 (1985)].
8. I. Hofmann, L. J. Laslett, L. Smith, and I. Haber, *Part. Accel.* **13**, 145 (1983).
9. J. Struckmeier and M. Reiser, *Part. Accel.* **14**, 227 (1984).
10. For other distributions $f(Q)$, functions of the quadratic form $Q = v^T W v$, a straightforward calculation shows that Eqs. (6) and (7) continue to hold, with the replacement of the factor 1/4 in Eq. (7) by $\alpha/4$, where $\alpha = \int_0^\infty dQ\, Q^2 f(Q)/\int_0^\infty dQ\, Q f(Q)$.
11. V. Bailey, *et al.*, *Proc. 1987 Particle Accelerator Conf.*, Washington, DC., pp 920–922.

APPENDIX B
Conference Presentations

1. "Envelope Stability for $\ell=0$ Focusing Systems," A. Mondelli and D. Chernin *APS/DPP Meeting*, Boston, MA (Oct.-Nov. 1984).

2. "Self-Consistent Treatment of Equilibrium Space Charge Effects in the $\ell=2$ Stellatron," D. Chernin, *Particle Accelerator Conference*, Vancouver (May 1985).

3. "A Strong-Focused Spiral Line Recirculating Induction Linac," A. Mondelli, D. Chernin, S. Putnam, and L. Schlitt, *Compact Accelerator Workshop*, LLNL (Oct. 1985).

4. "Orbital Resonances and Energy and Current Limits in High Current Cyclic Accelerators," D. Chernin and A. Mondelli, *Compact Accelerator Workshop*, LLNL (Oct. 1985).

5. "Collective Effects in the $\ell=2$ Stellatron," D. Chernin, *APS/DPP Meeting*, San Diego, CA (Nov. 1985).

6. "A Strong-Focusing Spiral Line Recirculating Induction Accelerator," A. Mondelli, D. Chernin, S. Putnam, and L. Schlitt, *APS/DPP Meeting*, San Diego, CA (Nov. 1985).

7. "Linear Orbital Resonances in the $\ell=2$ Stellatron," D. Chernin, *APS/DPP Meeting*, San Diego, CA (Nov. 1985).

8. "Radiation from Betatron Oscillations as a Diagnostic for High Current Cyclic Electron Accelerators," D. Chernin and B. Levush, *IEEE International Conference on Plasma Science*, Saskatoon, Saskatchewan (May 1986).

9. "A Strong Focused Spiral Line Recirculating Induction Linac," A. Mondelli, D. Chernin, S. Putnam, L. Schlitt, and V. Bailey, *BEAMS '86*, Kobe, Japan (June 1986).

10. "Strong Focused High Current Electron Accelerators," A. Mondelli and D. Chernin, Presentation to JASON Review Committee, La Jolla, CA (June 1986).

11. "Long Wavelength Beam Stability in High Current Cyclic Accelerators with Strong Focusing," D. Chernin, *NATO Advanced Study Institute on High Brightness Accelerators*, Pitlochry, Scotland (July 1986).

12. "Beam Break-Up Instability in Recirculating Induction Accelerators," A. Mondelli and D. Chernin, *APS/DPP Meeting*, Baltimore, MD (Nov. 1986).

13. "Non-Linear Particle Orbits in a Twisted Quadrupole Field," D. Chernin and B. Levush, *APS/DPP Meeting*, Baltimore, MD (Nov. 1986).

14. "Space Charge Effects on Beam Envelope Evolution in Magnetic Focusing Systems with X-Y Coupling," D. Chernin, *DARPA Annual Propagation Review*, Monterey, CA (Sept. 1987).

15. "Beam Break-Up Instability in Strong-Focused Accelerators," A. Mondelli, D. Chernin and J. Petillo, *APS/DPP Meeting*, San Diego, CA (Nov. 1987).

16. "Beam Propagation Simulations in the PSI-SAIC Recirculating Accelerator Using the Code SPIRAL," J. Petillo, D. Chernin and A. Mondelli, *APS/DPP Meeting*, San Diego, CA (Nov. 1987).

17. "Spiral Line Recirculating Induction Accelerator," V.L. Bailey, S.D. Putnam, M. Tiefenback, C. Eichenberger, A. Mondelli, D. Chernin and J. Petillo, *SPIE Meeting*, Los Angeles, CA (Jan. 1988).

18. "Effect of Energy Spread on the Beam Breakup Instability in the Spiral Line Induction Accelerator," D. Chernin and A. Mondelli, *DARPA Annual Propagation Review*, Newport, RI (Sept. 1988).

19. "Beam Focusing and Matching into the PSI-SAIC Spiral Line Induction Accelerator," A. Mondelli, J. Petillo and D. Chernin, *APS/DPP Meeting*, Hollywood, FL (Nov. 1988).

APPENDIX C
Computer Codes

BBUSH: Tracks a beam pulse through an arbitrary series of gaps and transport sections, calculating the transverse deflection due to the beam break-up instability.

CBDRP: Solves the long wavelength dispersion relation for stellatron in the smooth approximation and plots real and imaginary parts of the mode frequencies versus any of 11 system parameters (beam energy, current, quadrupole strength, etc.).

EMNAG: A dispersion relation solver for the Hughes-Godfrey instability.

ORBITT: Calculates single particle orbits in the field produced by four helically wound wires, superposed on a uniform longitudinal field; used to study the effect of nonlinearities on single particle motion.

RPLANE: Plots curves in stellatron parameter space on which certain resonances are excited.

SBSC: Solves the full eigenvalue problem (no smooth approximation) for long wavelength beam stability in the stellatron.

SPIRAL: A 3-D Biot-Savart field solver and single particle tracking code; used for beam matching studies.

SSRS: Calculates synchrotron radiation spectrum, including the effect of betatron oscillations, for a stellatron.

STELMAT: Calculates the matched launching condition for stellarator systems, including space charge; also calculates growth rates of unstable modes of envelope oscillation.

STELTUNE: Calculates stellatron resonance crossings.

XYENV: A code for tracking beam envelopes in coupled systems, including space charge effects.

Beam stability in a stellatron

D. Chernin

Science Applications International Corporation, 1710 Goodridge Drive, McLean, Virginia 22102

Collective effects in the $l = 2$ stellatron [Phys. Rev. Lett. **50**, 507 (1983)], a high-current electron accelerator, are studied. A thin-beam model is employed, and only long-wavelength, low-frequency modes are considered. The eigenvalue problem is formulated in general and solved analytically in the smooth approximation; comparison with a numerical solution of the eigenvalue problem is excellent. It is found that the dispersion relation in the smooth approximation is identical in form to that for the modified betatron, under a simple substitution. An analytical expression for the transition energy, obtained earlier by a simple dynamical argument, is confirmed. The stellarator field is found to reduce the growth rate of the negative mass instability.

I. INTRODUCTION

The $l = 2$ stellatron, a betatron with an added $l = 2$ stellarator winding, was originally proposed[1] in order to improve the tolerance of a betatron or modified betatron[2] to a mismatch between the average beam energy and the vertical magnetic field. Such a tolerance would be a desirable feature of any high-current accelerator, since injectors inevitably produce a beam with measurable energy spread as well as a variable average energy. Though the original analysis included space-charge effects in a simple, non-self-consistent way, the argument for improved momentum compaction can be based on single particle orbit considerations alone.

Treatment of space-charge effects in the stellatron is complicated by the lack of symmetry in the fields. Self-consistent, monoenergetic, KV-like[3] equilibria can be constructed,[4] however, and these give explicit relations among the beam radii (the beam is elliptical, in general), emittance, current, energy, and externally applied fields; the shifts in the betatron frequencies due to space charge are also obtained from these equilibrium studies.

In the present paper the stability of a beam confined in a stellatron is considered. This work was motivated, in part, by certain experimental results on the $l = 2$ stellatron at the University of California at Irvine.[5] Though beam currents have been increased in that experiment by the addition of the $l = 2$ windings, currents are still not as large as one might expect from the amount of injected charge. An instability of some kind may be responsible for the current loss. An attempt to discover possible current limiting mechanisms in the stellatron initiated the work presented here.

The present stability calculation makes the following approximations: All first-order fields are treated in the long-wavelength ($\lambda > a \equiv$ minor radius of toroidal chamber), low-frequency ($\omega < c/a$) limit; toroidal corrections to the first-order fields are neglected. We note in particular that the long-wavelength approximation may omit the potentially interesting case $\lambda \sim 2\pi r_0/m$, where r_0 is the major radius of the torus and m is the number of stellarator field periods around the device. The beam is treated as a structureless, thin, threadlike charge distribution so that the effects of betatron oscillations and energy spread on the equilibrium are ignored; the magnitude of these effects can be roughly estimated, however.[6] The beam environment, which has a critical

effect on beam stability, is treated simply: the beam is assumed to be contained in a perfectly conducting toroidal chamber. Only the longitudinal, or negative mass mode is unstable in these circumstances. Several comments are made below, however, regarding the effects of walls of arbitrary impedance on both longitudinal and transverse modes.

Under the above approximations we have the following findings to present: (1) the eigenvalue problem governing the longitudinal and transverse modes of a beam in a stellatron; (2) a dispersion relation, obtained from an approximate solution to the eigenvalue problem, which is identical in form to that obtained for the modified betatron,[7] with the redefinition of a certain symbol; (3) confirmation of an analytical expression,[8] obtained by a simple dynamical argument, for the so-called transition energy, below which the longitudinal mode is stable (in the absence of dissipative effects); (4) a quite favorable numerical comparison between the solution to the eigenvalue problem of (1) and the dispersion relation of (2) for the longitudinal mode.

This paper is organized as follows. Section II describes the derivation of the linearized equations of motion, assuming the applied fields are given near the axis of the torus. Section III outlines the derivation of the first-order charge and current densities in terms of the single particle variables using a summation over initial conditions. In Sec. IV the approximate solution to Maxwell's equations is obtained, and the total first-order fields to be used in the equations of motion are derived. In Sec. V the eigenvalue problem is formulated and is shown to reproduce the modified betatron dispersion relation in the absence of the twisted quadrupole field. An approximate solution based on a two-time scale analysis is presented and some comments are made on the form of the resulting dispersion relation. Finally, in Sec. VI, a numerical solution to the full eigenvalue problem is presented and compared to results from the dispersion relation of Sec. V.

Section VII summarizes these results and makes a few additional remarks.

II. EQUATIONS OF MOTION

We shall use a standard (r, θ, z) cylindrical coordinate system. In the unperturbed state we have a thin beam enclosed in a perfectly conducting torus of major radius r_0 and